Supra-molecular structures at the cytoplasmic periphery of the plasma membrane

Dissertation
zur
Erlangung des Doktorgrades (Dr. rer. nat.)
der
Mathematisch-Naturwissenschaftlichen Fakultät
der
Rheinischen Friedrich-Wilhelms-Universität Bonn

vorgelegt von

Eva Elisa Merklinger

aus

Bühl

Bonn 2017

Angefertigt mit Genehmigung der Mathematisch-Naturwissenschaftlichen Fakultät der
Rheinischen Friedrich-Wilhelms-Universität Bonn

1. Gutachter: Prof. Dr. Thorsten Lang

2. Gutachter: Prof. Dr. Christoph Thiele

Tag der Promotion: 17. November 2017

Erscheinungsjahr: 2018

Eidesstattliche Erklärung

Hiermit versichere ich, dass ich die vorliegende Dissertation eigenständig und ohne unerlaubte Hilfe angefertigt habe. Es wurden keine anderen als die angegebenen Hilfsmittel verwendet. Direkt oder indirekt übernommenes Gedankengut wurde nach bestem Wissen und Gewissen kenntlich gemacht. Die Arbeit liegt in dieser oder ähnlicher Form keiner anderen Prüfungsbehörde vor.

(Datum) (Unterschrift)

Anmerkung

Teile dieser Arbeit wurden bereits in folgenden Publikationen veröffentlicht:

Merklinger, E., Schloetel, J.-G., Spitta, L., Thiele, C. and Lang, T. (2016). "No Evidence for Spontaneous Lipid Transfer at ER–PM Membrane Contact Sites". In: *The Journal of Membrane Biology* 249.1-2, pp. 41–56.

Merklinger, E., Schloetel, J.-G., Weber, P., Batoulis, H., Holz, S., Karnowski, N., Finke, J., Lang, T. (2017). "The packing density of a supramolecular membrane protein cluster is controlled by cytoplasmic interactions." In: *eLife* 6, e20705.

Table of contents

Summary **11**

1 Introduction **13**
1.1 Cellular membranes . . . 13
1.2 Basic structural principles of membranes . . . 15
1.2.1 Hydrophobic effect . . . 15
1.2.2 Components of cellular membranes . . . 16
1.3 Macroscopic zones of the PM . . . 19
1.3.1 The hydrophobic core . . . 20
1.3.2 The cytoplasmic zone . . . 23
1.3.2.1 Lipid-protein interactions . . . 23
1.3.2.2 Protein-protein interactions . . . 25
1.3.3 Challenges for studying the cytoplasmic PM periphery . . . 29

2 Aim of the study **37**

3 Materials and Methods **39**
3.1 Materials . . . 39
3.1.1 Technical devices . . . 39
3.1.1.1 Appliances . . . 39
3.1.1.2 Microscopes . . . 40
3.1.2 Buffers and solutions . . . 41
3.1.3 Culture media and reagents . . . 42
3.1.4 Cell lines . . . 42
3.1.5 Antibodies . . . 43
3.1.5.1 Primary antibodies . . . 43
3.1.5.2 Secondary antibodies . . . 44
3.1.6 Plasmids . . . 44
3.1.7 Kits . . . 46
3.1.8 Software . . . 47
3.2 Methods . . . 47
3.2.1 Cloning . . . 47
3.2.2 Cell culture . . . 49
3.2.2.1 General cell culture procedures . . . 49
3.2.2.2 Cleaning and coating of coverslips . . . 50
3.2.2.3 Transfection and transduction . . . 50
3.2.2.4 Cell lysis . . . 51
3.2.3 SDS-PAGE and western blot . . . 51

3.2.4 PM sheets . . . 52
3.2.4.1 Preparation of PM sheets . . . 52
3.2.4.2 Treatments of PM sheets . . . 52
3.2.5 Staining and labeling for fluorescence microscopy . . . 53
3.2.5.1 Immunostaining . . . 53
3.2.5.2 Metabolic labeling of PC and cycloaddition reaction . . . 54
3.2.5.3 Labeling with membrane dyes and lipid probes . . . 54
3.2.6 Botulinum toxin co-expression . . . 55
3.2.7 Comparative epifluorescence-western blot experiment . . . 56
3.2.8 pH-quenching of GFP . . . 57
3.2.9 3D STED . . . 58
3.2.10 Fluorescence recovery after photobleaching (FRAP) . . . 58
3.2.11 Fluorescence loss after photobleaching (FLAP) and analysis . . . 59
3.2.12 STED microscopy and analysis . . . 60
3.2.13 Total internal reflection fluorescence (TIRF) microscopy and analysis 61
3.2.14 Trypsin treatment and ER spot tracking . . . 62
3.2.15 Image analysis . . . 63

4 Results 65

4.1 Inner architecture of the syntaxin 1A protein cluster . . . 65
4.1.1 Influence of cytoplasmic protein domains on lateral organization of syntaxin clusters . . . 67
4.1.1.1 Lateral organization of syntaxin and the variants syx-ΔS and syx-ΔCyt . . . 67
4.1.1.2 Lateral organization of syntaxin and the variants syx-CaaX and syx-ΔS-CaaX . . . 69
4.1.2 Influence of the cytoplasmic domain on packing density of the syntaxin cluster . . . 71
4.1.2.1 Testing of antibodies as molecular sensors for packing density in the current experimental system . . . 72
4.1.2.2 Influence of BoNT/C1-LC cleavage on extracellular myc accessibility of syntaxin . . . 73
4.1.2.3 Comparative analysis of packing density in syntaxin, syx-ΔS and syx-ΔCyt clusters . . . 75
4.1.3 Lateral mobility of syntaxin in the PM of non neuronal cells - implication of the cytoplasmic domain . . . 84
4.1.3.1 Mobility of syntaxin, syx-ΔS and syx-ΔS-Cyt in HepG2 cells 84
4.1.3.2 Mobility of syntaxin, syx-ΔS and syx-ΔS-Cyt in HepG2 PM sheets . . . 86
4.2 Spontaneous lipid transfer (SLT) at ER-PM membrane contact sites (MCS) 89
4.2.1 ER-PM MCS preparation . . . 89
4.2.1.1 Visualization of ER on PM sheets . . . 89
4.2.1.2 PC as a marker lipid for the ER membrane . . . 90

4.2.1.3 Lipid composition of ER-PM contact sites 95
4.2.2 Application and biological relevance of ER-PM contact preparation . 98
4.2.2.1 Functional ER-PM MCS 98
4.2.2.2 Tethering of ER-PM MCS 101
4.2.3 Spontaneous lipid transfer at ER-PM MCS 103
4.2.3.1 Spontaneous transfer of PC 104
4.2.3.2 Spontaneous transfer of cholesterol 108

5 Discussion **111**
5.1 Inner architecture of the supra-molecular syntaxin cluster at the cytoplasmic periphery of the PM 112
5.1.1 Physical properties of syntaxin clusters 112
5.1.2 Correlation between cluster packing density and attraction into the clustered state 117
5.1.3 Putative mechanism of protein-protein interaction mediated cluster density 118
5.1.4 Sketching an integrative view on syntaxin clustering factors 120
5.2 Functional aspects of a supra-molecular structure at the cytoplasmic periphery of the PM - ER-PM MCS 121
5.2.1 Relevance of the ER-PM preparation 121
5.2.2 Advantages and insights from the novel ER-PM MCS preparation . 122
5.2.3 Revisiting spontaneous lipid transfer at MCS 125
5.2.4 No evidence for SLT of PC and cholesterol 127
5.2.5 Possible role for lipid transfer proteins 131
5.3 Reduced dimensionality in supra-molecular structures 132

Bibliography **135**

List of Figures

1.1 Cellular membranes compartmentalize reaction spaces within cells 14
1.2 Three major lipid classes of cellular membranes 16
1.3 Membrane embedding and association of proteins 18
1.4 Segregation principles within the hydrophobic core of the PM 20
1.5 Lipid-protein interactions at the cytoplasmic periphery of the PM 23
1.6 Protein-protein interactions at the cytoplasmic periphery of the PM 26
1.7 Complex networks of interactions influence the cytoplasmic periphery of the PM 30
1.8 Cell unroofing for PM extraction 32
1.9 STED microscopy 34

4.1 Syntaxin1A domain structure and variants 66
4.2 Lateral organization dependent on cytoplasmic protein domains probed by super-resolution microscopy 68
4.3 Transmembrane domain independent lateral organization of syntaxin probed by super-resolution microscopy 70
4.4 Relation of cluster packing density and antibody labeling 72
4.5 Antibody labeling as a molecular sensor of cluster density 73
4.6 Myc accessibility upon intracellular cleavage of syntaxin 74
4.7 Subcellular distribution of syntaxin, syx-ΔS and syx-ΔCyt - pH quenching 77
4.8 Subcellular distribution of syntaxin, syx-ΔS and syx-ΔCyt - analyzed with 3D STED. 79
4.9 Western blot of myc tagged constructs and an IRES linked reporter protein 81
4.10 Comparative analysis of antibody labeling in intact PM versus western blot 83
4.11 The intact SNARE motif is involved in mobility restriction of syntaxin in non-neuronal cells 85
4.12 The intact SNARE motif is involved in mobility restriction of syntaxin in PM sheets of non-neuronal cells 87
4.13 Visualization of ER in whole cells and on PM sheets 90
4.14 Chemical sketch of pPC and sBP-PC 91
4.15 Specificity of metabolic PC labeling 92
4.16 ER membranes visualized by the marker lipid PC 93
4.17 Overlay of clathrin and caveolin with PC spots 95
4.18 Overlap of ER spots with membrane dyes and markers for cholesterol, $PI(4,5)P_2$ and PS 96
4.19 Application of ER-PM MCS preparation in different cell lines 98
4.20 STIM1 enrichment upon stimulation at PC spots on PM sheets 100

4.21 Tethering of the ER contact sites mediated by proteins 102
4.22 The lipid carrier HPαCD mediates PC transfer at ER-PM MCS 105
4.23 Probing loss of pPC from ER membranes after long incubations 106
4.24 No evidence for SLT when probed by FLAP 107
4.25 Cholesterol loading of ER membranes 109

List of Tables

3.1 Appliances 39
3.2 Buffers and solutions 41
3.3 Culture media and reagents 42
3.4 Primary antibodies 43
3.5 Secondary antibodies 44
3.6 Plasmids 44
3.7 Software 47
3.8 Immunostainings 53

Abbreviations

azido-sBP	azido-sulfo-Bodipy
BCA	bicinchoninic acid
BoNT/C1-LC	botulinum toxin C1 light chain from *clostridium botulinum*
BSA	bovine serum albumin
DMSO	dimethylsulfoxid
EDTA	ethylenediaminetetraacetic acid
EGTA	ethylene glycol-bis(2-aminoethylether)-N,N,N,N-tetraacetic acid
ER	endoplasmic reticulum
ER-PM MCS	endoplasmic reticulum - plasma membrane membrane contact site
FLAP	fluorescence loss after photobleaching
FRAP	fluorescence recovery after photobleaching
FRET	Förster resonance energy transfer
FWHM	full width at half maximum
GFP	green fluorescent protein
GPI	glycosylphosphatidylinositol
GPL	glycerophospholipid
HPαCD	(2-hydroxypropyl)-α-cyclodextrin
IRES	internal ribosome entry site
LTP	lipid transfer protein
MβCD	methyl-β-cyclodextrin
MCS	membrane contact sites
min	minute
MSD	mean square displacement
PALM	photo-activated localization microscopy
PBS	phosphate buffered saline
pbs	poly basic stretch
PC	phosphatidylcholine
pC	propargyl choline
PCC	Pearson correlation coefficient
PCR	polymerase chain reaction
PFA	paraformaldehyde
PH	pleckstrin homology
PI(4,5)P_2	phosphatidylinositol-4,5-bisphosphate
PLC	phospholipase C
PLL	poly-L-lysine
PM	plasma membrane
pPC	propargyl-phosphatidylcholine

PS	phosphatidylserine
RFP	red fluorescent protein
RIPA	radioimmunoprecipitation assay buffer
ROI	region of interest
s.d.	standard deviation
s.e.m.	standard error of mean
sBP-PC	sulfo-Bodipy-phosphatidylcholine
SDS-PAGE	sodium dodecyl sulphate-polyacrylamide gel electrophoresis
SL	sphingolipid
SLT	spontaneous lipid transfer
SM	sphingomyelin
SNARE	soluble N-ethylmaleimide-sensitive-factor attachment receptor
SOCE	store-operated calcium entry
STED	stimulated emission depletion
STIM1	stromal interaction molecule 1
$t_{1/2}$	half time
TIRF	total internal reflection fluorescence
TM	transmembrane
TMA-DPH	1-(4-trimethyl-ammoniumphenyl)-6-phenyl-1,3,5-hexatriene-*p*-toluolsulfonate
VAMP8	vesicle-associated membrane protein 8
WB	western blot
YFP	yellow fluorescent protein

Summary

The self-assembly of biomolecules into supra-molecular structures is an important principle underlying cellular organization. These structures define spatial environments for diverse biological processes. In particular, at the cytoplasmic periphery of the plasma membrane (PM) a rich variety of supra-molecular structures are found, relying on lipid-lipid, lipid-protein and protein-protein interactions. Examples include protein-lipid nano-clusters, membrane scaffolds or membrane-membrane contact points. Investigation of such fragile structures is challenging and requires minimally invasive methods. In this work, modern fluorescence microscopy techniques were applied in combination with physical unroofing of cells. This allows for imaging at high signal-to-noise ratio and access to the cytoplasmic leaflet of the basal PM, while preserving the integrity of the supra-molecular structures.

This study provides a detailed analysis of two exemplary supra-molecular structures: the syntaxin cluster and ER-PM membrane contact sites (MCSs).

Syntaxin, a transmembrane protein important for synaptic vesicle exocytosis, can be found in local accumulations of presumably 75 molecules within a diameter of 50 - 60 nm. In this work, the impact of cytoplasmic protein-protein interactions on the inner architecture of the cluster was studied. Analysis by high resolution microcopy revealed overall conserved physical dimensions of protein clusters even if major parts of the cytosolic protein domains were deleted or the transmembrane region was exchanged for a lipid anchor. Mobility measurements revealed that the N-terminal part of the SNARE motif conveys attraction into the clustered state. Deletion of this protein domain entailed the loosening of clusters as indicated by packing sensitive probes. From these results, it is postulated that there is a basic clustering reaction mediated by general attractive forces acting on the TM segment. For the formation of tight intermolecular packing, however, specific protein domains are necessary.

As a second example, ER-PM membrane contact sites (MCS) were chosen. It has been debated whether lipids are able to spontaneously move between two opposing membranes. For analyzing lipid transfer at the contact sites, metabolic labeling of the membrane lipid phosphatidylcholine (PC) in combination with "click chemistry" was applied. This success-

fully enabled the visualization of the lipid dynamics, but did not provide an indication for spontaneous lipid transfer (SLT) between the opposing membranes. Similar observations were made for cholesterol. It can be concluded that MCSs do not *per se* constitute hot spots for SLT of PC and cholesterol. This renders the here developed preparation method attractive for the study of protein-mediated lipid transfer in absence of other lipid transfer mechanisms such as SLT or vesicular transfer.

This work was laid out to characterize two multifaceted supra-molecular structures at the cytoplasmic periphery of the PM. In this context, experimental strategies were developed to probe features of the supra-molecular structures. The here presented results give detailed insights into very specific aspects of these structures. Future investigation could focus on unraveling further aspects of the inner architecture of nano-clusters or clarify the role of proteins associated with lipid transfer at ER-PM MCSs.

1 Introduction

All processes of life are defined by interactions between organic macromolecules. Their precursors derived 4 billion years ago from organic monomers by an important principle: the physical delimitation of the reaction space. Proposed boundary models in this context are the primordial soup (Oparin 1924), pyrite surfaces (Wächtershäuser 1988) or metal-sulfide-walled compartments (Martin et al. 2003). Despite context related differences, all those concepts stress the importance of high reactant concentration and their close proximity for the emergence of organic macromolecules.

Cells developed their own boundary for structural autonomy from the inorganic surrounding. The separation into closed compartments allows for competition and thus development by evolution. Furthermore, it protects molecules from the inorganic environment and enables regulation of biochemical reactions. Despite large variability in components, the overall structure confining the cell interior is similar amongst all living cells. Intriguingly, it is not a compact solid but a thin fluid layer, therefore called plasma membrane (PM).

In smaller dimensions, the aforementioned delimitation principle continues within the PM and its surroundings. The components, lipids and proteins, interact in complex networks to build up supra-molecular structures. Analogous to the example above they enable spatial separation of components for the generation of specific micro-environments. These sub-compartments meet important physiological functions such as signal transduction or cargo transfer.

1.1 Cellular membranes

Separation from the environment is an important feature of membranes. However, if its function was exclusively limited to this boundary property, cells would be plain reaction compartments with a stagnating number of reacting partners. This would ultimately result in the convergence of chemical potentials arresting all reactions.

Instead, cellular membranes are highly flexible structures with the ability to exchange, import or export material. Inherently, membranes are semi-permeable: uncharged mole-

cules can diffuse through membranes the easier the less polar and the smaller they are. For charged or larger molecules, transport across membranes is protein-mediated. It can be either passive along a concentration gradient or active and thus energy-dependent. The active transport of ions, for instance, enables the establishment of ion gradients across membranes, which in turn can be used for the synthesis of high energy bonds. This fundamental conversion principle between chemical and electrical energy is used by all known living cells.

Additional to the active or passive exchange of molecules, cellular membranes also function as communicators between inside and outside. They receive signals, translate and transmit them. In this way, cells can readily sense and adapt to environmental changes. In multicellular organisms, intercellular communication ensures effective collaboration and is essential for survival.

Prokaryotes, archaea and bacteria, possess only the cell surrounding PMs. Eukaryotes on the other hand exhibit a multitude of other intracellular membranes. They compartmentalize the interior of cells into additional physical spaces with specialized functions: the organelles (see figure 1.1).

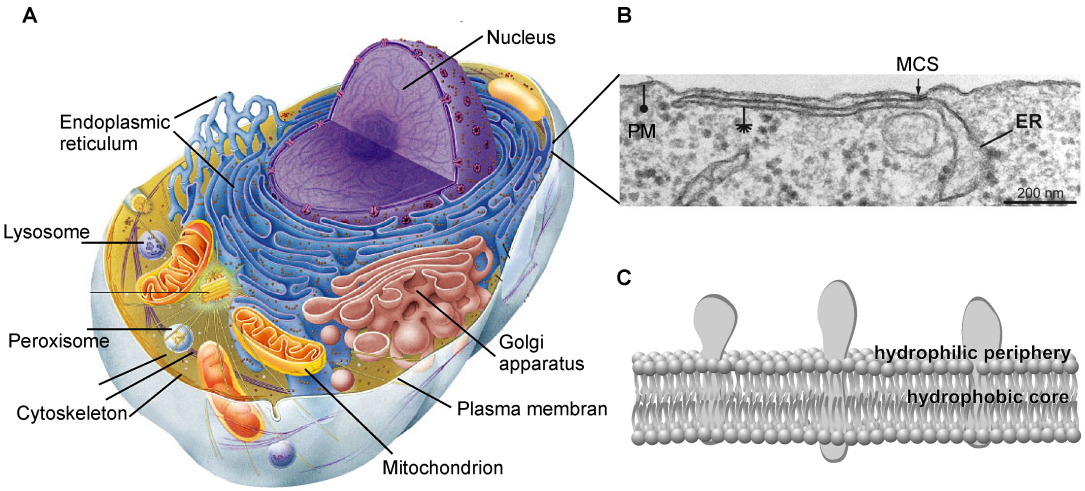

Figure 1.1: **Cellular membranes compartmentalize reaction spaces within cells. A** Schematic illustration of an animal cell. Specialized functions can be attributed to each of the organelles: the nucleus harbors and manages the majority of genetic material; the ER, a complex membrane enclosed compartment that spreads throughout the cell in a net-like structure, functions in e.g. lipid synthesis, Ca^{2+} homeostasis, protein synthesis, modification, quality control, and transport; the cellular energy current, ATP, is generated in the mitochondria; the Golgi apparatus is important for the vesicular transport of material and the establishment of lysosomes, the location of degradation and recycling of molecules; oxidative reactions for degradation are mainly processed in peroxisomes. (Image slightly modified from Campbell et al. 2001). **B** Electron micrograph of a ER-PM membrane contact site in HeLa cells. Image from Orci et al. 2009. **C** Schematic illustration of cellular membrane arrangement of hydrophobic core built up by hydrophobic lipid and protein parts and the hydrophilic periphery.

Commonly, biological textbooks present organelles as isolated structures surrounded by the cytoplasm. In this way, the visual presentation might be less cluttered, but it is far from being complete. Instead, organelles are connected to each other at highly abundant membrane contact sites (MCS) (see figure 1.1). The yeast strain *saccharomyces cerevisiae*, for example, contains more than 1000 MCS between PM and endoplasmic reticulum (ER) per cell (Pichler et al. 2001). In general, MCS are stabilized by tethering proteins. Most of these are integral membrane proteins of either of the interacting membranes that can bind to proteins or lipids of the other membrane. Depending on the length of the tethers, the two compartmental membranes exhibit close proximity of less than 30 nm (Helle et al. 2013).

1.2 Basic structural principles of membranes

As mentioned above, supra-molecular structures of the PM depend on a complex network of interactions. The general framework in which they occur underlies the basic physical principle of the hydrophobic effect that leads to the assembly of the building blocks, lipids and proteins.

1.2.1 Hydrophobic effect

The overall stability of cellular membranes can be assigned to the hydrophobic effect, which describes the tendency for hydrophobic and hydrophilic substances to separate from each other. With its dipolar structure, water is the predominant hydrophilic substance of cells. Water molecules assemble in solution to build up a network of dipole-dipole interactions. Hydrophobic molecules exhibiting mainly nonpolar and uncharged moieties therefore disturb the water network and force the water molecules to rearrange (Chandler 2005). To diminish the involved energy costs, the interface area between hydrophobic domains and hydrophilic solvent has to be minimized. Therefore, hydrophobic molecules tend to assemble to higher order structures such as membranes. Accordingly, the reverse reaction, desorption of hydrophobic molecules into the hydrophilic solvent, is restrained, which prevents the disassembly and stabilizes membranes.

Nonetheless, biological membranes have to remodel constantly to adapt to the environment, for cargo transport, cell division, intercellular communication etc. These processes are always accompanied by transition states that increase the hydrophobic-hydrophilic interface temporally (Jahn et al. 2003). Therefore, specific micro-environments have to be created to counteract the stabilizing forces, often with the expense of energy.

1.2.2 Components of cellular membranes

In the context of cellular membranes, the cytosol and extracellular space constitute the hydrophilic solvent, whereas hydrophobic lipid and protein parts separate and assemble. However, none of the cellular membrane components are purely hydrophobic but are characterized by an amphiphilic structure. The following section gives a short introduction of those amphiphilic building blocks, lipids and proteins.

Three major membrane lipid classes

There are three major classes of membrane lipids that build up cellular membranes: the glycerophospholipids (GPLs), sphingolipids (SLs) and sterols (see figure 1.2). The GPLs are the most abundant lipid group in eukaryotes. They are based on a glycerol backbone linked on two positions to hydrophobic carbon chains. These chains originate from fatty acids and can vary in their length and the amount of double bonds (degree of saturation). The major fatty acids in eukaryotic GPLs can vary from 16 to 20 carbon atoms in length and contain either none, one, two or four double bonds (Keenan et al. 1970). Chain length

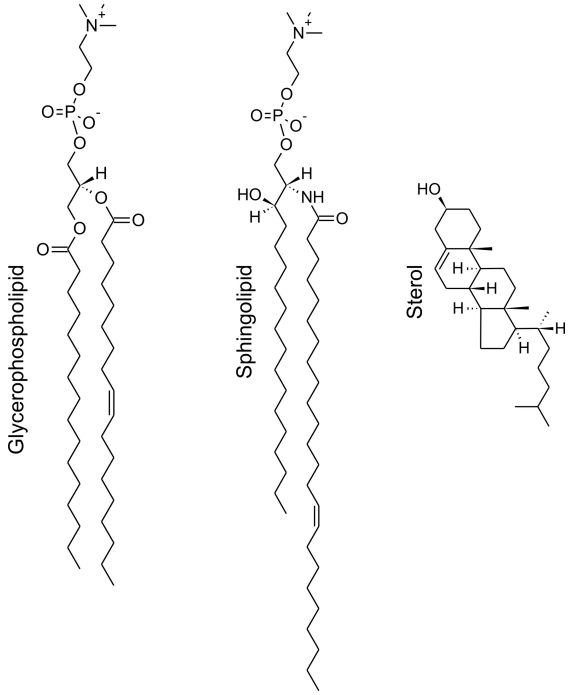

Figure 1.2: **Three major lipid classes of cellular membranes.** Schematic illustration of representatives of the three membrane lipid classes: *left*, glycerophospholipids (GPL): 1-hexadecanoyl-2-(9Z-octadecenoyl)-sn-glycero-3-phosphocholine (phosphatidylcholine, PC(16:0/18:1)); *middle* sphingolipids (SL): N-(tetracosenoyl)-sphinganine-1-phosphocholine (sphingomyelin, SM(18:0/24:1)); *right* sterols: cholest-5-en-3β-ol (cholesterol); Lipid structures from LIPID MAPS Structure Database (http://www.lipidmaps.org/)(Sud et al. 2007). Fatty acid chains in GPL and SL can vary in length and degree of saturation which influences physical properties of cellular membranes such as fluidity and order similarly to the content of cholesterol.

and saturation directly affect properties of the membrane: the longer and more saturated the chains are, the better chains can align. This higher order leads to stronger interactions among the lipids and increases rigidity of the membrane.

The different GPLs are defined by their headgroups, which are linked to the remaining hydroxyl group of the glycerol backbone by a phosphate ester. The most common headgroups are choline, serine, glycerol, inositol, and ethanolamine. Headgroups influence the charge of the lipid with phosphatidylcholine (PC) and phosphatidylethanolamine (PE) being zwitterionic and phosphatidylglycerol (PG), phosphatidylserine (PS) and phosphatidylinositol (PI) being anionic. The hydroxyl groups of the inositol in PI can be phosphorylated at different positions yielding mono-, di-, or triphosphates.

SLs are structurally similar to GPLs with two hydrophobic fatty acid chains and a hydrophilic head group attached to a backbone, in this case the amino acid L-serine. A choline headgroup is attached to yield sphingomyelin (SM) . In contrast to GPLs, SLs tend to contain more saturated and longer fatty acids. Additionally, SLs can be glycosylated for the formation of complex glycosphingolipids, which are mainly found in the outer leaflet of the PM.

The third class of membrane lipids is the sterols with cholesterol as the most prominent representative in mammalian cells. The synthesis is catalyzed in the cytosol and at the cytoplasmic face of the ER membrane leading to the inflexible four carbon rings forming the sterol backbone. Cholesterol is mainly apolar with the exception of one hydroxyl group at the C3 carbon atom, which can form hydrogen bonds.

Modular combination of the diverse GPLs, SLs and sterols enable cells to obtain cellular membranes of different basic physical properties. The PM, for example, contains a high amount of sterols and sphingolipids, which leads to an increased stability and makes it less permeable. On the contrary, the ER harbors less sterols and a higher amount of GPLs with cis-unsaturated acyl chains resulting in looser packing and thinner membranes (Schneiter et al. 1999, Meer et al. 2008).

Further, the asymmetric distribution of particular lipids alters the specific fingerprint of membrane surfaces through altered surface charges or specialized lipid functions. Phosphatidylinositol-4,5-bisphosphate ($PI(4,5)P_2$) for example occurs mainly at the inner leaflet of the PM (Di Paolo et al. 2006) where it functions as a recruitment site of specialized protein binding domains (see section 1.3.2.1).

Membrane proteins

Proteins are important structural and functional components of cellular membranes. In fact, 8% of all human proteins were found to reside in the PM (Uhlén et al. 2015) and around 50% of the PM mass results from membrane proteins (Alberts et al. 2002). Membrane proteins are commonly differentiated in peripheral or integral proteins (figure 1.3).

Integral membrane proteins are partly embedded into the core of the membrane. Hydrophobic interactions with lipids thereby stabilize the transmembrane (TM) protein parts. In addition, electrostatic interactions of charged protein moieties flanking the TM regions with charged lipid head groups further retain the proteins inside the membrane. Embedding can be achieved by a single or multiple helices that traverse the membrane. Another possibility is the formation of a hairpin structure, which enters and leaves the membrane at the same side or a beta-barrel that creates a membrane pore. Initially, the majority of integral PM proteins are synthesized at and inserted into the ER membrane. Protein modifications like glycosylation or formation of disulfide groups are processed in the ER or the Golgi before vesicular trafficking to the PM.

In contrast, peripheral proteins associate with headgroups of lipids or other proteins in the membrane. Thus, they are not in direct contact with the hydrophobic core and their protein parts can only face the side of the membrane to which they are attached to.

Some peripheral and integral membrane proteins are linked covalently to a fatty acid

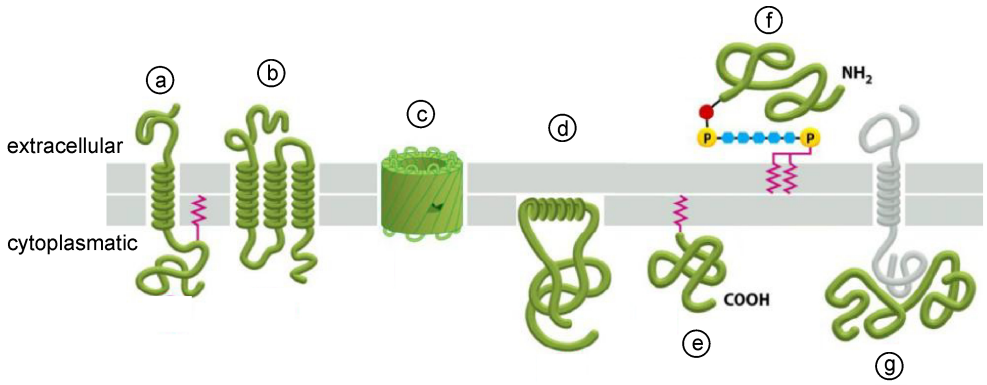

Figure 1.3: **Membrane embedding and association of proteins.** Diagrammatic view on different possibilities for proteins to be part of membranes; (**a-d**) integral membrane proteins exhibit direct contact of protein domains with the hydrophobic lipid core of the membrane with (**a**) one TM helix (single span), (**b**) multiple TM helices (multi span), (**c**) a barrel structure of β-sheets, (**d**) protein domains that are only embedded into one layer of the membrane. (**e**) Peripheral and integral proteins can be anchored to the membrane via fatty acid or prenyl groups at the intracellular leaflet of the PM. (**f**) Glycolipid attached to the C-terminus of certain proteins anchors them to the extracellular leaflet (GPI-anchor). (**g**) Peripheral membrane proteins bind to other membrane-anchored proteins or lipid headgroups without direct contact of protein domains with the hydrophobic core. (Illustration modified from Alberts et al. 2002).

chain or a prenyl group, further anchoring the proteins at the membrane. A special case of membrane anchoring is the glycosylphosphatidylinositol (GPI) anchor, which is post-translationally attached in the ER to proteins with a specific motif. GPI-anchored proteins are found at the extracellular leaflet of the PM.

1.3 Macroscopic zones of the PM

When considered from a rather macroscopic view, the PM can be dissected into three different zones: i) a carbohydrate-rich outer periphery, ii) the core build up by hydrophobic lipid and protein moieties and iii) a fringe region with the cytoplasm.

The outer periphery meets diverse demands in cell-cell and cell-matrix communication. An important structural element in these processes is the glycocalyx at the cell surface, which consists of a vast number of oligosaccharide chains linked to membrane proteins or lipids (Kleene et al. 2004). This complex meshwork is, for example, important for neuronal cell development and regeneration (Kleene et al. 2004), or can function in mechano-transduction in endothelial cells (Florian et al. 2003).

Hydrophobic lipid and protein parts build up the hydrophobic core of the PM separating the hydrophilic extra- and intracellular environment (see section 1.2.1). The core acts as a permeability barrier for charged and large molecules, therefore allowing regulated cargo transport across the PM.

The cytoplasmic zone of the PM is a highly occupied and busy area: signals approach from the outside and are processed and transmitted, cargo is transported via endo- or exocytosis, the structure of the PM is remodeled by interactions with the cytoskeleton, membrane channels are opened or closed, etc. The majority of these processes are implemented by supra-molecular structures, wherein multiple proteins and lipids interact to form specific micro-environments such as for example signaling platforms. Diverse interactions among the components contribute to the formation and stability of supra-molecular structures. Lipid phase separation, lipid wetting of embedded protein parts and hydrophobic mismatch are segregation principles mostly attributed to the hydrophobic core (see figure 1.4). Interactions between lipid headgroups and protein residues (see figure 1.5) amongst proteins in the hydrophilic surrounding (see figure 1.6) are located at the cytoplasmic interface of the PM. In the next sections, the hydrophobic core and the cytoplasmic periphery will be dissected for interactions localized in the respective zone.

1.3.1 The hydrophobic core

The components within the hydrophobic core are not distributed homogeneously. Instead, they interact with each other leading to local changes in physical properties of the membrane such as fluidity or thickness (figure 1.4). Formation and stabilization of supra-molecular assemblies are thereby promoted.

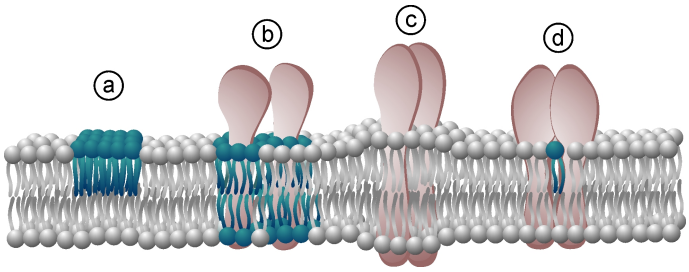

Figure 1.4: **Segregation principles within the hydrophobic core of the PM.** Components within the hydrophobic membrane core interact with each other and thus promote the formation and stabilization of supra-molecular assemblies at the cytoplasmic periphery of the PM. (**a**) Lipids can assemble due to their order parameters into lipid phases. (**b**) Protein domains in direct contact with the hydrophobic core are surrounded by annual lipids. Sharing lipid annuli can lead to capillary condensation. (**c**) Protein and lipid parts influence the thickness of membranes. Hydrophobic mismatch is an important sorting mechanism for proteins. (**d**) Proteins and lipids can exhibit specific interactions.

Lipid phases

One of the most studied organization principles in bilayers are the lipid phases. The term refers to the ability to organize the bilayer into lateral domains as revealed decades ago in simple lipid systems (Engelman et al. 1972). The idea that lipid phases are important for physiological functions arose from the observation that glycoproteins are sorted in the Golgi apparatus along with newly synthesized SLs before they are delivered to the epithelial PM in polarized cells (Simons et al. 1988). So-called *lipid rafts* of SM and cholesterol formed in the Golgi have been suggested to attract certain proteins, thus directing their co-segregation and transport (Simons et al. 1997).

When considering pure lipid systems, the lipid bilayer can be classified into three phases according to their order parameter and the lateral mobility: solid ordered (high order, low mobility), liquid-disordered (low order, high mobility), and liquid-ordered (high order, low mobility) (Meer et al. 2008). Transition between phases is fluent and occurs, for instance, upon temperature change (Ipsen et al. 1987).

In particular, structure and shape of the lipid species influence phase properties (see section 1.2.2). For example, SLs often contain long and saturated acyl chains and therefore assembles at higher order (D. A. Brown et al. 2000). In contrast, a bilayer composed of

unsaturated PC appears in a liquid-disordered phase (McMullen et al. 1994). Sterols, being smaller and more compact and rigid as the acyl chains, have a divergent effect on bilayers: On the one hand, they disturb the tight packing of, for example, SM and on the other hand they are able to compensate for packing defects between unsaturated acyl chains. This leads to a decrease of membrane fluidity, increased membrane thickness (Almeida et al. 2005) and the assembly of liquid ordered phases, which still provides high lateral mobility of the lipids (Meer et al. 2008).

Studies performed in artificial bilayer systems with lipid mixtures related to the lipid composition of PM were able to visualize the segregation into domains with fluorescence microscopy (Veatch et al. 2003, Kaiser et al. 2009, Dietrich et al. 2001). In live cells, SM and GPI-anchored proteins, putative lipid raft-associated proteins, were shown to be trapped in complexes in the PM (Eggeling et al. 2009). Those cholesterol-dependent complexes have been described to be short lived (up to 20 ms) and smaller than 20 nm in diameter (Eggeling et al. 2009) and thus differ vastly from the phases observed in artificial membranes. This questions the transferability of the studies on lipid phases in artificial lipid systems to biological membranes but, at the same time, stresses the influence of lipid phases on the formation of micro-domains inside cellular membranes. In fact, such phases were shown to be important for the formation of signaling platforms at the PM. For example, the human chemokine receptors partition into specific lipid domains upon binding of ligands where they come into close proximity with G proteins and activate them for further signal processing (Jiao et al. 2005).

Protein embedding into the hydrophobic core

Certainly, there is an influence of lipid assemblies on segregation of proteins as explained in the previous section. However, at the same time hydrophobic protein domains influence lipid behavior and thereby modulate membrane organization.

When protein domains are embedded into lipidic bilayers, the lipid molecules have to adapt structurally to the hydrophobic protein surface for a close contact in order to preserve the integrity of the membrane. Lipids in direct proximity to the protein are therefore less structured and are restricted in their movement (Brotherus et al. 1981). These so-called shell lipids are not rigid but readily exchange with the bulk lipids outside the shell (D. Marsh et al. 1998). Entropic effects promote the tendency to share lipid annuli. Capillary condensation effects thereby lead to joining forces between proteins and facilitate the formation and stabilization of protein accumulations within the membrane (Gil et al. 1998).

Consequently, proteins represent obstacles for lipid diffusion and thus reduce mobility of the adjacent lipids. Moreover, the insertion of proteins in membranes can lead to local disturbance of lipid order as demonstrated by enhanced capability of transbilayer movement upon insertion of certain peptides into model membranes (Kol et al. 2003).

From the examination of synaptic vesicles, it is known that the occupancy of proteins inside the membrane can reach more than 10^5 TM regions per µm^2 membrane area (Takamori et al. 2006). In red blood cells, the percentage of the protein-occupied area within the PM was determined to be more than 20 % (Dupuy et al. 2008). These numbers imply that a large portion of membrane lipids is influenced by proteins in the PM, which in turn affects protein segregation.

Thickness of the core region and hydrophobic mismatch

The thickness of the membrane core is modulated by the chain length of the lipid carbon chains and their outstretch due to the degree of saturation. In artificial lipid bilayers, cholesterol is able to increase membrane diameter (Wilkins et al. 1971) whereas in biological membranes, TM protein domains were suggested to be the more prominent regulator of membrane thickness (Mitra et al. 2004). In either case, TM segments of proteins usually match in length with the bilayer, because a positive or negative length difference, the hydrophobic mismatch, would lead to energetically disfavored increase in hydrophobic-hydrophilic interfaces (see section 1.2.1). The matching is achieved either by the restructuration of the membrane or the TM protein domain (Jesus et al. 2013) or by differential sorting of TM domains to different cellular membranes of appropriate thickness (Munro 1995). Hydrophobic mismatch is an important factor promoting the interaction between TM segments (Schmidt et al. 2008) and regulating, for instance, the specificity of interaction within protein clusters (Milovanovic et al. 2015).

Specific lipid-protein interactions

The forces described in the previous sections are throughout collective properties of bilayers that stabilize or promote the formation of supra-molecular assemblies in the PM. In addition, there are specific interactions between lipids and proteins that lead to the formation of higher order assemblies. For example, a direct and highly specific interaction of the TM protein p24 with SM was discovered involving the headgroup and the backbone of the lipid (Contreras et al. 2012). Binding of the lipid was shown to promote dimerization of p24 and thus the lipid was suggested to be a cofactor in the conversion of an inactive protein monomer to an active supra-molecular assembly (Contreras et al. 2012).

1.3.2 The cytoplasmic zone

When refocusing from the hydrophobic core further towards the cytosol, one approaches its interface with the hydrophilic periphery of the PM. Further complex interactions take place in this region to define the specific micro-environments of supra-molecular structures. Such interactions involve the recognition of specific lipid headgroups for the recruitment of soluble proteins or proteins integral to other cellular membranes. Furthermore, electrostatic interactions with lipids or among proteins, as well as other protein-protein interactions lead to higher order assemblies. In most cases, the different interaction types mutually depend on each other, challenging their investigation.

1.3.2.1 Lipid-protein interactions

Lipid-mediated protein recruitment

Specific lipids at the cytoplasmic periphery of the PM create platforms for the recruitment of proteins from the cytosol (see figure 1.5). In this way, interaction partners come in close proximity, which enables efficient reaction and allows for refined regulation.

One prominent example for such a specific lipid is the major phosphoinositide in mammalian cells, $PI(4,5)P_2$ (see section 1.2.2). For example, phospholipases C (PLC) are recruited to the PM via their $PI(4,5)P_2$ binding pleckstrin homology (PH) domains upon activation by signal cascades (Ferguson et al. 1995). The proximity to the PM enables the PLC to hydrolyze their target $PI(4,5)P_2$ into diacylglycerol (DAG) and inositol 1,4,5-trisphosphate (IP3). While the latter opens calcium channels in the ER, the former in turn acts as an additional recruiter of protein kinase C to the cytoplasmic periphery of the PM. This lipid-promoted binding entails the recruitment of further scaffolding pro-

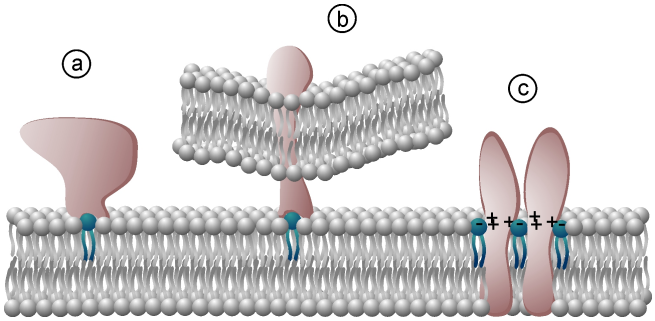

Figure 1.5: **Lipid-protein interactions at the cytoplasmic periphery of the PM.** Specific lipids such as e.g. $PI(4,5)P_2$ (depicted in blue) act as recruiter for cytosolic proteins (**a**) or membrane-embedded proteins from other cellular membranes such as the ER or vesicles (**b**). (**c**) Negatively charged lipids such as $PI(4,5)P_2$ interact with positively charged protein residues. This electrostatic interaction can promote e.g. the assembly of proteins to clusters (Bogaart et al. 2011).

teins (Mochly-Rosen et al. 1991), which again bind other signaling enzymes generating an intricate network of interactions at the cytoplasmic periphery of the PM.

Lipid-mediated membrane recruitment

Another lipid-mediated protein recruitment at the cytoplasmic periphery of the PM goes even beyond the described PI(4,5)P_2/PLC interaction: If the protein containing the lipid binding motif is anchored in another membrane, such as the ER, the recruitment mediates spatial proximity of the two membranes, which leads to the formation of a MCS (figure 1.5). One example for such supra-molecular structures is the ER-PM MCS.

First described in an electron microscopy study of muscle cells in 1957 (Porter et al. 1957), ER-PM MCS were neglected for a long time due to the lack of reliable methods for purification or observation. In recent years, however, they regained attention and their influence in lipid transfer is currently of high interest (Giordano et al. 2013, Saheki et al. 2016, Yu et al. 2016).

All of the identified tethering proteins, the human extended synaptotagmins, the Ist2 (corresponding to human TMEM16A-J), the VAP (vesicle-associated membrane protein-associated) proteins and the exclusively in mammals identified junctophilins are integral ER membrane proteins (Henne et al. 2015). They interact with lipids at the PM by multiple lipid recognition protein domains. Extended syntaptotagmins, for example, contain lipid-binding C2 and SMP domains (Schulz et al. 2004, Toulmay et al. 2012) and bind PI(4,5)P_2 in a calcium-dependent manner (Giordano et al. 2013). Ist2/TMEM16 likewise interacts with PI(4,5)P_2 via a polybasic protein domain (Fischer et al. 2009). Junctophilins contain a not fully investigated basic MORN (membrane occupation and recognition nexus) domain, that has been proposed to bind PI(3,4,5)P_3 (Bennett et al. 2013), a lipid that is, similar to PI(4,5)P_2, nearly exclusively found in the PM (Meer et al. 2008).

Electrostatic lipid - protein interactions

Just as the described specific interactions, also electrostatic lipid-protein interactions play a pivotal role in the organization of the cytoplasmic PM periphery (see figure 1.5). The most important lipids in this context are the phosphoinositides and PS. The net charge of PI(4,5)P_2, for instance, ranges from -3 to -5 depending on the pH and interactions with surrounding molecules (McLaughlin et al. 2002). Thus, it is able to electrostatically interact with positively charged protein residues proximal to the lipid headgroups.

The involvement of electrostatic lipid-protein interactions in micro-domain formation was demonstrated using syntaxin 1A clustering as an example (Bogaart et al. 2011).

Syntaxin 1A traverses the PM with a single TM domain linked to the cytoplasmic protein part by a polybasic amino acid stretch 260KARRKK265 (pbs). In the study of Bogaart et al. 2011, PI(4,5)P_2 formed cluster phases with a peptide corresponding to the pbs-TM domain dependent on the positive amino acids in giant lamellar vesicles. Additionally, high resolution microscopy revealed the formation of PI(4,5)P_2 domains in the PM of cells with similar size of syntaxin1A cluster, which were sensitive to PI(4,5)P_2 cleavage. In summary, it has been concluded that electrostatic lipid-protein interactions were sufficient for micro-domain formation. However, as suggested by Khuong et al. 2013, the more negative lipid PI(3,4,5)P3 could be the relevant charge counterpart in the process of syntaxin 1A micro-domain formation.

The supra-molecular structures of syntaxin 1A and phosphoinositides were reported to serve as docking platforms for neurotransmitter-containing vesicles at the synaptic cleft (Honigmann et al. 2013). Those vesicles are docked to the PM and fuse upon arrival of an action potential. The cytoplasmic periphery of the PM plays an important role in spatial and temporal regulation of this process, whereat SNARE protein interactions convey specificity and are the basic molecular engine for the fusion reaction (Jahn et al. 2012). Such protein-protein interactions at the cytoplasmic periphery of the PM are subject of the next chapter.

1.3.2.2 Protein-protein interactions

In general, protein-protein interactions (PPIs) can be classified into i) homomeric or heteromeric, ii) strong and weak, and iii) permanent or transient, whereby transitions between the interaction types are fluent (Nooren et al. 2003).

PPIs at the cytoplasmic fringe of the PM underlie the same principles as interactions in the cytosol with two major differences: i) PPIs, even if the interacting protein domains are located in the cytosol, often involve interactions within the hydrophobic core of the PM either with lipids or between TM domains of integral membrane proteins. ii) Interactions at the PM are spatially restricted to the 2D environment of the membrane. Integral as well as peripheral membrane proteins are mobile but manifold slower compared to cytosolic proteins (M. McCloskey et al. 1984, Kumar et al. 2010) and move only laterally. Additionally, the PM is highly packed with proteins (see section 1.3.1), which causes constant physical contact to multiple putative interaction partners.

Importantly, not only does membrane structure affect PPIs but PPIs in turn also impinge on the structure of the membrane. This complicates the analysis of cause and effect

of the interactions. In the following, PPI functions at the cytoplasmic periphery of the PM are introduced exemplary to provide insight into supra-molecular protein complexes (see figure 1.6).

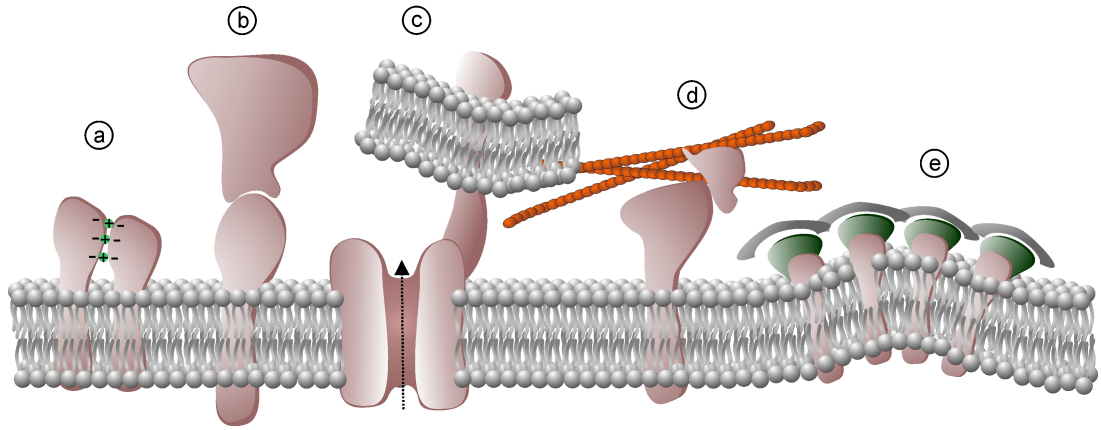

Figure 1.6: **Protein-protein interactions at the cytoplasmic periphery of the PM.** (**a**) Small ions such as calcium promote protein clustering via electrostatic charge bridges. (**b**) Membrane-embedded proteins can recruit soluble proteins via specific interaction domains. (**c**) PM proteins interact with integral proteins of other membranes such as the ER or vesicles e.g. for opening of calcium channels in the PM (depicted by black arrow). (**d**) Connections with the cytoskeleton allow for membrane remodeling and influence the organization of lipids and proteins within the membrane. (**e**) The combination of membrane-embedded proteins and adaptor proteins can lead to membrane deformation important for e.g. vesicle budding.

Electrostatics in protein clustering

Returning to the subject of electrostatics in membrane organization, ions are able to promote oligomerization of proteins similar to charged lipids. Calcium is one of the most important ions in this context. Its concentration in the cytosol is in the 100 nM range (Brini et al. 1995), but upon calcium channel opening the local concentrations at the cytoplasmic fringe of the PM can temporary exceed this value to values in the µM range (Rizzuto et al. 2006). This was shown to be sufficient for membrane protein interaction and the promotion of clustering for a variety of different membrane proteins (Zilly et al. 2011). Importantly, the calcium-dependent formation of those micro-domains is not due to specific calcium interaction sites within the proteins but purely mediated by electrostatics.

This distinction is exemplified by a study reporting on biphasic protein clustering in the interaction of the SNARE protein SNAP25 with calcium (Batoulis et al. 2016). Salt-bridges of calcium with negatively charged aspartate and glutamate residues are proposed to compensate the repulsion of negative charges among the proteins and therefore stabilize the formation of protein cluster at low calcium concentrations, whereas high calcium

concentration disband the bridging behavior due to overcharging (Batoulis et al. 2016). Interestingly, similar biphasic clustering behavior has been observed in the lipid-mediated sequestering of the syntaxin pbs-TM-peptide in giant membrane vesicles (GUV) used in the study of (Bogaart et al. 2011, see section 1.3.2.1), where sequestering was diminished at high $PI(4,5)P_2$ concentrations.

Protein recruitment via specific protein domains

Specific protein-protein interactions between membrane-embedded and soluble proteins play a pivotal role in the complex interaction networks of supra-molecular structures. These interactions are analogous to the previously explained protein recruitment of lipids. Similarly, they involve protein domains that specifically recognize their interaction partner.

Scr-homology (SH2) domains are classical examples of such a protein domain. Specificity for binding to membrane proteins is mediated by the recognition of C-terminal phosphotyrosine (pTyr) residues (Pawson et al. 2000). For example, the epidermal growth factor receptor (EGFR) contains several such pTyr sites in its activated state. Upon binding of a peptide ligand to the extracellular protein part, the receptor undergoes structural rearrangements and dimerizes. The thereby activated tyrosine kinase domain at the intracellular side of the PM catalyzes the phosphorylation of tyrosine residues at adjacent EGFRs. The binding of SH2 domain-containing proteins initiates the formation of a complicated network of more than 100 interacting molecules at the cytoplasmic periphery of the membrane for signal conveyance into the cytosol (Morandell et al. 2008). Protein interactions as the ones described are therefore integral parts of sophisticated networks in which even small changes can lead to severe phenotypes such as tumor development in case of the EGFR.

Protein-mediated ion channel activation

The previous sections introduced protein interactions within the PM, as well as between PM-embedded and soluble proteins. Interacting proteins of supra-molecular structures at the cytoplasmic periphery of the PM can also be anchored to different cellular membranes. This is for example important in ER-PM MCS-mediated store-operated calcium entry (SOCE). In this process, the integral ER protein STIM1 senses low calcium level in the ER, oligomerizes and translocates to MCS between the PM and the ER (Liou et al. 2007). STIM1 interaction with the pore forming protein ORAI1 in the PM opens calcium release-activated channels (CRAC) at the PM (Stathopulos et al. 2013) leading to local calcium influx (Wu et al. 2006).

Several layers of regulation contribute to the complexity of SOCE: for example, the oligomeric state of ORA1 assemblies at the PM defines ion specificity of the channel with the tetramer being specific for calcium (Thompson et al. 2013). Furthermore, SOCE is highly susceptible to changes in the STIM1:ORAI1 stoichiometry (Hoover et al. 2011). Trapping of the channels is thereby achieved by only two STIM1 molecules, full activation, however, requires eight STIM1s (Hoover et al. 2011). Mutations in the STIM1 consensus glycosylation site promote formation of STIM1 oligomers, which results in overactivation of ORAI1 channels and their subsequent degradation (Kilch et al. 2013). Such increased SOCE leads to severe pathological symptoms involving platelet defects and skeletal myopathies (Lacruz et al. 2015). Additionally, there are a variety of other possible regulations via lipid-protein interactions such as the suggested downregulation of SOCE by the specific binding of ORAI1 to cholesterol within the PM (Derler et al. 2016).

Although the connections between the different regulating mechanisms are unknown, the example of SOCE again demonstrates the necessity of fine orchestration in supramolecular assemblies like the ER-PM MCS.

Interaction of the PM with the cytoskeleton

Another layer of complexity at the cytoplasmic periphery of the PM is added by its connection with the cellular cytoskeleton. Many types of supra-molecular actin-based structures, as well as microtubuli and intermediate filaments interact tightly with the PM to control membrane tension, global cell shape and volume (Doherty et al. 2008).

In smaller dimensions, cytoskeleton-PM interactions also influence the organization of PM components. For example, the direct coupling of a membrane protein to actin filaments results in the formation of protein clusters (Gowrishankar et al. 2012). In addition, already existing supra-molecular protein assemblies are actively redistributed within the PM through the action of cytoskeleton elements, as demonstrated in the context of T cell receptor signaling (Varma et al. 2006).

However, the interaction of PM components with the cytoskeleton is bidirectional as exemplified by a study of Banjade et al. 2014, wherein the authors present protein cluster as the nucleation sites of actin filaments. This demonstrates the complexity of interactions at the cytoplasmic periphery of the PM. Open questions in this area of research are therefore difficult to tackle, since on the one hand slight changes in membrane organization or on the other hand minimal disintegration of the cytoskeleton meshwork could mutually influence each other leading to unintended restructuring of cytoskeleton-PM interactions.

Protein-induced remodeling of the membrane

Previous chapters introduced the various interactions at the cytoplasmic periphery of the PM that determine the micro-environments of supra-molecular structures. Conversely, the latter are able to influence the structure of the PM as illustrated in, for example, clathrin-mediated endocytosis (CME).

CME is important for the uptake of specific cargo proteins in and at the PM and their subsequent transport to other cellular destinations. This cellular process requires multiple cargo adaptors, accessory proteins and membrane remodeler being orchestrated in a supra-molecular network. In a first step, adaptor proteins are recruited to the cytoplasmic periphery of the PM. They interact with their respective PM-localized cargo proteins initiating clathrin binding and polymerization to a clathrin cage (Kirchhausen 2000). At this stage, the membrane forms a vesicle but is still connected to the PM. The GTPase dynamin surrounds the neck of the vesicle and triggers fission whereupon the clathrin cage dissociates.

It is highly debated how the described membrane curvature is generated during formation of vesicles. Intrinsically, lipid bilayers exhibit high elasticity. Therefore, shaping of membranes requires active mechanisms (McMahon et al. 2015). In context of CME, the insertion of Epsin1 at the cytoplasmic leaflet of the PM causes curvature by increasing the occupied area in the leaflet (Ford et al. 2002). However, mere crowding of Epsin1 without the insertion capacity already bends the lipid bilayer in artificial lipid vesicles (Stachowiak et al. 2012). Furthermore, Epsin1 was shown to interact with actin likely creating mechanical forces that pull the vesicular membrane away from the PM (Messa et al. 2014).

Overall, monitoring the formation of vesicles appears to be technically elusive due to the complex network of necessary adaptor proteins and mechanical forces. Cell free systems closely related to the natural environment were established to tackle this problem (Wu et al. 2012) and were e.g. applied to unravel a regulatory mechanism for the size of internalized membrane fragments during endocytosis (Wu et al. 2010).

1.3.3 Challenges for studying the cytoplasmic PM periphery

As expounded in the last chapter, the cytoplasmic zone of the PM is a highly crowded place. Multiple cellular processes are implemented by supra-molecular assemblies, such as signal processing into the cytosol, modulation of cell shape and motility, exo- and endocytosis and the connection to other organelles. Interactions within the supra-molecular

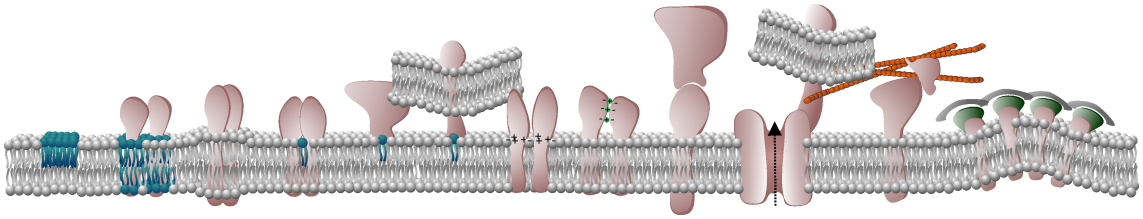

Figure 1.7: **Complex network of interactions influence the cytoplasmic periphery of the PM.** Interactions within the hydrophobic core of the PM (see figure 1.4), lipid-protein interactions at the cytoplasmic periphery (see figure 1.5) and protein-protein interactions (see figure 1.6) build up a complex network of supra-molecular structures at the cytoplasmic periphery of the PM. Their mutual dependency challenges the technical approach and call for integrative experimental systems.

structures are complex and always require multiple layers of the introduced interactions, which mutually depend on each other (figure 1.7).

Those mutual dependencies challenge the investigation of the cytoplasmic periphery of the PM both on the technical level as well as on the level of interpreting the findings. The major difficulties are hereby the combination of hydrophobic and hydrophilic environments, the impeded accessibility in contrast to the outer periphery of the PM and the "crosstalk" between the PM and the remainder of the cell.

The first attempts to study proteins and lipids at the inner side of the PM were conducted in red blood cells. Unlike other eukaryotic cells, they lack organelles or a nucleus. Thus, their PM can be easily isolated without contaminations of other intracellular membranes (Alberts et al. 2002). Homogenization and resealing of the resulting "ghosts" generates a population of vesicles where the inner leaflet points to the outside (Steck et al. 1970). This opens up the possibility to access the inner surface of the PM and to investigate orientation and arrangement of PM proteins (Steck 1974). It further lead to the recognition that lipids are asymmetrically distributed among the two membrane leaflets (Kahlenberg et al. 1974).

Detergent-based solubilization of PM components

Necessary prerequisite for proteins to be embedded in the hydrophobic core of the membrane is the exposure of hydrophobic amino acids to the lipid interface. Purification and structural analysis of membrane proteins and their complexes therefore often involve the usage of detergents. Those amphiphilic molecules can provide a membrane mimicking environment and prevent hydrophobic protein parts from aggregation. Membrane solubilization with the detergent Triton X-100 at 4°C followed by density gradient centrifugation extracts detergent-resistant membrane (DRM) parts. These DRMs were found to be en-

riched in SM and cholesterol and were closely connected with membrane rafts for a long time (see section 1.3.1). Proteins associated to DRMs were claimed to partition in lipid rafts in intact cells. However, detergents themselves are in principle able to induce ordered and detergent-resistant domains in lipid bilayers and that behavior could be confounded with natural partitioning of the PM (Heerklotz 2002). Comparative analysis of raft partitioning in giant lipid vesicles and DRM revealed that only a third of the investigated proteins partitioned into the ordered lipid phase in vesicles, whereas they separated entirely into the DRMs upon TritonX-100 solubilization (Kahya et al. 2005). Therefore, the application of detergents cannot be seen as an appropriate and reliable method to extract sub-partitions of the PM.

Mechanical PM extraction

To prevent the usage of detergents, several PM purification protocols based on mechanical forces have been established. Most of those protocols rely on mechanical cell disruption and subsequent differential centrifugation to separate the PM from intracellular membranes according to their respective density. However, such membrane purification protocols achieve accessibility to the inner part of the PM at the expense of PM integrity. The extracted components can be analyzed and interactions with covalent or strong interacting partners can be detected. However, it is challenging to investigate supra-molecular structures that are held together by weak and transient interactions or that are susceptible to membrane curvature and integrity.

Cell unroofing for PM extraction

An option for the detergent free extraction of the PM that partly preserves membrane integrity is the sheeting technique (see figure 1.8). With this technique a short ultrasound pulse is applied to adherent cells, which decapitates cells and therefore causes the physical abrasion of cytoplasmic structures (Heuser 2000). The resulting planar membrane sheets, henceforth referred to as PM sheets, offer accessibility to the cytoplasmic as well as to the extracellular periphery of the PM. The preparation is simple and applicable to a large set of cells with the prerequisite of cell attachment to a surface suitable for imaging.

Cell unroofing ceases exchange of the PM and the cytosol and thereby simplifies the experimental system. The technique has been applied for the investigation of supra-molecular structures at the cytoplasmic periphery of the PM. Namely, it was used to resemble formation of clathrin-coated pits (Moore et al. 1987), which lead to the conclusion that there are limited pit assembly sites on the PM and that the assembly is independent

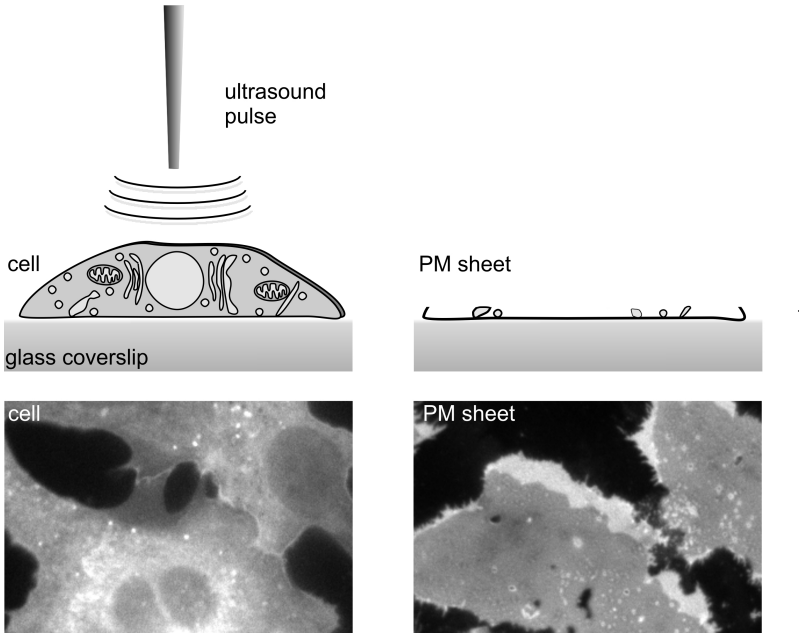

Figure 1.8: **Cell unroofing for PM extraction.** Illustration of cell unroofing technique. A short ultrasound pulse is applied to adherent cells, which removes major parts of cytosolic structures as well as the apical membrane. The resulting planar PM sheets offer accessibility to the cytoplasmic periphery of the PM and allow for high signal-to-noise imaging in epifluorescence microscopy. *Lower panel*: Cells (*left*) and PM sheets (*right*) stained with a fluorescent membrane marker.

of ATP. A similar experimental system of PM sheets was used to identify the involvement of tubular endocytic intermediates in endocytosis (Wu et al. 2010) (see section 1.3.2.2). Furthermore, PM sheets in combination with high resolution microscopy were used to quantitatively describe a protein cluster in terms of physical dimensions and molecule number (Sieber et al. 2007).

Microscopic examination of the PM

Most of the supra-molecular structures at the cytoplasmic side of the PM involve sensitive lipid-lipid or lipid-protein interactions. To investigate the structures and the underlying processes, the experimental system needs to contain necessary interaction partners in the cytoplasmic periphery and in the hydrophobic core of the membrane. Thus, application of microscopic methods increasingly gained ground in this field, because it enables the preservation of the natural surroundings and at the same time provides important spatial as well as temporal resolution.

The major difficulty in the investigation of the PM and its proximal environment by fluorescence microscopy is the intracellular fluorescence that conceals fluorescent signals from structures at the PM. To overcome these obstacles, several microscopic methods have been developed additional to the aforementioned mechanical PM dissection.

For example in confocal microscopy, a pinhole in front of the detector diminishes out-of-focus light which results in the detection limited to light from the focal spot. Thereby, the restricted detection of a planar section of about 500 nm to 1 µm thickness allows for spatial selection. Total internal reflection fluorescence (TIRF) microscopy permits even smaller depth discrimination, which, in contrast to confocal microscopy, occurs through selective illumination. Total reflection of a laser on the oil-water interface generates an evanescent wave that protrudes only about 100 nm into the cytosol and selectively excites fluorophores at the basal PM (Steyer et al. 2001). TIRF microscopy was used, for instance, for the first recording of single synaptic vesicles in docking and fusion with the PM (Zenisek et al. 2000).

High-resolution imaging

Despite the improvement concerning out-of-focus light, confocal and TIRF- microscopy are still subjected to the diffraction limited resolution, which depends on the numerical aperture of the system and the wavelength of imaging. In standard setups of fluorescence microscopes, this limit usually exceeds 200 nm. However, some of the supra-molecular structures of the PM are smaller and thus appear in a blurry fluorescence spot lacking detailed structural information on the distribution of their components. To overcome the diffraction limit, high resolution microscopy techniques were developed mainly in the last two decades such as photo-activated localization microscopy (PALM), stochastic optical reconstruction microscopy (STORM) and stimulated emission depletion (STED) mircoscopy.

PALM/STORM resorts to stochastic detection of individual fluorophores in sequential imaging frames. From each image the localization of single signals can be calculated by the point spread function. Superimposition of these localization maps reveals images at 2 - 25 nm resolution (Betzig et al. 2006).

In STED, stimulated depletion is used to transfer molecules in a non-fluorescent state by a donut-shaped laser of high intensity (see figure 1.9). This de-excitation laser superimposes the excitation laser leaving only the fluorescence from the center of the spot. With this technique, resolution of less than 40 nm can be achieved in recent setups (Vicidomini et al. 2011).

Both methods were implemented successfully in the investigation of supra-molecular structures at the PM periphery. A high-speed version of PALM (hsPALM), for example, was used to characterize the PM distribution of the T cell receptor clusters in relation to those of an adaptor protein important for signal transduction (Lillemeier et al. 2010). A

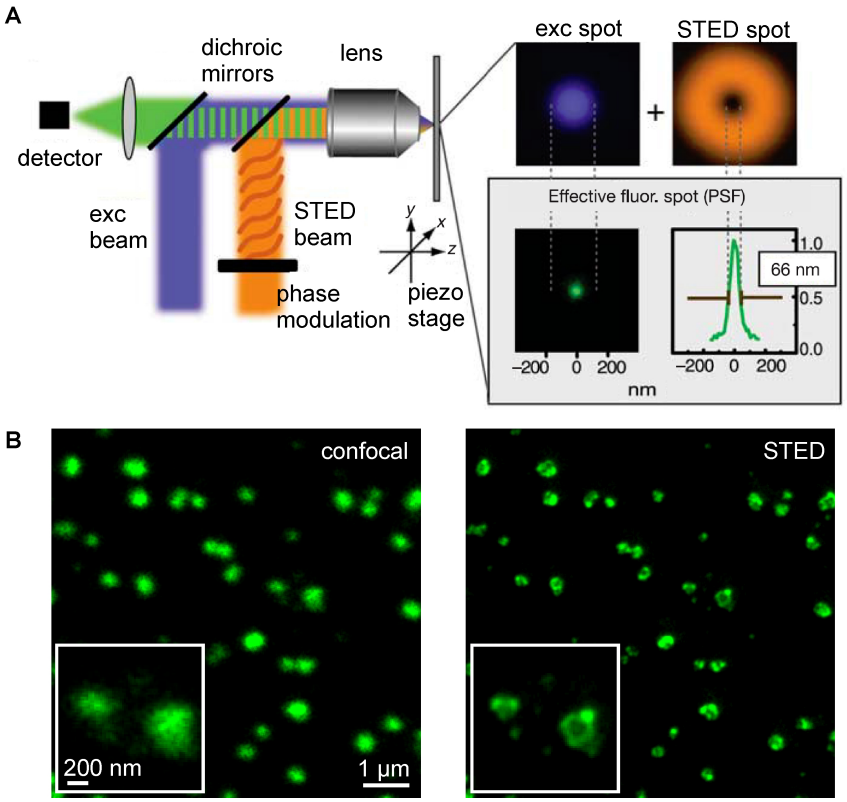

Figure 1.9: **STED microscopy. A** Schematic illustration of STED principle. The STED beam (depicted in orange) de-excites fluorophores via stimulated emission. A phase modulator generates the doughnut-shaped form of the STED laser, which superimposes the diffraction-limited excitation spot (depicted in blue). This confines the fluorescence emission to the center of the doughnut, which is narrower than the excitation spot. Image modified from Willig et al. 2006. **B** Comparison of images obtained in confocal (*left*) and STED (*right*) mode of a clathrin immunostaining on fixed PM sheets from mouse embryonic fibroblasts (kindly provided by Martina van Uelft).

spatial resolution of roughly 25 nm enabled to observe that previously separated clusters of T cell receptor and the adaptor protein merge upon activation. Further, the combination of STED and fluorescence correlation spectroscopy has proven useful in the investigation of lipid dynamics within the natural surroundings of the PM (Eggeling et al. 2009). Intriguingly, this technique is able to distinguish strong and specific lipid-protein interactions (see section 1.3.1) from lipid phase-mediated interactions (see section 1.3.1) in live cells (Mueller et al. 2011).

Tackling supra-molecular structures at the PM periphery

In conclusion, the investigation of the cytoplasmic periphery of the PM is challenging due to the combination of hydrophilic and hydrophobic environments and the lack of direct accessibility.

Biochemical extraction methods of the PM are helpful for the quantification of explicit components or the identification and analysis of strong and/or permanent interactions.

Similarly, artificial lipid systems such as liposomes or supported lipid bilayers can be used to reconstitute and examine specific interactions. These simplified experimental systems have been proven particularly useful in the discovery of lipid phases (section 1.3.1).

However, supra-molecular structures are often mediated by a complex network of interactions involving weak and transient protein-protein, lipid-lipid and protein-lipid interactions. Complexes therefore tend to disintegrate upon isolation. Furthermore, the single components show differential needs in purification due to different proportions of hydrophobic and hydrophilic domains. Even more important in this context is the mutual dependency of interactions as pictured in section 1.3.2.

Experimental approaches such as the above displayed microscopy methods and the sheeting technique bear the potential to overcome these obstacles since they are able to capture the natural cellular environment. In addition, they provide sufficient spatial and temporal resolution for the direct visualization as well as open up the possibility to investigate anatomy and function of supra-molecular structures in the cytoplasmic periphery of the PM.

2 Aim of the study

The cytoplasmic periphery of the PM is a zone of utmost importance for all cells. Communication with the surrounding or metabolic maintenance are only few examples of the diverse biological processes implemented in this cellular region. The distinct functions are thereby fulfilled in specific microenvironments that are created by the formation of supra-molecular structures. Their organization is accomplished by a complex network of interactions of lipids and proteins that rely on an intact membrane environment. The investigation of this cellular region thus appears technically challenging and demands the integration of hydrophobic and hydrophilic surroundings.

In this study I aimed to explore PM sheets in combination with modern imaging and lipid labeling techniques to obtain a better understanding of supra-molecular structures at the cytoplasmic periphery of the PM in terms of i) structural and ii) functional aspects.

i) The first aim of the study was to investigate the influence of cytoplasmic protein-protein interactions on the inner architecture of a membrane protein cluster using the syntaxin cluster as an example.

ii) For the functional characterization of a supra-molecular structure I chose a more complex assembly integrating lipid-protein and protein-protein interactions between two different cellular membranes: ER-PM membrane contact sites.

3 Materials and Methods

3.1 Materials

Standard chemicals and reagents used in this study were purchased from *Carl Roth* (Karlsruhe, Germany), *Sigma Aldrich* (Hamburg, Germany), *AppliChem* (Darmstadt, Germany), *Merck* (Darmstadt, Germany), *Thermo Fisher Scientific*, formerly *Life Technologies*, (Waltham, USA) unless stated otherwise. All consumables for cell culture were obtained from *Sarstedt* (Nümbrecht, Germany), other consumables were from *Carl Roth* (Karlsruhe, Germany), *VWR* (Darmstadt, Germany), *Labomedic* (Bonn, Germany), *Eppendorf* (Hamburg, Germany), or *Bio-Rad* (Munich, Germany). Glass coverslips for microscopy were purchased from *Marienfeld* (Lauda-Königshofen, Germany). Cell culture media and reagents were obtained from *PAN Biotech* (Aidenbach, Germany) and *Biochrom* (Berlin, Germany).

3.1.1 Technical devices

3.1.1.1 Appliances

Table 3.1: Appliances

Instrument	Name/Manufacturer	Application
Microplate reader	Infinite® 200 PRO multimode microplate reader (*Tecan*, Maennedorf, Switzerland)	determination of protein concentration by bicinchoninic acid assay (BCA)
Imaging system	Odyssey® CLx Imaging System (*LI-COR Inc.*, Lincoln, USA)	western blot imaging
Thermocyclers	TPersonal and TProfessional basic gradient(*Biometra*, Goettingen, Germany)	polymerase chain reaction (PCR)
Spectrophotometer	NanoDrop2000 (*Thermo Fisher Scientific*, Waltham, USA)	DNA concentration measurements
Bright-field microscope	Inverted microscope ECLIPSE TS100, CFI60 Infinity Optical System (*Nikon*, Tokyo, Japan)	cell culture

3.1.1.2 Microscopes

Epifluorescence/total internal reflection fluorescence (TIRF) microscopes: For epifluorescence microscopy, an inverted Olympus IX81-ZDC fluorescence microscope with a 60x 1.49 NA or a 10x 0.4 NA apochromat objective (*Olympus*) was used with additional magnification (1.6x and 2x or 4x). A MT20E illumination system (*Olympus*) with a 150 W xenon lamp and the filter sets DAPI HC (F36-500), EGFP HC (F36-525), TRITC HC (F36-503) and Cy5 ET (F46-009) (*AHF Analysentechnik*, Tuebingen, Germany) were used for fluorescence excitation and detection. For imaging, a 16 bit EMCCD camera (ImagEM C9100-13, *Hamamatsu Photonics*, Hamamatsu, Japan) with 512 x 512 pixels (16 µm x 16 µm pixel size) was coupled with the microscope. For imaging in TIRF mode, a 488 nm Argon-Laser (LAS/488/20, *Olympus*) in combination with a CMR-U-MTIR-488-HC filter set (*Olympus*) was used. The microscope was controlled via the CellR® (*Olympus*) software.

Additionally, an Axio Observer D1 epifluorescence microscope (*Zeiss*, Jena, Germany) was used, equipped with a Plan-Apochromat 100x/NA 1.4 oil immersion objective (*Zeiss*), a N XBO 75 (75 W xenon arc lamp) (*Zeiss*), a 12 bit CCD Seniscam QE camera with 1376 × 1040 pixels (6.45 µm x 6.45 µm pixel size) (*PCO*, Kelheim, Germany). Following filter sets were used for imaging: UV filter set (F11-000), EGFP HC filter set (F36-525), TRITC HC filter set (F36-525), Cy5 HC filter set (F36-523) (*AHF Analysentechnik*). For operation of the microscope the CamWare software (*PCO*) was employed.

Confocal laser scanning microscope: For confocal microscopy, an inverted Olympus FluoView™ FV1000 (*Olympus*) was employed. The microscope was equipped with an oil immersion objective UPlanSApo 60x NA 1.35 (*Olympus*), 405, 488 and 543 nm lasers and a climate chamber (*Evotec*, Hamburg, Germany). The microscope was controlled by the Fluoview 3.0 software (*Olympus*).

Stimulated emission depletion (STED) microscopes: STED microscopy was performed partly on a TCS SP8 gated-STED microscope (*Leica*, Mannheim, Germany) equipped with a 100x 1.4 NA oil immersion objective, a pulsed white-light laser for fluorescence excitation and a 592 nm continuous wave (CW) laser for STED and hybrid detectors (HyD) (*Leica*). The microscope is located at the Light Microscopy Facility of the German Centre for Neurodegenerative Diseases (DZNE) in Bonn.

Further STED microscopy was performed on an easy3D STED microscope (*Abberior Instruments*, Göttingen, Germany) equipped with an UPlanSApo 100x/NA 1.4 oil immer-

sion objective (*Olympus*), a UPlanApo 60x/NA 1.2 water immersion objective (*Olympus*), pulsed excitation lasers (485 nm, 518 nm, 561 nm, 640 nm; *Abberior Instruments*), a pulsed 775 nm STED laser (*MPBC*, Montreal, Canada), filter sets (500 - 520 nm, 532 - 558 nm, 580 - 630 nm, 650 - 720 nm; *Abberior Instruments*), and single photon counting modules as detectors (*Excelitas*, Waltham, USA). The microscope was controlled by the Imspector software (*Abberior Instruments*).

3.1.2 Buffers and solutions

All buffers were prepared with fully desalinated or deionised water and autoclaved or sterile filtered when necessary.

Table 3.2: Buffers and solutions

Name	Composition/Preparation
Phosphate buffered saline (PBS)	137 mM NaCl, 2.7 mM KCl, 1.76 mM KH_2PO_4, 10 mM Na_2HPO_4, pH 7.4
Sonication buffer	20 mM HEPES-KOH, 120 mM potassium glutamate, 20 mM potassium acetate and 10 mM EGTA, pH 7.2
HEPES/KCl	140 mM KCl, 20 mM HEPES-KOH, pH 7.2
HEPES/KCl/EGTA	140 mM KCl, 20 mM HEPES-KOH, 10 mM EGTA, pH 7.2
Ringer solution for FRAP	130 mM NaCl, 4 mM KCl, 1 mM $CaCl_2$, 1 mM $MgCl_2$, 48 mM D(+)glucose, 10 mM HEPES-NaOH, pH 7.4.
Ringer solution for TG stimulation	155 mM NaCl, 4.5 mM KCl, 2 mM $CaCl_2$, 1 mM $MgCl_2$, 10 mM D(+)glucose, 5 mM HEPES-NaOH, pH 7.4. For a calcium free Ringer solution, $CaCl_2$ was exchanged for $MgCl_2$ yielding 3 mM $MgCl_2$ in total.
Tris-Acetat-EDTA (TAE) buffer	40 mM Tris, 1 mM EDTA and 0.11% (v/v) acetic acid
Poly-L-Lysine (PLL) stock solution (20x)	2 mg/mL PLL (*Sigma Aldrich*, # P1524) in ddH_2O
4xLaemmli	8% (w/v) SDS, 40% (w/v) glycerol, 0.008% (w/v) bromophenol blue, 0.25 M Tris HCl, pH 6.8; shortly before usage 20% (v/v) β-mercaptoethanol was added to gain complete 4x solution.
Sodium dodecyl sulfate (SDS) running buffer	25 mM Tris, 0.1 % (w/v) SDS, 192 mM glycin
Towbin buffer	25 mM Tris, 192 mM glycine, 20% (v/v) methanol

Table 3.2 – *Continued from previous page*

Name	Composition/Preparation
Paraformaldehyde (PFA) solution	For a PFA stock solution, water was heated to 55 °C. Then the appropriate amount of PFA was added for a 16% (w/v) solution and stirred with addition of a few drops of a 1 M NaOH until the solution became clear. Aliquots of this solution were kept at -20°C for a medium-term storage. For the fixation of cells and PM sheets, the stock solution was diluted with water and 10x PBS to gain a 4% PFA in 1x PBS.

3.1.3 Culture media and reagents

Table 3.3: Culture media and reagents

Medium/Reagent	Composition/Supplier
HepG2 growth medium	MEM Eagle (*PAN Biotech*, # P04-08509) supplemented with 10% (v/v) fetal calf serum (FCS) (*Biochrom*, # S0615), 2 mM stable glutamine (*PAN Biotech*, # P04-82100) and 1% (v/v) penicillin/streptomycin (*PAN Biotech*, # P06-07100)
PC12 growth medium	DMEM (*PAN Biotech*, # P04-03550) supplemented with 5% (v/v) FCS, 10% (v/v) horse serum (*Biochrom*, # S9135) and 1% (v/v) penicillin/streptomycin
Jurkat growth medium	RPMI 1640 (*Invitrogen*, # 21875091) supplemented with 10% (v/v) FCS and 1% (v/v) penicillin/streptomycin
Dulbecco's PBS (DPBS)	Dulbecco's PBS without Ca^{2+} and Mg^{2+} (*PAN Biotech*, # P04-36500)
Trypsin	Trypsin (0,05 %) with 0,02 % EDTA in PBS, without Ca^{2+} and Mg^{2+} (*PAN Biotech*, # P10-0231SP)
LB medium	10 g/L tryptone, 5 g/L yeast extract, 5 g/L NaCl, purchased as complete powder from *Carl Roth* (Karlsruhe, Germany), for plates medium was supplemented with 2 % (w/v) agar-agar

3.1.4 Cell lines

HepG2 cells: HepG2 cells are human liver hepatocellular cells isolated from a hepatoblastoma. For this study they were purchased from *CLS*, Eppelheim, Germany, (# 300198). Cells were passaged every three to four days and used for experiments until a maximum passage number of 30.

PC12 cells: PC12 cells are rat pheochromocytoma cells obtained by radiation of adrenal gland cells. Cells were a kind gift of Rolf Heumann, Ruhr University Bochum and are similar to clone 251 described in Heumann et al. 1983. Every three to four days, cells were passaged and used for experiments until a maximum passage number of 30.

Jurkat cells: Human leukemic T cell lymphoblast cell line Jurkat E6.1 was obtained from *ECACC Generel Collection* (# 88042803). Suspension cell culture was diluted to 2 x 10^5 cells per mL every three to four days and used until a maximum passage number of 35.

3.1.5 Antibodies

3.1.5.1 Primary antibodies

Table 3.4: Primary antibodies, IF: immunofluorescence; WB: western blot

Target	**Host species**	**Supplier/ Catalogue number**	**Application/ (dilution)**
Syntaxin 1A (HPC1)	mouse	*Sigma*, # S0664	IF (1:200)
Myc-tag	mouse	*ThermoFisherScientific*, # MA1-21316	IF (1:200 - 1:400) WB (1:1000)
Clathrin	goat	*Santa Cruz*, # sc-6579	IF (1:200)
Caveolin	rabbit	*abcam*, # ab2910	IF (1:200)
Pan-cadherin	mouse	*Santa Cruz*, # sc-59876	WB (1:1000)
GRP78	rabbit	*abcam*, # 21685	WB (1:1000)
GFP	rabbit	*abcam*, # ab290	IF (1:200) WB (1:1000)
RFP	rabbit	*Rockland*, # 600-401-379	WB (1:1000)
Transferrin receptor	rabbit	*Abcam*, # ab84036	WB (1:1000)

3.1.5.2 Secondary antibodies

Table 3.5: Secondary antibodies, IF: immunofluorescence; WB: western blot

Target species	Host species	Coupled fluorophore	Supplier/ Catalogue number	Application/ (dilution)
goat	rabbit	CF™647	*Biotium*, # 20049	IF (1:200)
rabbit	goat	Alexa Fluor®647	*ThermoFisherScientific*, # A21245	IF (1:200)
mouse	goat	Alexa Fluor®488	*ThermoFisherScientific*, # A11001	IF (1:200)
mouse	goat	Atto647N	Sigma, # 50185	IF (1:200)
mouse	goat	Alexa Fluor®647	*ThermoFisherScientific*, # A-21235	IF (1:200)
rabbit	goat	IRDye®800CW	*LI-COR*, # 926-32211	WB (1:10000)-(1:15000)
mouse	goat	IRDye®800CW	*LI-COR*, # 926-32210	WB (1:5000)-(1:8000)

3.1.6 Plasmids

Table 3.6: Plasmids

Name	Origin	Plasmid backbone / Tag	Comment
pmEGFP-N1	*Clontech*, Mountain View, USA; GenBank No.: U55761	pEGFP-N1 / C-terminal EGFP	EGFP carries a mutation to abolish GFP dimerization (Zacharias et al. 2002); from Sieber et al. 2006
RFP-Sec61β	kindly provided by Lars Kürschner (Kuerschner et al. 2005)	pmRFP / N-terminal RFP	integral ER protein used for identification of ER on PM sheets
PH-GFP	*Addgene*, No.: 21179, Stauffer et al. 1998	pEGFP-C1 / N-terminal GFP	PH domain of PLCdelta for $PI(4,5)_2$ binding
YFP-STIM1	kindly provided by Barbara Niemeyer (Kilch et al. 2013)	pEXP1 / N-terminal YFP	
mRFP-GL-GPI	kindly provided by Lars Kürschner	pmRFP / mRFP	N-terminal signal sequence of rabbit lactase phlorizin hydrolase, C-terminal N-glycosylation site and GPI attachment signal

Table 3.6 – *Continued from previous page*

Name	**Origin**	**Plasmid backbone / Tag**	**Comment**
GFP-SNAP25	Halemani et al. 2010	pmEGFP-C1 / N-terminal mEGFP	rat SNAP-25B (NP112253.1)
BoNT/C1/LC-GFP	Raj Halemani	pmEGFP-N1 / C-terminal mEGFP	light chain of botulinum neurotoxin C1 from Zilly et al. 2006
pDL208 (AUP1-3myc)	kindly provided by AG Thiele (Lohmann 2013)	pcDNA 3.1Hygro(+) / C-terminal triple myc tag	used for cloning of syntaxin with C-terminal triple myc tag
VAMP8-mCherry	kindly provided by Jens Rettig (Marshall et al. 2015)	pC1-EGFP / C-terminal mCherry	used for cloning of VAMP8-GFP
syntaxin-GFP	from Sieber et al. 2006	pmEGFP-N1 / C-terminal mEGFP	corresponding to Sx1A-GFP in Sieber et al. 2006
syx-ΔCyt-GFP	from Sieber et al. 2006	pmEGFP-N1 / C-terminal mCherry	corresponding to TMR-GFP in Sieber et al. 2006
myc-syntaxin	from Sieber et al. 2007	pBob5.1 (Schütz et al. 2005) / N-terminal myc tag	
IPP-CaaX	kindly provided by Silvio Rizzoli, from Malecz et al. 2000	pcDNA3.1 / N-terminal mRFP	used for cloning of syntaxin-Caax and syx-ΔS-CaaX
syx-ΔS-GFP	E. Merklinger	pmEGFP-N1 / C-terminal mEGFP	syntaxin 1A-(1-192 + 218-288) with C-terminal linker LVPRARDPPVAT as in Sieber et al. 2006
syntaxin-myc	E. Merklinger	pDL208 / C-terminal triple myc tag	syntaxin 1A-(1-288) with C-terminal linker LV PRARDPPVATSRG
syx-ΔS-myc	E. Merklinger	pDL208 / C-terminal triple myc tag	syntaxin 1A-(1-192 + 218-288) with C-terminal linker LVPRARDPPVATSRG
syx-ΔCyt-myc	E. Merklinger	pDL208 / C-terminal triple myc tag	syntaxin 1A-(1-28 + 259-288) with C-terminal linker LVPRARDPPVATSRG

Table 3.6 – *Continued from previous page*

Name	Origin	Plasmid backbone / Tag	Comment
syntaxin-myc-IRES	E. Merklinger	pmEGFP-N1 / C-terminal triple myc tag	syntaxin 1A-(1-288) with C-terminal linker LV PRARDPPVATSRG
syx-ΔS-myc-IRES	E. Merklinger	pmEGFP-N1 / C-terminal triple myc tag	syntaxin 1A-(1-192 + 218-288) with C-terminal linker LVPRARDPPVATSRG
syx-ΔCyt-myc-IRES	E. Merklinger	pmEGFP-N1 / C-terminal triple myc tag	syntaxin 1A-(1-28 + 259-288) with C-terminal linker LVPRARDPPVATSRG
myc-syntaxin-CaaX	E. Merklinger	pcDNA3.1 (IPP-CaaX) / N-terminal myc tag	syntaxin1A-(1-258)-AAAKSKTKCVIM
myc-syx-ΔS-CaaX	E. Merklinger	pcDNA3.1 (IPP-CaaX) / N-terminal myc tag	syntaxin 1A-(1-192 + 218-258)-AAAKSKTKCVIM
VAMP8-GFP	E. Merklinger	pmEGFP-N1 / C-terminal mEGFP	

3.1.7 Kits

Kits were used according to the manufacturer's instructions.

NucleoSpin Gel and PCR clean-up® *Macherey und Nagel*, Düren, Germany, # 740609

NucleoSpin Plasmid® *Macherey und Nagel*, # 740588

NucleoBond Xtra Midi® *Macherey und Nagel*, # 740410

Pierce™ BCA Protein Assay Kit *Thermo Fisher Scientific*, # 23225

Neon™ Transfection System 100 µL **Kit** *Thermo Fisher Scientific*, # MPK10096

3.1.8 Software

All instruments (see table 3.1) were controlled by the software provided by the manufacturer. Other software used is listed in table 3.7.

Table 3.7: Software

Software	**Supplier**	**Application**
CorelDraw X4	*Corel*	preparation of figures and illustrations
ImageJ (MBF and Fiji bundle)	developed by *Wayne Rasband* (NIH)	image analysis
MSExcel	*Microsoft corporation*	data analysis and organization
SigmaPLot 11.0	*Systat software GmbH*	data plotting
OriginPro 8G	*OriginLab*	data analysis and organization
ApE	developed by *Wayne Davis*	DNA sequence editor
MiKTeX2.9	developed by *Christian Schenk*	typesetting
Texmaker	developed by *Pascal Brachet* and *Joel Amblard*	typesetting

3.2 Methods

All experiments were carried out at room temperature, unless stated otherwise.

3.2.1 Cloning

Cloning was performed following the standard methods described in Sambrook et al. 2001. Enzymes for cloning were purchased from *NEB*, Ipswich (MA), USA and were used with the accompanied buffers and according to the manufacturer's instructions. DNA amplification via polymerase chain reaction (PCR) was performed with a Q5® High-Fidelity DNA polymerase (*NEB*, # M0491S). Plasmids used as templates for cloning PCR or as target vectors after amplification are listed in table 3.6. Primers for PCR were designed manually and purchased from *MWG-Biotech*, Ebersberg, Germany. The optimal annealing temperatures for PCR reaction was calculated using the NEB Tm calculator tool ([1]). By default, plasmids were dephosphorylated after restriction digest using an antarctic phosphatase (*NEB*, # M0289S) prior to ligation with T4 ligase (*NEB*, # M0202T).

[1] http://tmcalculator.neb.com/

E.coli XL10-Gold® (*Stratagene*, San Diego, USA, # 200314) were transformed with ligated plasmids for plasmid amplification. Bacteria were selectively grown in LB medium containing the antibiotics kanamycin or carbenicilin (analogue of ampicilin) depending on the antibiotic resistance encoded by the inserted plasmid. Kanamycin or carbenicilin were used at a concentration of 50 µg/mL or 100 µg/mL, respectively, for liquid LB cultures and plates.

Screening for successful cloning was performed by colony PCR employing an OneTaq® DNA polymerase. Alternatively, a restriction digestion of purified plasmids was performed. All constructs were finally verified by sequencing (*GATC*, Konstanz, Germany).

All syntaxin constructs are based on the sequence of rat syntaxin 1A (NP_446240.2). For obtaining syx-ΔS (syntaxin 1A-(1-192 + 218-288)) either for C-terminal GFP or triple-myc tagging, a two-step fusion PCR was performed. For deletion of the part corresponding to the n-SNARE domain, an overlapping primer pair was designed containing 10 bases before and 11 bases behind the requested deletion. Sequences of those two primers are CGAAGCAGGCCATGGCCATGC (forward syx-ΔS) and GCATGGCCATGGCCTGCTTCG (reverse syx-ΔS). In the first PCR step, two parts of syntaxin were amplified using either of two fusion primers in combination with appropriate forward or reverse primers carrying specific restriction sites. PCR reactions were subjected to agarose gel electrophoresis, the two syntaxin parts were extracted from the gel and a mixture of both was used as a template for the second joining PCR step.

For generating syx-ΔS-GFP, syntaxin-GFP (see table 3.6) was used as a template in the first step of the two-step fusion PCR. After the second joining PCR step, the restriction sites NheI and NotI were used for insertion of the PCR product into the backbone of the expression vector pmEGFP-N1 (see table 3.6).

For the myc-tag syntaxin variants, syntaxin-GFP and syx-ΔCyt-GFP were used as templates. Both constructs contain the C-terminal linker LVPRARDPPVATSRG (Sieber et al. 2006), which was crucial for staining of the C-terminal myc tag (data not shown). Amplification was performed as a single step PCR for syntaxin and syx-ΔCyt and as a two-step fusion PCR (see above) for syx-ΔS, generating PCR products with HindIII and XbaI restriction sites for insertion into the vector. As a target vector pDL208 was used (see table 3.6), from which AUP1 was cut out beforehand using HindIII and XbaI restriction sites.

For the IRES fusion constructs, three parts were inserted via PCR into the pmEGFP-N1 vector, where the mEGFP was cut out beforehand: (i) the syntaxin variants with

a C-terminal linker and triple myc tag, (ii) an internal ribosome entry site (IRES2) of the encephalomyocarditis virus and (iii) a mRFP, N-terminally tagged with the signal sequence of rabbit lactase phlorizin hydrolase, and C-terminally fused to a consensus N-glycosylation site and a GPI attachment signal of LFA-3 (based on a mRFP-GL-GPI (see table 3.6). For insertion into the vector, the following restriction sites were used: EcoRI and XhoI for syntaxin constructs, SpeI for IRES, and SpeI and NotI for the mRFP-GL-GPI.

VAMP8-GFP was obtained by subcloning. To this end, VAMP8 was cut out from the vector VAMP8-mCherry (see table 3.6) using NheI and KpnI restriction sites and subsequently inserted into a pmEGFP-N1 (see table 3.6).

For myc-syntaxin-CaaX (MEQKLISEEDLNS- syntaxin1A-(1-258)-AAAKSKTKCVIM and syx-ΔS-CaaX (MEQKLISEEDLNS-syntaxin 1A-(1-192 + 218-258)-AAAKSKTKCVIM myc-syntaxin (see table 3.6) was used as a template for PCR (single step for syntaxin-CaaX and fusion PCR for syx-ΔS-CaaX). Restriction sites NheI and NotI were used to insert the PCR product into the target vector IPP-CaaX (see table 3.6), from which the mRFP tagged synaptojanin was cut out beforehand using NheI and NotI restriction enzymes.

3.2.2 Cell culture

All general cell culture procedures and transfections were performed under a sterile LaminarFlow cell culture hood (*BDK*, Sonnenbühl, Germany). Cells were cultivated at 37 °C and 5% CO_2 in a cell incubator (*Binder*, Tuttlingen, Germany).

3.2.2.1 General cell culture procedures

Thawing: Cryostocks of cells were instantly transferred into a 37 °C waterbath, thawed for 2 min and resuspended in pre-warmed cell specific medium. The cell suspension was centrifuged for 3 min at 200 g. The supernatant was discarded and the cell pellet resuspended in pre-warmed medium. Cells were transferred to a cell culture flask and were used for experiments two to four passages after thawing.

Freezing: For cryo-conservation of cells, cell suspensions were adjusted to 10^7 cells per mL freezing medium (70% (v/v) medium, 20% (v/v) FCS, 10% (v/v) dimethylsulfoxid (DMSO)). Aliquots of 1 mL cell suspension per cryo vial were transferred to a cryo-freezing container for slow reduction of temperature below −70 °C before storage in a liquid nitrogen tank.

Passaging: Adherent cells (HepG2 and PC12) were cultivated to a maximal confluency of 80% and passaged every 3 to 4 days. To do so, cells were briefly washed with PBS and incubated with trypsin for 3 - 5 min at 37 °C. To stop the protease activity, cell specific growth medium was added and the cell suspension of the detached cells was centrifuged for 3 min at 200 g. The supernatant was removed and cells were resuspended in the appropriate medium. Afterwards, cells were either counted for transfection (see below) or seeding to coverslips (see below) using a Neubauer chamber, or directly transferred to a new cell culture flask for further cultivation. For passaging of Jurkat cells, cells were counted and an appropriate amount of cells was transferred into a new flask to gain a concentration of 2 x 10^5 cells per mL.

3.2.2.2 Cleaning and coating of coverslips

For microscopy, cells were settled onto glass coverslips with a thickness of "0" (0.085 to 0.115 mm) or "1" (0.13 to 0.16 mm) for epifluorescence, TIRF and confocal microscopy. For STED microscopy, high precision coverslips (thickness "1.5H", 0.170 mm ± 0.005 mm) were used. For cleaning, the coverslips were consecutively incubated with agitation in 1 M HCl, in 1 M NaOH and in 100% ethanol for 1 h each. In between the incubation steps, coverslips were washed thoroughly in fully deionised water. After the last incubation step, ethanol was discarded and the coverslips were sterilized and dried at 180 °C. For coating, the coverslips were incubated for 30 min with 500 µL PLL solution per coverslip. The solution was removed, the coverslips were dried and subsequently sterilized by exposure to UV light for 20 min. Typically, 2 - 4 x 10^5 HepG2 cells, 5 x 10^5 PC12 cells and 1 x 10^6 Jurkat cells were settled onto one coverslip.

3.2.2.3 Transfection and transduction

The Neon® electroporation system was used for transfection of HepG2 cells according to the instructions of the manufacturer. In brief, the cells were detached from the culture flasks, counted and centrifuged. For each transfection, 1.5 - 3 x 10^6 cells were resuspended in 125 µL buffer R (*ThermoFisherScientific*) and mixed with 1 - 10 µg plasmid DNA. Subsequent transfection was conducted using a single 50 ms pulse at 1200 V. Transfected cells were transferred into antibiotics-free medium and cultivated for 24 h before the experiment. For visualization of ER on PM sheets, HepG2 cells were transduced with CellLight® ER-RFP, BacMam 2.0 (*ThermoFisherScientifc* formerly *Life Technologies* # C10591) according to the manufacturer´s instructions, adding 20 particles per cell for 16 h.

3.2.2.4 Cell lysis

During cell lysis all centrifugation steps were performed at 4 °C, all other steps on ice, if not stated otherwise. Transfected cells were rinsed three times with ice-cold DPBS. Then cells were carefully scraped off the bottom of the cell culture flask in ice-cold DPBS. The cell suspension was centrifuged for 3 min at 200 g, the cell pellet was resupended in RIPA buffer (Santa Cruz, # sc-24948) and incubated for 30 min at 4 °C. During this incubation, the cell containing solution was vortexed every 5 min for 10 s. Then, the lysate was incubated for another 5 min in an ultrasound bath followed by a centrifugation step for 15 min at 1.4 x 10^4 g. The supernatant was transferred to a new vial and its protein concentration was determined by BCA assay as triplicates in comparison to a standard curve obtained from different albumin concentrations in RIPA buffer. Samples were mixed with Laemmli buffer, boiled for 10 min at 95 °C and stored at −20 °C.

3.2.3 SDS-PAGE and western blot

Gels for SDS-polyacrylamide gel electrophoresis (PAGE) were either casted with a stacking and running gel containing 4% acrylamid / 0.11% bisacrylamid and 12% acrylamid / 0.32% bisacrylamid, respectively. Alternatively, gradient gels (4–20% Mini-PROTEAN® TGX™, *Bio-Rad*, Hercules, USA; # 4561094) were used. Samples in Laemmli buffer were loaded to the gel with 15 to 20 µg of total protein per lane. The gel was run in SDS running buffer for 20 min at 70 V and for additional 60 - 80 min at 110 V.

For transfer of proteins from the gel to a nitrocellulose membrane (*Carl Roth*, # HP40.1), a wet electroblotting system (*BioRad*) was employed. The transfer was performed in cold Towbin buffer at 100 V for 1 h. Afterwards, the membrane was rinsed with PBS and blocked for 1 h in Odyssey Blocking Buffer (*LI-COR Inc.*, # P/N 927-4000) 1:1 diluted with PBS. For staining of membranes with two different first antibodies, the membrane was cut prior to blocking. First antibody incubation was done over night at 4 °C in Odyssey Blocking Buffer with PBS/0.1% Tween20 (PBS-T) (1:1). The membrane was then washed four times for 5 min with PBS-T followed by incubation with the secondary antibody in Odyssey Blocking Buffer with PBS-T (1:1) for 1 h at RT. Finally, membranes were washed again four times with PBS-T for 5 min and three times with PBS for reduction of detergent concentration before imaging with the Odyssey imager at 150 dots per inch (dpi). The analysis of western blot images was performed using the "gel analyzer" option in ImageJ. Peak areas for each signal were related to the corresponding peak area of the loading control in the same lane.

3.2.4 PM sheets

3.2.4.1 Preparation of PM sheets

Coverslips with adhered cells were rinsed shortly with PBS and then transferred into ice-cold sonication buffer. The tip of a sonifier (Sonopuls HD 2070, *Bandelin*, Berlin, Germany) was placed into the solution and above the center of the coverslip at a distance of approximately 5 mm. A 100 ms pulse was applied at an intensity empirically determined for each cell line. PM sheets were either used in native condition or were directly fixed with 4% PFA in PBS for 30 - 45 min followed by quenching of the fixative with 50 mM NH_4Cl in PBS for 15 min.

3.2.4.2 Treatments of PM sheets

Phospholipase: Treatment with 0.25 U/mL phosphatidylcholine-specific phospholipase C (PC-PLC) from *Clostridium perfringens* (EC 3.1.4.3) (*Sigma-Aldrich*, # P7633) was performed on PM sheets from metabolically labeled cells in a buffer containing 250 mM Tris-HCl and 50 mM $CaCl_2$ (pH 7.2) for 1 h at 37 °C. After treatment, PM sheets were washed three times with PBS prior to cycloaddition.

HPαCD: For pPC transfer assay, freshly prepared sheets from metabolically labeled cells were incubated with 50 mM (2-hydroxypropyl)-α-cyclodextrin (HPαCD)(*Sigma-Aldrich*, # 390690) in sonication buffer for 30 min at 37 °C. Afterwards, PM sheets were washed two times with sonication buffer and once with PBS prior to cycloaddition reaction.

Cholesterol-MβCD: For loading with cholesterol, cells overexpressing RFP-Sec61β were sonicated and the PM sheets were incubated with 1.5 mM of a cholesterol-methyl-β-cyclodextrin (MβCD)(*Sigma-Aldrich*, # P4555)-complex in sonication buffer or only sonication buffer as a control for 10 min at 37 °C followed by three washing steps with sonication buffer. The Cholesterol-MβCD complex was obtained essentially as described in Klein et al. 1995. In brief, sonication buffer containing 10 mM MβCD was heated to 80 °C. Then 25 mM cholesterol solution in ethanol was added under vigorous stirring. This yielded a ratio of approximately 25 mg cholesterol per gram MβCD. Afterwards, the solution was sonicated for 15 min at 40 °C and subsequently centrifuged for 30 min at 20000 g. The supernatant was used for cholesterol loading of PM sheets.

Calcium: For treatment with calcium (figure 4.5), PM sheets from cells overexpressing myc-tagged syntaxin variants were prepared in ice-cold HEPES/KCl/EGTA buffer, briefly

washed with HEPES/KCl buffer and incubated for 10 min at 37 °C with 10 mM $CaCl_2$ in HEPES/KCl or with HEPES/KCl/EGTA as a control. Afterwards, PM sheets were directly fixed with 4% PFA and stained for the myc tag.

3.2.5 Staining and labeling for fluorescence microscopy

3.2.5.1 Immunostaining

Cells or PM sheets were fixed with 4% PFA in PBS for 30-45 min followed by quenching of the fixative with 50 mM NH_4Cl in PBS for 15 min. Samples were washed twice with PBS and blocked with 3% BSA in PBS for 1-2 h. Incubation with the first antibody (1st AB) and secondary antibody (2nd AB) was performed in 3% BSA in PBS. Incubation times are summarized in table 3.8. Both antibody incubation steps were followed by three washing steps with PBS for 5 min. Samples were either directly imaged or stored over night at 4 °C in PBS prior to imaging. In the case of 2D STED, samples were embedded with ProLong® Gold antifade mountant (*ThermoFisherScientific*, # P10144) on microscopy slides, sealed with colorless nail polish and stored at 4 °C.

Table 3.8: Immunostainings; o/n : over night; AB: antibody

Antibody	**Experiment/Figure**	**Incubation time 1st AB**	**Incubation time 2nd AB**	**2nd AB conjugate**
α-myc-tag	BoNT/C1/LC coexpression / figure 4.6	1.5 h at RT	1 h at RT	Atto-647N
α-myc-tag	comparative Epi-Western / figure 4.10	o/n at 4°C	1.5 h at RT	Alexa-488
α-myc-tag	pulsed STED / figures 4.2 and 4.3	o/n at 4°C	2 h at RT	Atto-647N
α-myc-tag	CW-STED / figure 4.2	24 h at 4°C	o/n at 4°C	Alexa-488
α-myc-tag	calcium induced clustering/ figure 4.5	1 h at RT	1 h at RT	Alexa-488
α-caveolin/ α-clathrin	co-staining with BP-pPC/ v 4.17	1 h at RT	1 h at RT	Alexa-647
α-myc-tag/ α-GFP	3D STED/ figure 4.8	2 h at RT	1 h at RT	Atto-647N

3.2.5.2 Metabolic labeling of PC and cycloaddition reaction

For visualization of PC, a metabolic labeling strategy was employed as described previously (Jao et al. 2009). To this end, cells were fed with 0.5 mM propargyl-choline (pC) in cell specific medium containing 10% delipidated FCS (kind gift from AG Thiele) instead of normal FCS or HS for 8-12 h or 14 h followed by chasing with normal medium for 4 h for TIRF imaging (figure 4.16, panel A). pC was a kind gift of C. Thiele and synthesized as described in Jao et al. 2009.

For the copper-catalyzed azide-alkyne cycloaddition of the propargyl groups and azide-linked fluorophores, a reaction mix containing 625 µM TBTA (Tris[(1-benzyl-1H-1,2,3-triazol-4-yl) methyl] amine) (*Sigma-Aldrich*, # 678937), 500 µM Tetrakis (acetonitrile) copper(I) tetrafluoroborate (*Sigma-Aldrich*, # 677892) and 100 µM azido-sulfo-Bodipy (see below) or 2 µM azido-coupled Atto647N (*ATTO-Tec*, Germany, # AD647N-101) was prepared in PBS buffer directly before the reaction. The PM sheets or cells on coverslips were incubated with 40 µL per coverslip of the reaction mix in a humid reaction chamber protected from light. Incubation lasted for 30 min at RT, except for the experiment presented in figure 4.16, panel B, where the incubation was performed for 10 min on ice. After the reaction, coverslips were washed three times with PBS.

The azido-coupled Atto647N showed elevated background staining of unlabeled cellular membranes. To prevent this unspecific labeling, samples were blocked with 5% peptone and 5% BSA in PBS followed by a brief wash with 3% BSA in PBS prior to cycloaddition with azido-Atto647N. This was not necessary in case of the azido-sulfo-Bodipy.

The azido-sulfo-Bodipy (i.e. 8-(5-Azidopentyl)-4,4-difluor-1,3,5,7-tetramethyl-4-bora-3a,4a-diaza-s-indacene-2,6-disulfonic acid disodium salt) was kindly provided by C. Thiele and synthesized as described in Hofmann et al. 2014.

3.2.5.3 Labeling with membrane dyes and lipid probes

TMA-DPH: For visualization of membranes, the supernatant of a saturated 1-(4-Trimethyl-ammoniumphenyl) - 6 - Phenyl - 1,3,5-Hexatriene p-Toluenesulfonate (TMA-DPH) (*ThermoFisher Scientific*, # T204) solution was used directly in 1:10 (v/v) dilution in the imaging solution. TMA-DPH is a membrane dye, which only fluoresces upon incorporation into the PM. It was used to ensure integrity of PM sheets and as a reference staining for image analysis.

CellMask™ and R18: CellMask™ (*ThermoFisher Scientific*, formerly *LifeTechnologies*, # C10046) and R18 (Octadecyl Rhodamine B Chloride) (*ThermoFisher Scientific*, formerly *MolecularProbes*, # O-246) are general membrane dyes. For staining, CellMask™ was incubated with PM sheets at a concentration of 5 µg/mL in PBS for 5 min before fixation and three washing steps with PBS. R18 was added to already fixed PM sheets after cycloaddition at a concentration of 1.46 µg/mL (2 µM) for 15 min followed by three washing steps with PBS.

Lactadherin: For staining of PS, PM sheets were incubated with 80 nM FITC-labeled bovine lactadherin (*HTI*, # BLAC 1200) in PBS for 15 min after the cycloaddition reaction followed by three washing steps with PBS.

Filipin: Cholesterol labeling was achieved by incubation of PM sheets with 80 µg/mL Filipin III from *Streptomyces filipinensis* (*Sigma-Aldrich*, # F4767) in PBS for 45 min followed by three washing steps with PBS.

FAST DiO™: For a membrane reference staining for pulsed 2D STED microscopy, PM sheets were incubated after immunostaining with 0.3 µM FAST DiO™ (*ThermoFisher Scientific*, # D-3898) in PBS for 10 min followed by three washing steps for 5 min with PBS prior to embedding.

3.2.6 Botulinum toxin co-expression

HepG2 cells were co-transfected with syntaxin-myc or syx-ΔS-myc and the light chain of botulinum neurotoxin C1 (C-terminally fused to GFP (BoNT/C1/LC-GFP)). For preventing cell death (observed in preliminary experiments for high concentrations of the protease), BoNT/C1/LC-GFP plasmid was used at a 10-fold lower concentration (w/v) compared to the syntaxin constructs. Single syntaxin-myc and syx-ΔS-myc transfections were used as controls.

One day after transfection, cells were fixed and underwent immunostaining for the myc tag (see table 3.8 and section 3.2.5.1). Cells were imaged (Olympus IX81-ZDC, 60x objective) in PBS with TMA-DPH in the blue (TMA-DPH), green (GFP) and the far-red (Atto647N) channel. For analysis, cell footprints were traced in the far-red channel. The resulting regions of interest (ROIs) were used to measure size of the footprints and the average fluorescence in the green and far-red channel for each cell. Fluorescence intensities were background corrected. For identification of BoNT/C1/LC-GFP cotransfected

cells, a threshold of autofluorescence was determined in single transfected cells without BoNT/C1/LC-GFP. Cells from double transfection with lower values in the GFP channel were not included in the further analysis. Averaged fluorescence intensities in the far-red channel (myc immunostaining) were normalized to the averaged syntaxin-myc single transfection condition. Since cell footprint size decreased in all conditions compared to the syntaxin-myc single transfection, the intensity of the myc-signal was multiplied by the respective average footprint size.

3.2.7 Comparative epifluorescence-western blot experiment

For a comparison of epifluorescence and western blot signals of different syntaxin constructs, HepG2 cells were split after transfection with syntaxin-myc, syx-ΔS-myc or syx-ΔCyt-myc into two fractions: 2.75 x 10^6 cells were transferred into a cell culture flask for western blot and 2.5 x 10^5 cells were seeded to two coverslips for microscopy. After 24 h cells for western blot were lysed (see section 3.2.2.4) and subjected to SDS-PAGE and western blot (see section 3.2.3). Cells for microscopy were fixed and immunostained as described in section 3.2.5.1 and table 3.8.

Immunostained cells were imaged in PBS buffer containing TMA-DPH on the Olympus IX81-ZDC using the 60x objective. For determination of transfection efficiency, cells were selected in the TMA-DPH channel and imaged in both, TMA-DPH and green (immunostaining), channels. Cells were classified as transfected when background corrected intensity was higher than the average intensity of untransfected cells. From the resulting transfection efficiencies a factor was calculated. Western blot signals (determined as described in section 3.2.3; with 3 – 4 technical replications for each independent experiment) were multiplied by this factor before normalization to the syntaxin-myc value.

Additional images of randomly chosen transfected cells were obtained to ensure a sufficient number of cells for the analysis of epifluorescence intensity. For analysis, ROIs were placed at the cell periphery in the TMA-DPH channel, transferred to the green (immunostaining) channel, measured and background corrected. From equally stained and analyzed non-transfected cells the average fluorescence intensity was determined and set as a threshold for unspecific signal (resulting from autofluorescence and from unspecific binding of antibodies). Only values higher than this threshold were averaged per construct and normalized to the value of syntaxin-myc. The normalized values from three independent experiments were averaged. For the calculation of epifluorescence/western blot ratios, western blot signals of each individual experiment were corrected for different

subcellular localization of the constructs as determined by pH quenching. The ratio was calculated for each individual experiment and then averaged.

3.2.8 pH-quenching of GFP

Subcellular distribution of GFP-tagged syntaxin constructs was analyzed by pH quenching. To this end, HepG2 cells were transfected with syntaxin-GFP, syx-ΔS-GFP, syx-ΔCyt-GFP, GFP-SNAP25 as a control for intracellular PM-localized GFP. Additionally, VAMP8-GFP was used as control for a partially lysosomal and endosomal localized protein with lumenal GFP. Prior to imaging, cells were treated 24 h after transfection with 0.2 µM bafilomycin A1 from *Streptomyces griseus* (*Sigma-Aldrich*, # B1793, in DMSO) or with an equal volume of DMSO as a control for 45 min. The treatment was performed in HepG2 growth medium.

Bafilomycin A1 specifically inhibits vacuolar H^+-ATPases and thus degrades intracellular pH gradients. VAMP8-GFP signal was monitored over time directly after drug treatment. This revealed that for dequenching of GFP signals in acidic compartments the optimal incubation time is 45 min (data not shown).

Solutions for imaging were phosphate buffer (30.5 mM NaCl, 81 mM Na_2HPO_4, 19 mM NaH_2PO_4) at pH 7.4, and a solution containing 30.5 mM NaCl, 8 mM Na_2HPO_4, 92 mM NaH_2PO_4 adjusted to pH 4.3 by adding HCl. Cells were imaged on the Olympus IX81-ZDC employing the 10x objective. The same cells were subsequently imaged at pH 7.4 and pH 4.3. In between the imaging steps, coverslips were briefly washed three times and incubated for 2 min with the solution at pH 4.3.

For analysis, cells footprints were traced manually. Intensity in the resulting ROIs was measured and corrected for background fluorescence. Intensity values at pH 4.3 were related to the intensity at pH 7.4 for every cell and averaged per condition and construct. Cells were categorized into three classes: i) cells of normal size and regular shape (comparable to non-transfected cells), ii) smaller cells with spiky membrane extensions and iii) very small and rounded cells. Generally, class ii) and iii) cells showed higher overall as well as intracellular GFP signal. Class iii) cells occurred most often in syntaxin-GFP expressing cells followed by syx-ΔCyt-GFP and syx-ΔS-GFP. For the calculation of subcellular distribution, all cell types were included into the analysis. The average values were calculated for each day and construct and averaged among the independent experiments.

3.2.9 3D STED

Subcellular distribution of myc- and GFP-tagged syntaxin variants was tested by 3D STED. To this end, transfected HepG2 cells underwent immunostaining with antibodies raised against the respective tag (GFP or myc)(see table 3.8). The classical protocol (see section 3.2.5.1) was slightly adapted in that after fixative quenching the coverslips were washed 3 times with HBSS (Hanks balanced salt solution, *Gibco, ThermoFisher Scientific*, # 14025092) before being incubated with 100 µg/mL concanavalin A conjugated to Alexa Fluor® 594 (*ThermoFisher Scientific*, # C11253) in HBSS for 30 min. Afterwards, cells were permeabilized with 0.5% Triton-X100 in PBS for 10 min and from there all solutions contained 0.05% Triton-X100. After the last washing step cells were washed with PBS twice and samples were stored over night at 4 °C prior to imaging.

Imaging was performed in PBS with the easy3D STED microscope (*Abberior Instruments*) using the water immersion objective. Samples were screened for transfected cells in the epifluorescence mode of the microscope. Cells were then recorded in confocal mode in x,y for an overview image (110 x 110 µm, pixel size 300 nm) of concanavalin and antibody staining. The overview image was divided horizontally into 10 sections with a distance of 10 µm, which were imaged in concanavalin and antibody channel in x,z employing 3D STED modus of the microscope (100%) and 200 mW STED laser deexcitation power. Pixel size for those vertical dissections were 50 nm in x and 96.3 nm in z.

For STED images, 6% Alexa-594 bleed-trough was found in single stains (ConcanavalinA-Alexa594 only), which was subtracted from all STED (Atto647) images.

For analysis, the cell membrane was traced by a ROI in the concanavalinA image in each slice of one cell. This ROI was expanded by 5 pixels yielding an inner ROI delineating the cytosol and an outer ROI delineating the cell and the ROI between inner and outer ROI tracing the PM. ROIs were then transferred to the corresponding STED images of the antibody staining. The integral of the fluorescence signal was measured in all ROIs (PM, cytosol and whole cell) and was summed up for the slices of one cell. Averaged values of non transfected control cells were subtracted for background correction and the values for PM and cytosol were related to the total fluorescence signal of the respective cell.

3.2.10 Fluorescence recovery after photobleaching (FRAP)

For measurement of protein mobility within the PM, FRAP was employed. Live HepG2 cells in Ringer solution or freshly prepared native PM sheets in sonication buffer were imaged at 37 °C using the Olympus Fluoview 1000 laser scanning microscope (see section

3.1.1.2) for no more than 40 min per cell sample and 25 min per PM sheet sample. Pixel size was adjusted to 414 nm and samples were recorded at 1 Hz. 10 frames were recorded before the bleaching step in a 12 x 12 pixel ROI (R_{bleach}) for 500 ms with full intensity of the 488 nm and 405 nm lasers . The sample was monitored for another 200 frames post-bleach.

For analysis, additional 12 x 12 pixel ROIs were placed next to the cell or PM sheet for determining the background fluorescence (R_{BG}). Another ROI was set in an unbleached region of the cell or PM sheet ($R_{control}$) and was used to identify out-of-focus drift or cell movement. To do so, fluorescence intensity in R_{BG} was subtracted from $R_{control}$ for each frame. The pre-bleach intensity was averaged for all 10 frames and compared to the averaged intensity in the last three frames. If the difference in intensity was bigger than ± 15%, the cell or PM sheet was not included in the further analysis.

Intensity in the R_{bleach} was likewise corrected for background fluorescence and post-bleach frames were normalized to the averaged pre-bleach intensity. The resulting normalized values were plotted against the time and averaged for each experiment. Average traces were fitted to a hyperbolic function (see equation 3.1) with a fixed offset (y_0) to obtain the half time of recovery ($t_{1/2}$) and the maximal recovery (Rec_{max}).

$$y(t) = y_0 + \frac{Rec_{max} * t}{t_{1/2} + t} \tag{3.1}$$

To determine the effect of pre-bleach intensity on the half time of recovery, the traces of individual cells or PM sheets were fitted. Fits with a lower R^2 than 0.7 were excluded and the remaining half times were plotted against the background corrected intensity of the pre-bleach frames.

3.2.11 Fluorescence loss after photobleaching (FLAP) and analysis

In order to probe for BP-pPC transfer from the ER to the PM, a FLAP experiment was performed. To this end, HepG2 cells were fed with pC as described in section 3.2.5.2. PM sheets obtained from these cells underwent cycloaddition with azido-sulfo-Bodipy and were subsequently imaged at 37 °C using the Olympus Fluoview 1000 laser scanning microscope (see section 3.1.1.2) with the pixel size adjusted to 207 nm. A bleaching ROI was defined covering one half of a sheet prior to the recording. Then a pre-bleach frame was recorded followed by a bleaching step in the defined ROI at full laser intensity of the 405 nm and 488 nm laser immediately followed by a post-bleach frame. Another post-bleach recording

was made after 20 min.

For analysis, spot intensities were analyzed from PM sheets that were not bleached as a control and bleached PM sheets on the non-bleached half of the sheet. An adjacent spot in the uniform PM layer was chosen for each ER spot and the measured intensities of all spots were background corrected. Values from each uniform layer spot were then subtracted from the values of the respective ER spot. The change in intensity between pre- and the post-bleach picture after 20 min was calculated for control and FRAP spots. For each of three independent experiments 80-180 spots from 6-14 sheets were analyzed.

3.2.12 STED microscopy and analysis

For CW-STED high resolution imaging the TCS-SP8 gated-STED microscope (see section 3.1.1.2) was used. Pixel size was adjusted to 20 nm and images were recorded at 200 Hz with excitation at 488 nm employing the white-light laser at 20% power and depletion at 592 nm with a CW-STED beam at 50% intensity and time-gating between 1 and 6.5 ns.

Pulsed STED high resolution imaging was performed using the *Abberior Instruments* easy-3D STED module (see section 3.1.1.2). To check for membrane integrity, FAST DiO membrane stain was imaged exciting at 488 nm and detection at 500-520 nm and 532-558 nm. From the antibody staining (Atto-647N) images were obtained exciting at 640 nm and detecting at 650-720 nm either without depletion (confocal image) or in STED mode using the pulsed 775 nm laser at 350 or 450 mW with time-gating between 1.25 and 8 ns. Pixel size was adjusted to 20 nm.

For analysis of spots, a custom ImageJ macro was used (developed by Dr. Jan-Gero Schloetel): Identification of spots was achieved by the ImageJ "Find Maxima" function in difference of Gaussians (DOG)- filtered STED images within a squared ROI (180 x 180 pixel for CW-STED images, 130 x 130 pixel for pulsed STED images for figure 4.2 and 55 x 55 pixel for figure 4.3). Circular ROIs with a 5 pixel diameter were placed at the identified spot positions on raw STED images. Spots with low mean intensities (100 arbitrary units (a.u.) for CW-STED or 4 a.u. for pulsed STED) were excluded from the analysis. Following parameters were extracted from the raw STED images: number of spots, mean intensity of the spot ROI, the spot size based on a Gaussian fit of a line scan in a 15 x 3 pixel ROI (either horizontal or vertical depending on fit quality) and the nearest neighbor distance based on the centre of the spot ROIs. Number of spots, spot intensities and spot sizes were averaged for each PM sheet. For number of spots and spot intensity all spots were included, whereas for mean size only spots with suitable

Gaussian fit quality ($R^2 \geq 0.9$) were included assuring a well-centered peak, reasonable offset and peak height. For figure 4.2 spots were additionally filtered for at least 5-6 pixels nearest neighbor distance for FWHM analysis. For calculation of average spot sizes in figure 4.3, panel C, PM sheets were excluded when the density of spots was too high for reliable separation of single clusters. Spot parameters were averaged for each PM sheet and compared to the background-corrected mean intensity of the PM sheets in the confocal channel.

For CW-STED, values from three independent experiments with a total of 38-39 sheets (2924-3185 spots) per condition for cluster size and 39-49 sheets (4678-9385 spots) for cluster counts and intensities were included. For pulsed STED for figure 4.2, plots show values from three independent experiments with a total of 22-45 sheets (1336-2010 spots) per condition for cluster size and 33-48 sheets (2407-6054 spots) for cluster counts and intensities. For pulsed STED for figure 4.3 a total of 13-24 sheets (243-606 spots) per condition for cluster size and 13-24 sheets (562-1142 spots) for cluster counts and intensities were analyzed.

3.2.13 Total internal reflection fluorescence (TIRF) microscopy and analysis

The Olympus IX81-ZDC (see section 3.1.1.2) was used for imaging in TIRF mode. Prior to imaging, the incident angle of the 488 nm laser was adjusted in that it was totally reflected at the interface between the glass and the sample and created an evanescent wave for excitation. The angle was maintained for all conditions of one independent experiment.

For TIRF imaging of BP-pPC at the cytosolic periphery of the PM (figure 4.16, panel A), metabolically labeled cells (see section 3.2.5.2) were fixed for 45 min 4% PFA in PBS, quenched with 50 mM NH_4Cl in PBS, followed by the cycloaddition reaction (section 3.2.5.2) and TIRF imaging in PBS.

For monitoring YFP-STIM1 signal in intact cells (see figure 4.20), transfected cells were recorded in TIRF mode essentially as described previously (Wu et al. 2006). In brief, cells were rinsed twice with Ringer solution for with calcium, then the solution was exchanged for either Ringer solution without calcium containing 1 µM thapsigargin (TG)(*Enzo Life Science*,# BML-PE 180-0001) in DMSO (stimulation), or for Ringer solution with calcium and DMSO only (control). Directly after buffer exchange, a reference image was obtained in epifluorescence mode. Cells were subsequently recorded in TIRF mode every 15 s for about 5 min. For analysis, three ROIs were placed in the area covered by one cell in the

reference epifluorescence image and then transferred to the TIRF frames. Fluorescence intensity was measured in each frame, background corrected and related to the intensity of the first TIRF frame. Values of each frame of one condition were averaged. 5 - 8 cells were recorded per independent experiment.

3.2.14 Trypsin treatment and ER spot tracking

Treatment with 0.5 mg/mL trypsin in PBS (*PAA*, # L11-004) was performed on non-fixed PM sheets after cycloaddition reaction (see section 3.2.5.2) either for 45 min or directly on the microscope. Trypsin pre-incubated with 0.5 mg/mL trypsin inhibitor type II-O (*Sigma-Aldrich*, # T9253) was used in both cases as a negative control. For tracking, PM sheets were monitored every 10 s for 200 s in PBS before treatment. Afterwards, solutions were exchanged for trypsin-containing solution or control solution, incubated for 1 min and monitored for another 900 seconds during treatment.

For analysis, performed by Dr. Jan-Gero Schloetel, lateral image drift was corrected employing the Image Stabilizer plugin for ImageJ ([2]). Upon focus drift, up to 5 frames after treatment had to be deleted. Spots were tracked manually using the ImageJ plugin MTrackJ (Meijering et al. 2012). For all spots within an 50 x 50 pixel ROI that were traceable for minimally 20 frames before and after treatment, calculation of mean-square displacement (MSD) was performed essentially as described previously (Qian et al. 1991, Kusumi et al. 1993). MSD plots were averaged for each condition (trypsin and control) and diffusion coefficients (D) were calculated from linear regression (instrumental weighting using MSD variance) according to equation 3.2.

$$\mathrm{MSD} = 4D\Delta t \tag{3.2}$$

For monitoring fluorescence intensity of spots during tracking, the image series was convoluted after drift correction with a normalized 3x3 pixel kernel (1,1,1/1,1,1/1,1,1). Using the MTrackJ plugin raw intensities were measured in a 1x1 pixel ROI (effectively revealing the mean spot intensity within a 3x3 pixel ROI). Background fluorescence was measured in a 10x10 pixel ROI outside of the PM sheet and subtracted from the spot intensities. Spot intensities of every single spot were averaged over all frames that did not show focus drift or spot collision yielding a track average. The spot intensity in each frame was normalized to this track average and the deviation (in %) from the track average was

[2] `www.cs.cmu.edu/~kangli/code/Image_Stabilizer.html`

averaged for the spots observed for each frame in one condition followed by averaging over 3 independent experiments.

3.2.15 Image analysis

Microscopy images were analyzed with the program ImageJ. Images are shown at arbitrary scaling unless specified otherwise.

Average fluorescence intensity: For determining average fluorescence intensity, ROIs were placed next to the PM sheets or cells. The fluorescence intensity averaged over the pixels of this ROI was subtracted from the average fluorescence intensity of the pixels in the cell/PM sheet ROI.

Correlation coefficient: Images of two channels were aligned either manually or using tetraspeck microspheres (*ThermoFisher Scientific*, formerly *Invitrogen*, # T7284) as a spatial reference. Pixel-wise Pearson correlation coefficient (PCC) between fluorescence intensities in defined ROIs was determined employing the ImageJ plugin Intensity Correlation Analysis (Li et al. 2004).

Overlap on single spot level: Circular ROIs were centered on randomly selected individual spots in one channel and then transferred to the other channel. Spots were rated as overlapping when the location of the spot center did not differ by more than one pixel. Correction for random overlap was performed on mirrored images as described previously (Lang et al. 2002). For each individual experiment 10 - 25 spots per PM sheet (10 - 22 PM sheets in total) were analyzed.

Relative standard deviation: The standard deviation of fluorescence intensity in a ROI was divided by the background corrected intensity of the same ROI to obtain the relative standard deviation.

Signal fraction of spots: The total PM sheet area (traced manually) and the area of the spots (segmented by a local threshold) were segmented for each PM sheet. The segmented spot areas were excluded from the total sheet area yielding the area of homogeneously distributed signal. The mean fluorescence intensities of the total PM sheet area and the homogeneous signal area were multiplied with the number of pixels defining the PM sheet. The difference between these integrated intensities reflects the signal arising from spots

and its percentage of the total integrated intensity was calculated for 10 - 14 PM sheets for each of three independent experiments.

Spot intensity above background: Circular ROIs were centered on randomly selected individual spots. The same ROIs were placed on the uniform layer of the PM sheet in the vicinity of the spot. Mean fluorescence intensities of all ROIs were background corrected and the intensity increase of the spots above background was calculated as a percentage of the uniform background intensity. 20 spots were analyzed per PM sheet. Values of 5 - 20 PM sheets were averaged followed by averaging over the three independent experiments.

4 Results

In this study, two different supra-molecular structures at the cytoplasmic periphery of the PM were investigated.

The first part (4.1) focuses on the influence of cytoplasmic protein domains on the inner architecture of the syntaxin protein cluster.

The second part (4.2) describes the preparation of ER-PM membrane contact sites (MCS) for the study of spontaneous lipid transfer (SLT).

4.1 Inner architecture of the syntaxin 1A protein cluster

The supra-molecular syntaxin 1A cluster is deemed to be an exemplary research object for the investigation of the clustering phenomenon in general. Multiple layers of interaction within the PM and at the periphery were proposed to contribute to syntaxin 1A clustering such as electrostatic interaction with charged lipids (section 1.3.2.1) or hydrophobic mismatch (section 1.3.1), whereas also interactions between cytoplasmic protein domains were suggested to mediate clustering (Sieber et al. 2006). The implication of cytoplasmic protein domains for inner architecture of the syntaxin1A cluster is subject of the following section.

Syntaxin1A, in the following referred to as syntaxin, is a single span PM protein extending its major part into the cytosol. This cytoplasmic domain consists of the large globular H_{abc} domain, the SNARE motif (SM) and a polybasic stretch (pbs) close to the transmembrane region (tmr) (figure 4.1). To test for the impact of protein interactions in the cytoplasmic domain of syntaxin on cluster architecture, two different variants based on rat syntaxin1A were employed in the following (figure 4.1): In one variant the N-terminal half of the SNARE motif (n-SM) is deleted from aminoacid 192 to 218. The second construct lacks the entire cytosplasmic domain except for the N-terminal peptide and the pbs. A triple myc tag or a GFP variant (mEGFP) was fused via a linker to the C-terminus of syntaxin and the variants, therefore pointing to the outside of the cell. In the further course

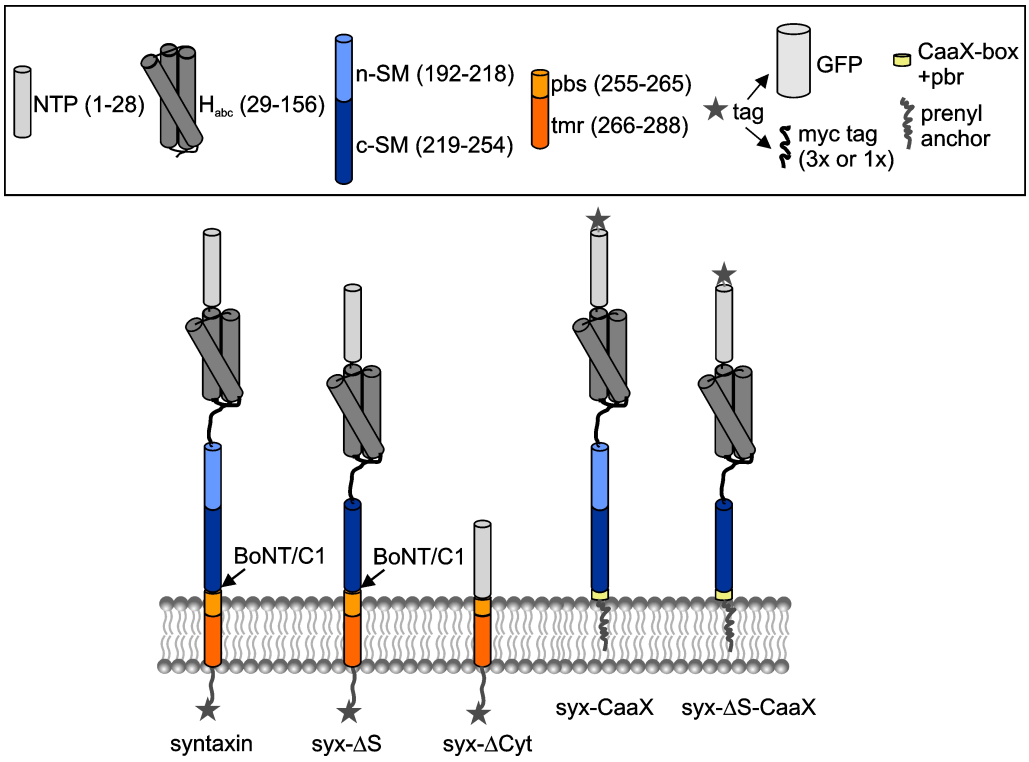

Figure 4.1: **Syntaxin1A domain structure and variants.** *Upper panel*: schematic illustration of syntaxin1A domain structure: syntaxin consists of a N-terminal peptide (NTP, grey), a large globular domain (H_{abc}, dark grey) attached via a linker region (black) to a SNARE motif, that is divided into an N- and a C-terminal part (n-SM and c-SM in light and dark blue, respectively). The following polybasic stretch (pbs, light orange) precedes the transmembrane region (tmr, orange). *Lower panel*: illustration of the tagged syntaxin construct and variants lacking either only n-SM (syx-ΔS), or H_{abc}, SM and small parts of the pbs (syx-ΔCyt). For detection, a monomeric variant of GFP or a triple myc tag were fused to the C-terminus via a short linker. Botulinum neurotoxin C1 (BoNT/C1) cleavage site is indicated by an arrow. In myc-syx-CaaX and myc-syx-ΔS-CaaX constructs, pbs and tmr region are exchanged for a CaaX box from K-Ras (Malecz et al. 2000) (yellow) for anchoring in the PM via a prenyl anchor (grey line) and a single myc tag was linked N-terminal for detection.

of the work the constructs are referred to as syntaxin, syx-ΔS and syx-ΔCyt, respectively. Additionally, syntaxin and syx-ΔS were further modified by replacing the tmr and pbs by a C-terminal CaaX box and the adjacent poly basic region of K-Ras (Malecz et al. 2000), which mediates anchoring to the PM via prenylation. These constructs, termed syntaxin-CaaX and syx-ΔS-CaaX, respectively, were tagged N-terminally with a single myc tag (figure 4.1).

Following issues were addressed for the characterization of cluster architecture depending on the cytoplasmic protein domain: i) lateral PM distribution, ii) packing density within the cluster, and iii) lateral mobility in the PM

4.1.1 Influence of cytoplasmic protein domains on lateral organization of syntaxin clusters

Syntaxin is organized in protein clusters at the inner periphery of the PM (Lang et al. 2001). Those cluster are, with sizes ranging between 50 - 60 nm (Sieber et al. 2007), smaller than the diffraction limited resolution. Therefore, high resolution STED microscopy was employed to investigate the lateral organization of syntaxin and its variants syx-ΔS and syx-ΔCyt (section 4.1.1.1) as well as variants lacking the TM domain (section 4.1.1.2).

4.1.1.1 Lateral organization of syntaxin and the variants syx-ΔS and syx-ΔCyt

HepG2 cells were transfected transiently with the myc-tagged constructs. Using this non-neuronal cell line offers the advantage of observing the proteins without the influence of endogenous syntaxin. One day after transfection cells were subjected to a short ultrasound pulse to generate PM sheets. The basic features of a PM like fluidity and composition are preserved in this cell free preparation and permits accessibility to the inner leaflet (see section 1.3.3, and 3.2.4.1). To ensure equal staining conditions among the constructs, the myc tag was attached to the C-terminus (see figure 4.1). In this way, the tags face similar surroundings and distance to the PM and staining should be independent of the large alteration of domain structure at the cytoplasmic periphery of the PM.

In order to visualize syntaxin clusters, a classical immunostaining with first and secondary antibody was employed (3.2.5.1). The first antibody used was raised either against the myc tag or the N-terminal part of syntaxin, called HPC-1, when indicated. While the myc tag antibody detects all constructs, the HPC-1 antibody is only able to stain syntaxin-myc and syx-ΔS-myc, but not syx-ΔCyt-myc. The myc tag is located at the outside of the cell. Accordingly, the antibody has to diffuse underneath the sheet into the interspace between membrane and coverslip. The adherence of the sheet to the surface hinders antibody diffusion resulting in a staining gradient from the periphery towards the sheet center, as depicted in figure 4.2, panel A. Further analysis of protein clusters, indicated by local enrichment of antibody signal, was performed at the periphery of the sheet.

STED microscopy outperforms standard confocal microscopy in terms of resolution (section 1.3.3) as illustrated in figure 4.2, panel A. In contrast to the confocal image (left), where clear separation of the single spots was difficult, the STED image (middle/right) provided sharp spot boundaries and clearly separated clusters of less than 100 nm size. As depicted in figure 4.2, panel B, syntaxin-myc formed homogenous clusters, predomi-

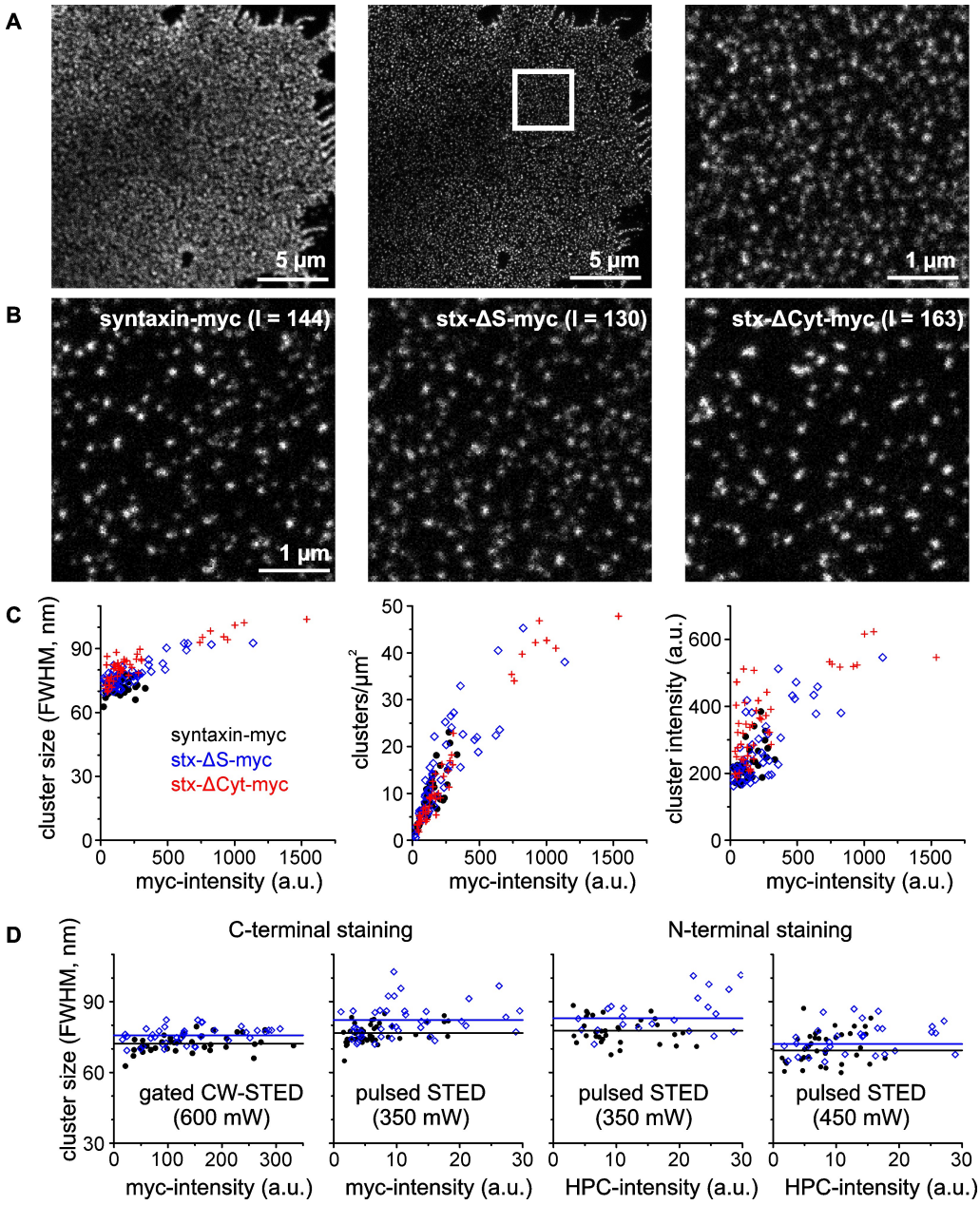

Figure 4.2: **Lateral organization dependent on cytoplasmic protein domains probed by super-resolution microscopy. A** PM sheets with overexpressed and immunostained syntaxin-myc in confocal (*left image*) and STED mode (*middle and right image*). Note the staining gradient for myc due to antibody diffusion underneath the membranes. ROIs for analysis were placed at the membrane peripheries (white square; magnified in the right image). **B** STED images from the different syntaxin variants as indicated, stained for the myc tag. Images were selected for similar average intensities (respective values are given in a.u.). **C** FWHM as a measure for cluster size, measured by line scan analysis, number of clusters per area and intensity of clusters were plotted against the average image intensity of the confocal image. **D** Cluster size of syntaxin-myc and syx-ΔS-myc at variable conditions. For analysis, only low intensities in overlapping ranges were considered. As indicated, samples were either stained at the extracellular C-terminus for the myc tag or with an antibody raised against the intracellular N-terminus. Imaging and analysis was performed by Dr. Jan-Gero Schlötel.

nantly with round shape. This was likewise the case for syx-ΔS-myc and syx-ΔCyt-myc, although occasionally both exhibited elongated structures. This phenomenon was found most often in syx-ΔCyt and occurred more likely in sheets with higher intensity.

For analysis, three parameters were extracted from the obtained images: i) cluster size expressed by the full width at half maximum (FWHM), ii) number of clusters per µm^2 membrane area, and iii) cluster intensity as a measure for antibody occupancy of each cluster (figure 4.2, panel C). For a detailed description of the analysis please see 3.2.12. These parameters were plotted against the average sheet intensity as a rough measure for the concentration of syntaxin in the membrane.

The number of clusters depended strictly on the average sheet intensity for all three constructs. In contrast, cluster size and cluster intensity only slightly increased upon elevated protein concentrations, suggesting that the clusters are limited in their capacity to expand laterally, which is in line with previous studies (Sieber et al. 2006).

When focusing on a lower intensity range syntaxin-myc and syx-ΔS-myc cluster size appeared independent of sheet intensity (figure 4.2, panel D). In this range syx-ΔS-myc clusters were slightly enlarged. This small difference remained, no matter if the constructs were detected at the extracellular C-terminus or the intracellular N-terminus, independent of the secondary antibody used or the microscopical settings. The absolute size, however, differed mainly according to the power of the depletion laser. Therefore, it can be deduced that obtaining absolute cluster sizes is not feasible with this setup, while comparative measurements are reliable.

In summary, the constructs exhibit similar lateral distributions with a slight tendency towards larger clusters for syx-ΔS and syx-ΔCyt over syntaxin-myc. However, the most considerable difference among the constructs are the staining intensities: while syntaxin-myc staining appears rather low, syx-ΔS-myc and syx-ΔCyt-myc intensities distribute over a broad range. Accordingly, their average intensity highly exceeds the average intensity of the full-length construct.

4.1.1.2 Lateral organization of syntaxin and the variants syx-CaaX and syx-ΔS-CaaX

The question arose whether cytoplasmic protein interactions between syntaxin molecules were sufficient for the cluster formation independent of the TM region. To this end syntaxin was compared to the two prenyl anchored constructs lacking the tmr and pbs domains (see syx-CaaX and syx-ΔS-CaaX in figure 4.1). For reasons of comparability, all constructs were tagged N-terminally with a single myc tag. The technical implementation

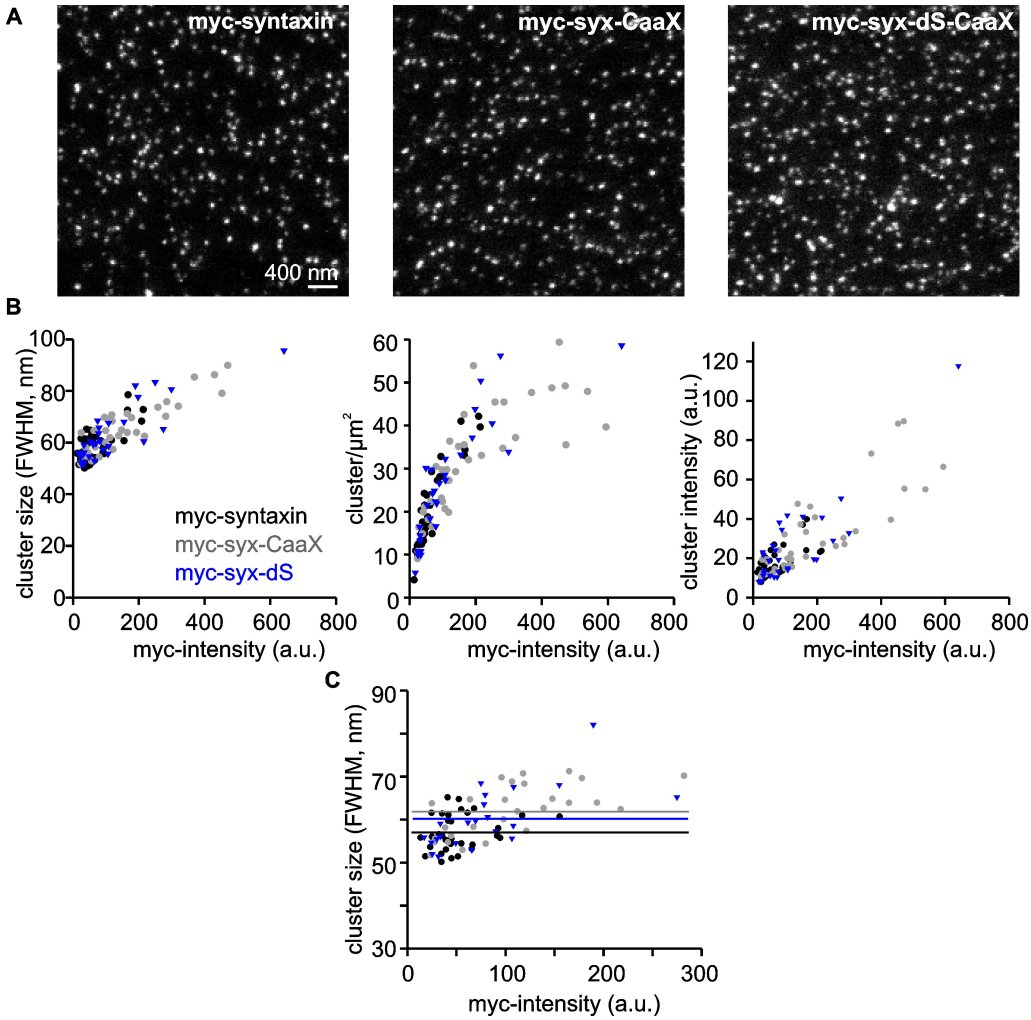

Figure 4.3: **Transmembrane domain independent lateral organization of syntaxin probed by super-resolution microscopy. A** PM sheets from cells expressing the different myc tagged syntaxin variants as indicated, stained for the myc tag and imaged with a pulsed STED at 450 mW depletion laser intensity. Images were selected for similar average intensities. **B** FWHM as a measure for cluster size, measured by line scan analysis (*left*), number of clusters per area (*middle*) and intensity of clusters (*right*) were plotted against the average sheet intensity of the confocal image. **C** Data from **B**, *left plot*, were filtered additionally for sheets for which separation of single spots was reliable. Black (myc-syntaxin), grey (myc-syx-CaaX) and blue (myc-syx-ΔS-CaaX) lines indicate the average cluster size. **B** and **C** Each data point represents averaged spot values of one PM sheet. Plots include values from two independent experiments.

matched the previous experiment (4.1.1.1) and the same parameters were extracted from the obtained high resolution images as described before.

It becomes apparent from figure 4.3, panel A, that all three constructs, myc-syntaxin, myc-syx-CaaX and myc-syx-Δ-CaaX showed the same staining pattern when observed at similar average sheet intensities. Clusters distributed homogeneously on the PM sheet, were well separated and predominantly of round shape. Cluster size of all constructs increased slightly with the overall intensity of the respective sheet (figure 4.3, panel B), though there was no correlation in lower intensity ranges for syntaxin (figure 4.3, panel C). This matches the previous results for C-terminally tagged syntaxin-myc and syx-ΔS-myc (section 4.1.1.1). In contrast, syx-CaaX and syx-ΔS-CaaX cluster sizes appeared more susceptible to their overall concentration in the sheets even at low ranges, suggesting an involvement of the TM domain in the limitation of cluster size. Thus, it is not surprising that the average cluster size was slightly increased in the CaaX variants in comparison to the full-length construct. Deletion of the TM region seemed to overrule the slight difference between syntaxin and syx-ΔS in terms of average cluster size (compare figure 4.3 and figure 4.2). Therefore, it could be inferred that, additionally to the cytoplasmic protein domains, the TM region affects cluster size.

Similar to previous results, the number of spots strictly depended on the average sheet intensity for all constructs. At high expression levels, however, the spot number per μm^2 reached saturation. This is probably due to technical limitation in separating single clusters in these intensity ranges.

As explained in the previous section, the cluster intensity provides information on the antibody occupancy of each cluster. No difference between the constructs was found in this context (figure 4.3, panel B, right plot). A slight increase of cluster intensity with the average sheet intensity could be observed for all constructs, which indicates an increase of molecule number in single clusters upon elevation of total protein concentration in the sheet. From this experiment it can be concluded that syntaxin is able to form clusters independent of the TM region and that those clusters exhibit similar properties compared to the full-length syntaxin clusters but slightly differ in their limitation of cluster size.

4.1.2 Influence of the cytoplasmic domain on packing density of the syntaxin cluster

Protein clusters are characterized by the local enrichment of a certain protein in the PM. The first quantitative study of the syntaxin cluster calculated roughly 75 molecules on an average cluster area of 2.4 x 10^{-3} μm^2 (Sieber et al. 2007). In order to achieve such high

local concentration within the cluster, the proteins have to be packed densely. Therefore, the question arose, if cytoplasmic domains of syntaxin participate in the formation of those close intermolecular distances.

To address this question, I employed antibody labeling as a molecular sensor for cluster packing density. If epitopes are located in close distance of a few nanometers, binding of an antibody to its epitope can be hindered sterically by another antibody binding to an adjacent epitope (see illustration in figure 4.4). Such close proximities occur particularly

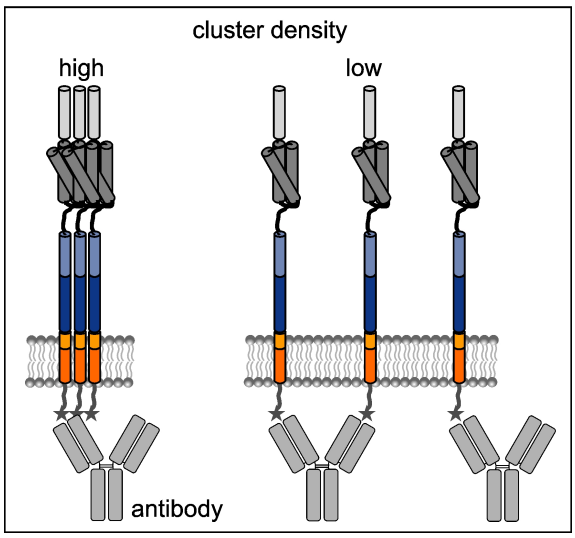

Figure 4.4: **Relation of cluster packing density and antibody labeling.** Pictogram illustrating different packing densities of syntaxin clusters. At high cluster density (*left*) the antibody cannot access all epitopes. Accessibility of epitopes is elevated at low cluster density (*right*).

in protein clusters in native PMs as corroborated by the data on syntaxin: assuming equal distribution of proteins within the cluster, the maximal intermolecular distance ranges between 6 - 7 nm (Sieber et al. 2007). This value is lower than the average distance between the two epitope recognition sites in a common IgG1 antibody (Zhang et al. 2015). Therefore, high packing density of epitopes leads to substoichiometric binding of the antibody and thus reduced staining intensity.

4.1.2.1 Testing of antibodies as molecular sensors for packing density in the current experimental system

To set the experimental framework, I first tested whether an antibody is capable of sensing differences in packing density in the system used. To this end, I used calcium to increase cluster density as described previously (Zilly et al. 2011, Batoulis et al. 2016) (see section 1.3.2.2) and monitored the response of the antibody signal. To do so, HepG2 cells were

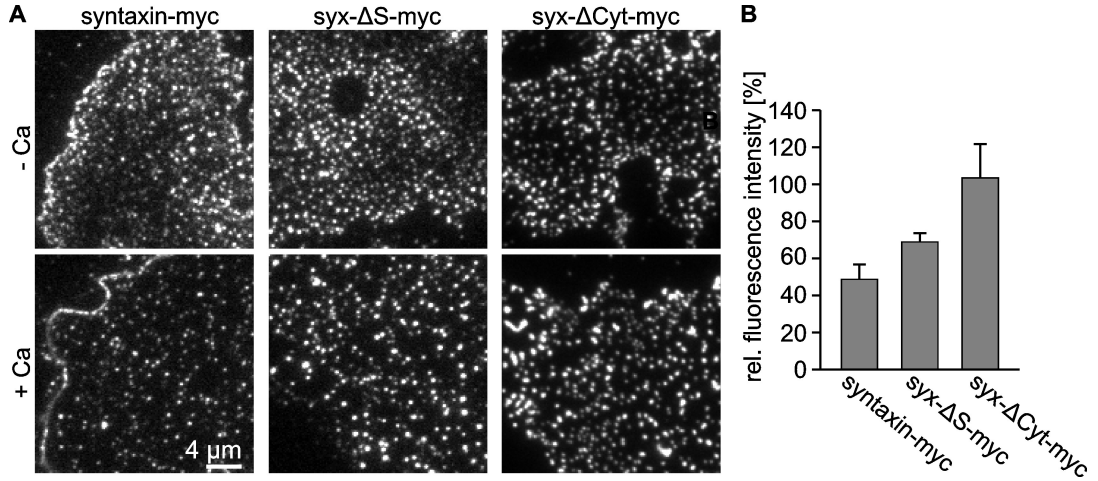

Figure 4.5: **Antibody labeling as a molecular sensor of cluster density. A** PM sheets from cells expressing syntaxin-myc, syx-ΔS-myc or syx-ΔCyt-myc as indicated. Freshly prepared sheets were incubated with buffer containing EGTA as a control (*upper panel*) or 10 mM $CaCl_2$ (*lower panel*) for 10 min at 37 °C, fixed and stained for the myc tag. Images of the same construct are shown at equal scaling. Scaling between the different constructs is arbitrary. **B** Fluorescence intensity was quantified and the calcium condition was related to the respective control condition for each construct (9-25 sheets per independent experiment and condition, n = 3 ± s.e.m.).

transfected with syntaxin-myc, syx-ΔS-myc or syx-ΔCyt-myc. Freshly prepared sheets of these cells were incubated with calcium containing solution or buffer supplemented with EGTA as a control, fixed and immunostained for the myc tag. Epifluorescence micrographs of representative sheets are depicted in figure 4.5, panel A.

Quantification of the fluorescence antibody signal revealed a calcium mediated decrease to 49% for syntaxin-myc, 69% for syx-ΔS-myc and nearly no change for syx-ΔCyt-myc when compared to the respective control conditions. The gradation in calcium sensitivity in the order syntaxin-myc<syx-ΔS-myc<syx-ΔCyt-myc possibly results from the consecutive degrease in overall negative charge from -19 to -15 to -6 for syntaxin-myc, syx-ΔS-myc and syx-ΔCyt-myc, respectively. This finding is in line with previously noticed charge dependence of the calcium effect (Zilly et al. 2011) and endorses the applicability of the antibody as a molecular sensor for cluster density in the current experimental system.

4.1.2.2 Influence of BoNT/C1-LC cleavage on extracellular myc accessibility of syntaxin

If the aforementioned packing density is indeed influenced by cytoplasmic domains of syntaxin, their depletion should affect intermolecular distances within the protein cluster. In order to test for this hypothesis, I deployed the light chain of botulinum toxin C1 from *clostridium botulinum*, hereinafter referred to as BoNT/C1-LC. BoNT/C1-LC is a

highly specific syntaxin1A protease, that cleaves the protein at the C-terminal end of the SNARE motif (figure 4.1, the black arrow indicates the cleavage site). To study the effect of BoNT/C1-LC on the clustering of syntaxin, GFP tagged BoNT/C1-LC was co-expressed in HepG2 cells with syntaxin-myc or syx-ΔS-myc. As a control, cells solely transfected with syntaxin-myc or syx-ΔS-myc were used. Cells were immunostained against the myc tag and the intensity of the staining was measured in epifluorescence micrographs

Overseeing the images, cells double transfected with BoNT/C1-LC-GFP and syntaxin-myc appeared to be smaller compared to the other conditions. Analysis of the cell footprint area confirmed this observation (figure 4.6, panel C). In comparison to the single syntaxin-

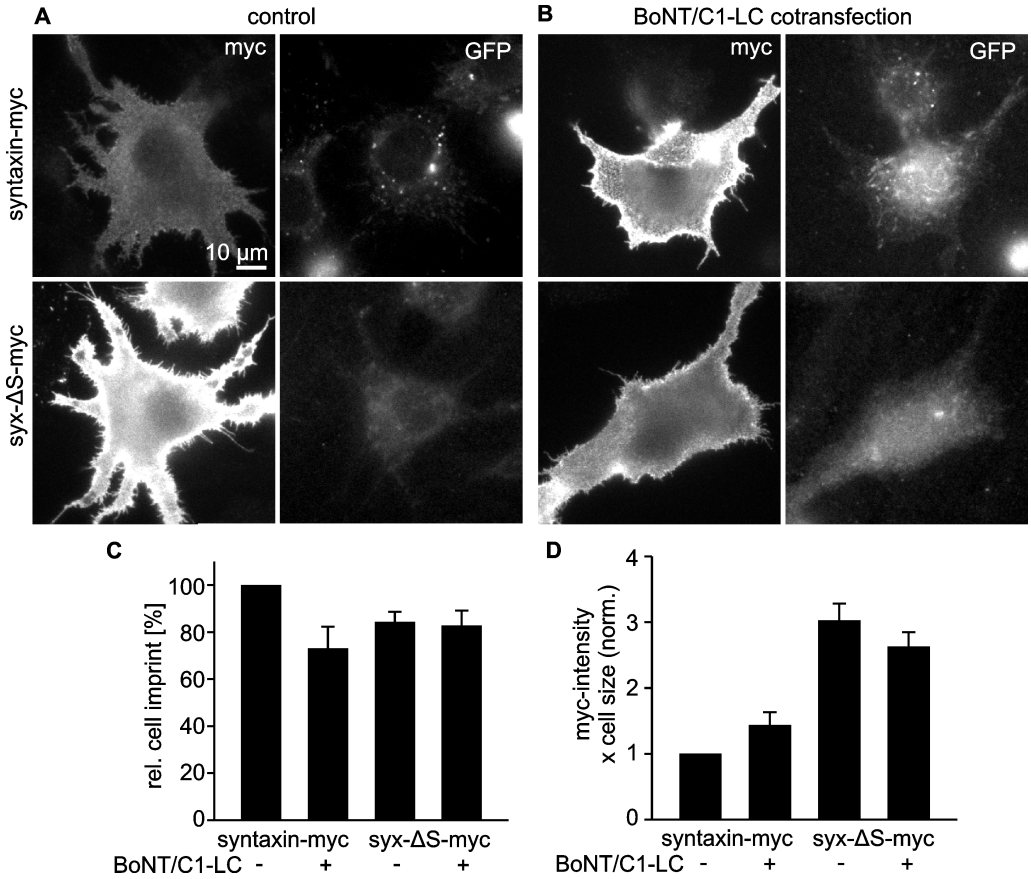

Figure 4.6: **Myc accessibility upon intracellular cleavage of syntaxin.** Cells were transfected with syntaxin-myc or syx-ΔS-myc alone (**A**), or cotransfected with with syntaxin-myc or syx-ΔS-myc and the light chain of botulinum neurotoxin C1 (BoNT/C1-LC) fused to GFP (**B**). Fixed cells were stained for myc and imaged for quantification of myc (*left* images in **A** and **B**) and GFP-intensity (*right* images in **A** and **B**). Images are shown at the same scaling in the respective channel. **C** Area of cell footprints (traced in the myc images) related to syntaxin-myc single transfection. **D** Antibody staining intensities, quantified from cell footprints, were related to syntaxin-myc single transfection. While BoNT/C1-LC did not influence the size of syx-ΔS cells, it resulted in approximately 25% smaller footprints of syntaxin-myc cells (see plot C) indicating that these cells concentrate their fluorescence on a smaller membrane area. As this effect may lead to an overestimation of the BoNT/C1-LC induced staining increase, intensities are multiplied by the respective footprint-size. **C**/**D** Values are given as means ± s.e.m. from three independent experiments (22 - 45 cells per independent experiment and condition).

myc transfection the decrease in footprint area was about 25% for syntaxin-myc/BoNT double transfected cells, while there was no difference between single syx-ΔS-myc and syx-ΔS-myc/BoNT transfected cells. One possible explanation for the decrease in cell size for syntaxin-myc/BoNT double transfected cells could be cellular stress linked to the overexpression of large amounts of protein. Such decrease in cell size accompanies a decrease in membrane surface. The number of proteins per membrane area would therefore raise causing higher antibody intensities. To correct for a possible influence of cell size, the measured antibody intensities of the four different conditions were corrected for the respective average footprint area of the cells. It should be noted here, that using the cells footprint is limited in its ability to reflect cell size. However, since there was no observable change in cell height between the conditions, the actual cell size might even be less affected than suggested by the change in footprint.

In single transfected cells the syx-ΔS-myc signal exceeded the syntaxin-myc signal approximately 3-fold, as observed similarly in previous experiments (see e.g. section 4.1.1.1). Upon co-expression with BoNT/C1-LC-GFP the staining intensity of syntaxin-myc increased by 43%. However, when BoNT/C1 was present, syx-ΔS-myc signal was even diminished by 10% related to the single transfection. Since syx-ΔS-myc contains the necessary protease interaction motif as well as the cleavage site (Schiavo et al. 1995), it should be equivalently susceptible to BoNT/C1 co-expression. The decrease in syx-ΔS-myc signal could be caused by the cellular stress resulting from the simultaneous overexpression of two proteins. Therefore, increase of antibody staining of syntaxin-myc hints to elevated accessibility to the myc epitope upon cleavage of cytoplasmic protein parts.

4.1.2.3 Comparative analysis of packing density in syntaxin, syx-ΔS and syx-ΔCyt clusters

As covered by the last sections, the intensity of an antibody signal is influenced by the accessibility of epitopes. More precisely, the signal is reduced at higher protein packing within the cluster (see section 4.1.2.1). In general, the intensity of an immunostaining (I_x) is proportional to the total amount of the protein of interest (N_{total}) and the accessibility of the epitopes (f_{access}) (see equation 4.1).

$$I_x \sim N_{total} * f_{access}$$
$$x = micr \text{ (epifluorescence microscopy) or } wb \text{ (western blot)} \tag{4.1}$$

If the intensity determined in epifluorescence microscopy (I_{micr}) is determined at the PM and N_{total} in whole cells, a correction factor for the subcellular distribution (f_{sort}) has to be included to dissect for the contribution of PM localized proteins. Accordingly, comparison of relative packing densities requires information on i) the amount of protein of interest, ii) the subcellular distribution, and iii) the antibody staining intensity in the intact PM (see equation 4.2 with k_{micr} being the proportionality factor for epifluorescence microscopy).

$$f_{access} = k_{micr} * \frac{I_{micr}}{N_{total} * f_{sort}} \tag{4.2}$$

Subcellular localization of syntaxin variants

In order to address the aforementioned amount of the myc tagged syntaxin variants in the PM, knowledge of their subcellular distribution was required to determine f_{sort} (see eq. 4.1). Two approaches were applied: i) pH quenching of GFP and ii) 3D STED analysis.

pH quenching of GFP: GFP is known to decrease reversibly in fluorescence intensity at pH lower than 6. The used variant EGFP, in particular, drops to lower than 10% fluorescence at pH 4.3 (Patterson et al. 1997). In the syntaxin constructs introduced in section 4.1 and figure 4.1, GFP is fused to the C-terminus of syntaxin, facing the extracellular periphery of the PM. This enables to quantify the intracellular GFP content simply by lowering the pH of the cell surrounding buffer and measuring the remaining fluorescence. Live HepG2 cells expressing either of the constructs syntaxin-GFP, syx-ΔS-GFP or syx-ΔCyt-GFP were monitored by sequential imaging at pH 7.4 and pH 4.3 (figure 4.7). The fluorescence intensity at pH 4.3 was compared to the respective value at pH 7.4 (see section 3.2.8 for details on the analysis). GFP-SNAP25 was employed as a control for PM localized intracellular GFP signal.

Acidic intracellular compartments such as lysosomes could potentially conceal GFP fluorescence of mis-targeted proteins. To avoid this, the pH gradient was degraded by bafilomycin (see section 3.2.8). VAMP8-GFP served as a control for a predominantly intracellular SNARE protein with a GFP tag facing the lumen of acidic cell compartments.

As depicted in figure 4.7, the GFP-SNAP25 signal was nearly unaffected by pH drop and bafilomycin treatment, as expected. The slight reduction by 14% for control and 18% for the bafilomycin condition could be due to bleaching effects or occasional cell disrup-

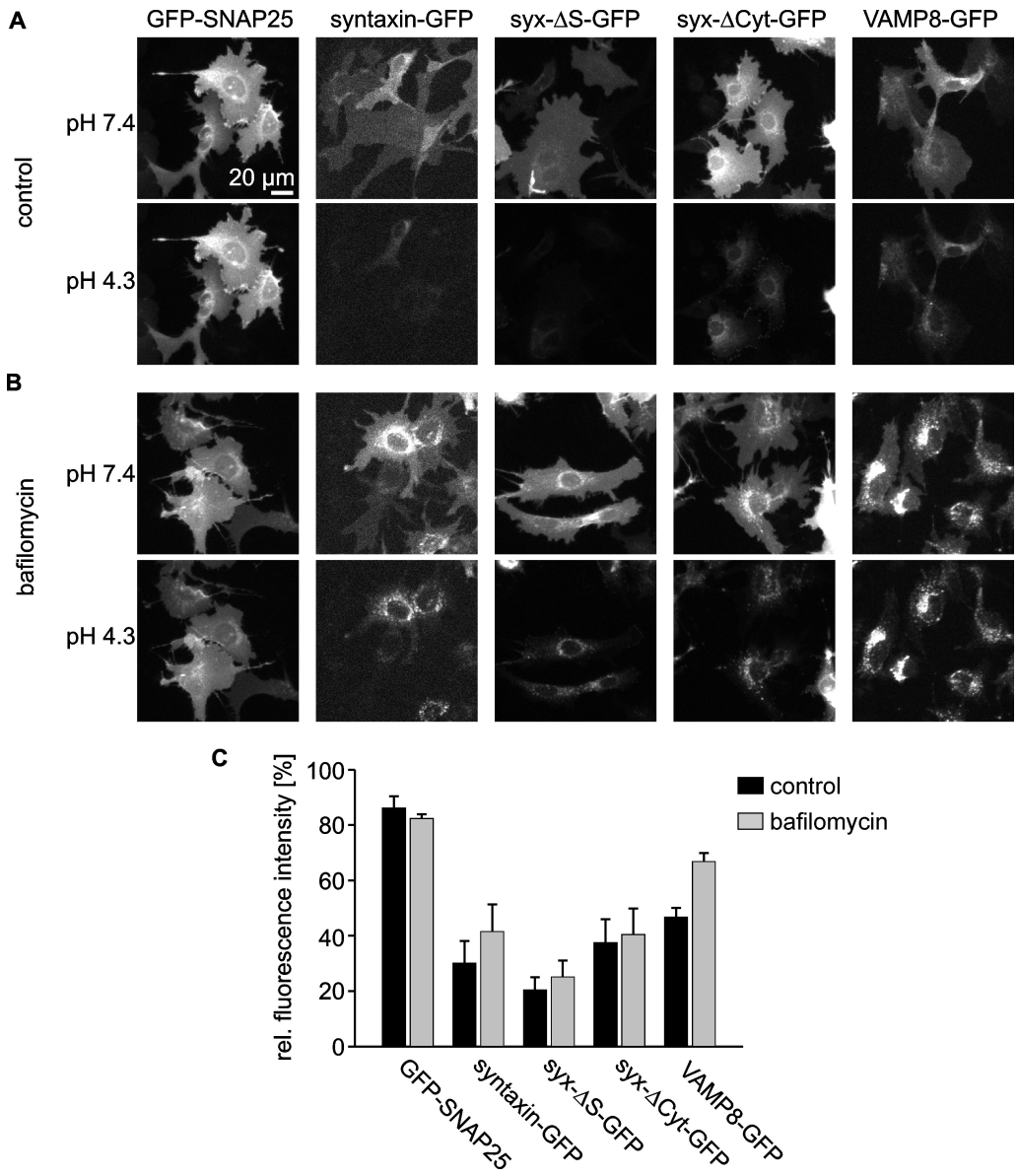

Figure 4.7: **Subcellular distribution of syntaxin, syx-ΔS and syx-ΔCyt - pH quenching.** Fraction of the expressed proteins in intracellular compartments by pH quenching of the extracellular and pH sensitive GFP (Patterson et al. 1997). Cells were either treated for 45 min with 0.2 µM bafilomycin to degrade intracellular pH gradients (**B**) or not (**A**). Two control constructs were used: GFP-SNAP25 (GFP localized to cytoplasmic periphery of the PM) and VAMP8-GFP (lysosomal and endosomal localized SNARE protein with luminal GFP). **A**/**B** HepG2 cells expressing the constructs as indicated were imaged consecutively at pH 7.4 (*upper panel*) and pH 4.3 (*lower panel*) with a 10x objective for large focal depth. Images of one construct are shown at the same scaling. **C** For analysis, cell imprints were traced, average fluorescence intensity was measured and the values at pH 4.3 were related to the starting condition at pH 7.4 for each cell. Values are given as means ± s.e.m. (n = 3 independent experiments with 16 - 38 cells per independent experiment).

tion. VAMP8-GFP, in contrast, was sensitive to pH drop and exhibited a bafilomycin sensitive pool indicating that VAMP8 is partly localized to the PM but for the most part to intracellular compartments. The intracellular signal of syntaxin increased from 30% to 41% upon bafilomycin treatment accompanied by the appearance of spotty fluorescence

in the cytosol, which is typical for lysosomal signal. Thus, a substantial pool of syntaxin is localized in intracellular compartments in HepG2 cells either through mistargeting or in the course of protein degradation. Similarly, the syx-ΔCyt-GFP showed an intracellular protein pool of 37% without bafilomycin treatment, which was mainly localized in net-like structures around the nucleus pointing towards ER retention. In line with this finding, the signal did only change marginally upon bafilomycin treatment. Syx-ΔS-GFP contained with 25% the lowest intracellular pool, which was likewise only slightly sensitive to bafilomycin.

In summary, the majority of syntaxin and its variants are targeted to the PM in HepG2 cells. However, syxtaxin and syx-ΔCyt yielded approximately 1.5-fold relative intracellular signals compared to syx-ΔS. Mistargeting to bafilomycin sensitive compartments seemed to be mediated by the intact SNARE motif, while the strong overexpression of syx-ΔCyt might be the cause for the observed ER retention.

Microscopic dissection: Additionally to the GFP quenching approach the subcellular distribution of the syntaxin variants was analyzed by STED microscopy (figure 4.8). To this end HepG2 cells were transfected with GFP- or myc-tagged syntaxin variants and the aforementioned VAMP8 as a control for an intracellular SNARE protein. Cells were fixed, permeabilized and immunostained for GFP or the myc tag. X,Z-scans were obtained every 10 µm with a confocal laser scanning microscope in STED mode, yielding a series of X,Z-sections. As a measure for the intracellular signal the integral of cytoplasmic fluorescence in all slices was related to the total fluorescence (figure 4.8).

For the GFP tagged variants of syntaxin, trends similar to the previous experiment could be observed: Syntaxin-GFP and syx-ΔCyt-GFP displayed nearly equal intracellular signals, while the variant lacking the N-terminal half of the SNARE motif, syx-ΔS-GFP, exhibited slightly higher preference for the PM. VAMP8-GFP was nearly equally distributed between PM and intracellular structures.

The pattern of intracellular distribution appeared slightly different in the myc tagged constructs: Syntaxin-myc yielded the highest localization at the PM. The proportion of intracellular signal for syx-ΔS-myc was slightly higher, however, the largest intracellular fraction could be observed for the syx-ΔCyt-myc. Note here a strong increase in absolute signals of syx-ΔCyt-myc over syxntaxin-myc, which could be responsible for the enhanced intracellular fraction.

When comparing the GFP tagged constructs, the differences among the constructs are less pronounced in contrast to the pH quenching experiment. This particularly applies for

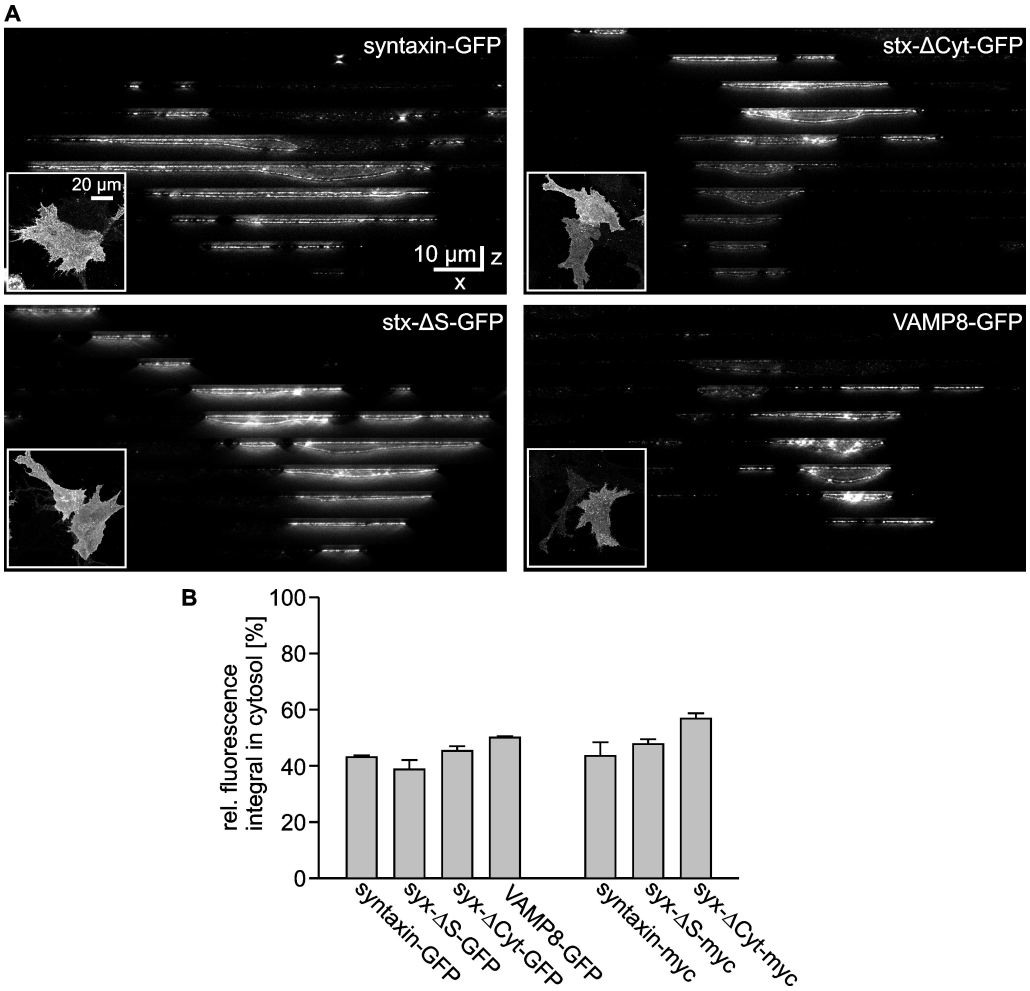

Figure 4.8: **Subcellular distribution of syntaxin, syx-ΔS and syx-ΔCyt - analyzed with 3D STED.** Fraction of myc or GFP tagged syntaxin variants in intracellular compartments by imaging with 3D STED. Cells were fixed and permeabilized prior to immunostaining with an antibody raised against the respective tag (GFP or myc). PM was labeled with concanavalin A (conjugated to Alexa-594). **A** Cells stained for the GFP tag, imaged in x/y for overview in confocal mode of the microscope (*insets*) and sliced in x/z every 10 µm for vertical dissection in STED mode (using 200 mW depletion laser intensity and 100% 3D STED mode). **B** Integral of fluorescence was summed up for all slices of one cell in ROIs tracing the whole cell or tracing the cytosol. Values of non transfected cells were subtracted and the values of the cytosol were related to the whole cell value for each cell. Cells for each construct were averaged for each independent experiment. Values are given as mean ± s.e.m. (n = 2-3 independent experiments with 7 - 26 cells per condition and experiment). Parts of sample preparation, data acquisition or analysis were conducted by Jerome Finke, Nora Karnowski and Dr. Jan-Gero Schlötel.

the control VAMP8, for which there was approximately a 20% difference in intracellular signal between pH quenching and the 3DSTED imaging. Following issues probably evoked these differences: Firstly, sample size is much smaller in confocal imaging compared to the pH quenching experiment and the insensitivity of STED requires the selection of high expressing cells for imaging. Secondly, the flat appearance of HepG2 cells impedes the separation of PM and intracellular fluorescence even when applying high resolution imaging. Nevertheless, the results presented here confirm the pH quenching experiment, in

principle, suggesting the prevailing localization of all syntaxin constructs at the PM with slight differences in manifestation among the different variants. For later quantification of the protein amount in the PM, the values of the GFP quenching approach were used due to the apparent higher accuracy in comparison to the 3D STED approach.

Direct relation of the antibody staining intensity to the expression level in intact PMs

For comparison of the cluster packing density between the three different syntaxin variants I attempted to access the antibody staining in native PMs (I_{micr}, see eq. 4.2) simultaneously with the protein amount (N_{total}, see eq. 4.2) by using a bicistronic expression system.

For this purpose the sequence of an internal ribosomal entry site 2 (IRES2) was placed between the sequence coding for the myc tagged variants of syntaxin upstream and a mRFP linked to glycosylphosphatidylinositol (GPI)- anchor as a reporter gene downstream. The obtained constructs are transcribed as one mRNA. From this mRNA the sequence upstream of IRES is translated in a normal 5′-cap-dependent manner, whereas the specific secondary structure of the IRES sequence conveys translation initiation for the downstream sequence. Therefore, the signal of the reporter should, in theory, correlate with the expression level of the myc-tagged syntaxin variants and give a measure of N_{total}.

To check for this technical prerequisite, protein amounts of syntaxin constructs and the reporter were quantitatively analyzed by western blot (figure 4.9). HepG2 cells were transfected with the IRES containing constructs and lysates from these cells were prepared after 24 h and subjected to SDS-PAGE followed by western blot.

As shown in figure 4.9, panel A, the height of the protein bands detected by the myc tag antibody matched roughly the expected size of the overexpressed syntaxin variants. syx-ΔS-myc is slightly lighter than the full lentgh syntaxin-myc, expressed by lower running height. As expected, syx-ΔCyt-myc shows the lowest running height, since it lacks almost the entire intracellular domain.

Decoration with an RFP antibody revealed multiple bands for all three constructs. Different stages of GPI anchor processing during biogenesis in the ER and Golgi might contribute to the bands obtained at about 35 kDa, 32 kDa and 29 kDa. However, degradation of the reporter protein cannot be excluded here. Intensity distribution of the single bands differed among the constructs: In syntaxin the 32 kDa band predominated in contrast to the pattern of syx-ΔS and syx-ΔCyt with the major band at 35 kDa. Since maturation of the reporter protein is irrelevant for mere comparison of upstream and downstream protein

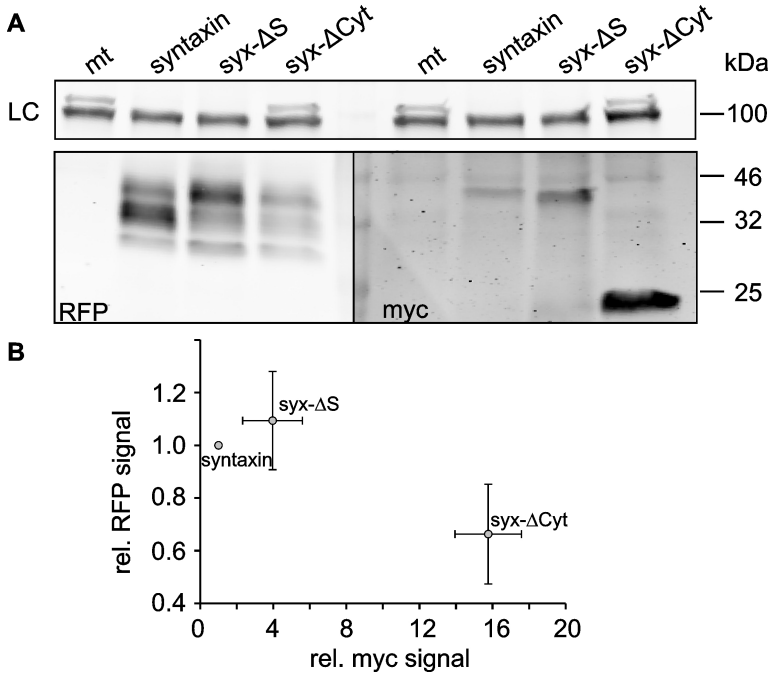

Figure 4.9: **Western blot of myc tagged constructs and an IRES linked reporter protein.** **A** Western blot from lysates of cells transfected with a bicistronic vector containing the sequence for the syntaxin variant as indicated (syntaxin-myc, syx-ΔS-myc or syx-ΔCyt-myc) and the reporter protein RFP, fused to a GPI attachment signal linked via an IRES2 sequence for translation from one mRNA. Mt: mock transfected cells; LC: loading control (transferrin receptor). Each lysate was loaded twice per gel, resulting in two identically loaded halves. Blots were cut after blotting as indicated for incubation with either myc tag, RFP or transferrin receptor antibody. **B** The RFP and the myc signals were quantified including all antibody specific bands, normalized to the LC and related to the values for RFP or myc of syntaxin-myc. Values are shown as mean ± s.e.m. (n = 3).

ratios, all RFP bands were included in the quantification and the values were related to the myc signal (figure 4.9, panel B).

In order to be able to use GPI linked RFP as a reporter for N_{total}, it is mandatory that its signal in the western blot correlates linearly with the corresponding myc signal. However, when syx-ΔS and syx-ΔCyt signals for myc and RFP were normalized to syntaxin the increase in myc signal did not entail an increase of RFP signal. In syx-ΔCyt samples the signal of the reporter was even diminished despite high protein content of syx-ΔCyt. Apparently, the theoretical considerations about ratio of reporter and upstream protein of interest do not hold true in our experimental system. Possible reason could be the pronounced overexpression of syx-ΔCyt saturating protein translation. The IRES approach therefore seems to be unsuitable to correct quantitatively for differences in expression level and thus impede the direct relation of I_{micr} and N_{total} via epifluorescence microscopy.

Comparison of epitope accessibility depending on cytoplasmic syntaxin domains

IRES was not applicable to determine I_{micr} and N_{total} directly by microscopy for comparing cluster packing density in syntaxin-myc, syx-ΔS-myc and syx-ΔCyt-myc. Therefore, I turned to a comparative study of microscopy and western blot. Formally, protein signal in the latter follows a similar principle as described by equation 4.1 in section 4.1.2.3. However, the influence of detergents and reducing agents in a non-native SDS-PAGE preceding the western blot disassembles protein clusters. Hence, f_{access} should be similar among the different constructs. Furthermore, using whole cell lysates renders the factor f_{sort} unnecessary. The western blot therefore allows for comparative access of N_{total} for the different constructs.

For the experiment HepG2 cells overexpressing syntaxin-myc, syx-ΔS-myc or syc-ΔS-myc were split into two fractions: one was used for immunostaining with a myc tag antibody and the appropriate fluorescently labeled secondary antibody to access I_{micr}. The other fraction was lysed and subjected to SDS-PAGE followed by western blot analysis for determination of relative N_{total}. Figure 4.10, panel A, shows cells expressing the three different constructs imaged with focus on the basal membrane of the cells. As illustrated, I_{micr} increased substantially in the order syntaxin-myc, syx-ΔS-myc and syx-ΔCyt-myc.

The intensity distribution among the constructs slightly differed in the corresponding western blots. In the particular experiment shown in 4.10, panel B, the strongest signal arose from the syx-ΔS-myc followed by syntaxin-myc and syx-ΔCyt-myc. However, this order changed between the independent repetitions of the experiment despite identical conduction. This inconsistency is also expressed by the large standard errors of the quantitative analysis of N_{total} represented in figure 4.10, panel C.

Comparing the quantitative analysis of microscopy (I_{micr}) and western blot (N_{total}) a stepwise increase in relative signal from syntaxin to syx-ΔS to syx-ΔCyt can be observed. However, the increase is more pronounced in the packing sensitive microscopy than in the packing insensitive western blot.

For comparing f_{access} (see equation 4.2) as a measure for cluster packing density, the relative signal of I_{micr} was divided by N_{total}, which was corrected for different intracellular distributions according to section 4.1.2.3 (figure 4.10, panel D). When syntaxin ratio is set to 1, syx-ΔS and syx-ΔCyt obtain elevated ratios of 3.9 and 3.2, respectively. This result suggests, that the accessibility of the syx-ΔS-myc and syx-ΔCyt-myc epitope is similarly elevated in comparison to syntaxin-myc. Possible explanation for this observation is increased intermolecular distances within protein clusters of the two constructs that

lack parts of the cytoplasmic domain. However, this result has to be treated with caution because of the high variability within one construct. A detailed discussion on this matter is provided in section 5.1.1.

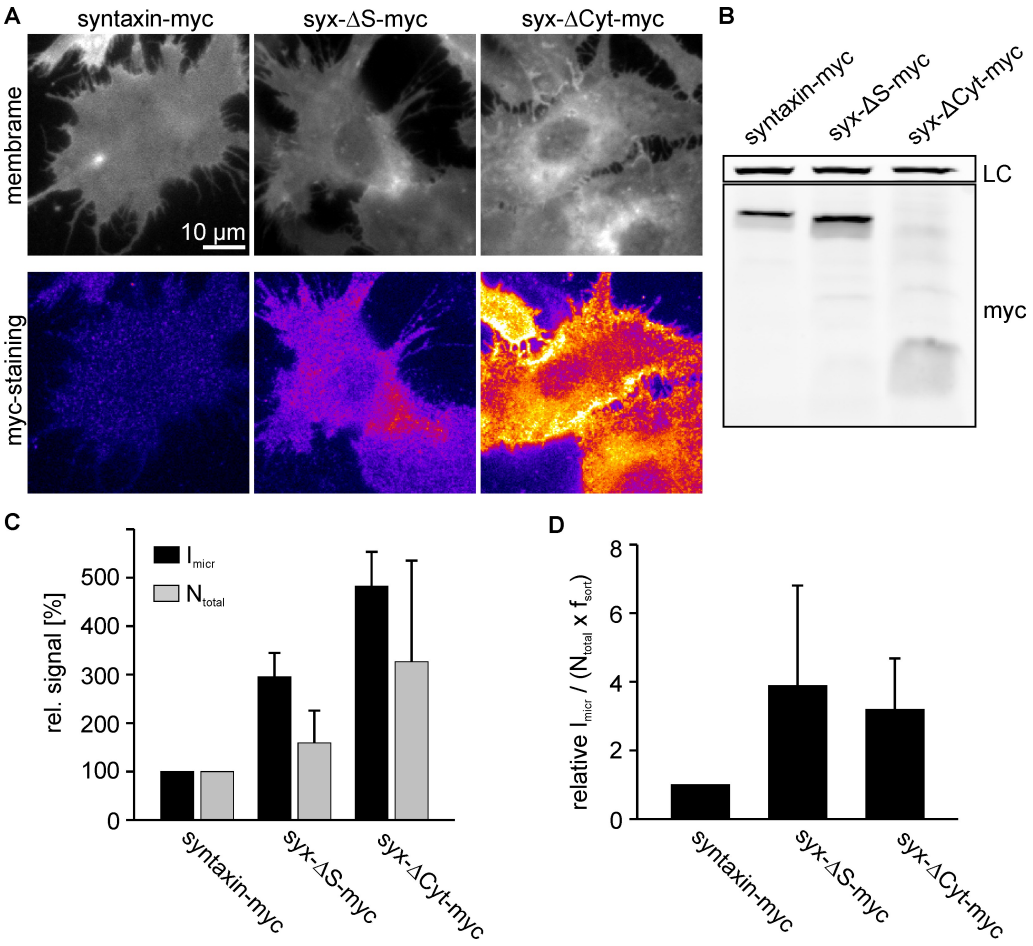

Figure 4.10: **Comparative analysis of antibody labeling in intact PM versus western blot.** Cells are transfected with the constructs as indicated and split into two fractions for microscopy and western blot. **A** For microscopy, fixed cells underwent immunostaining for the myc-tag (lower panels; shown applying the 'fire' lookup table). The membrane dye TMA-DPH was used for identification and selection of cells (*upper panel*). Per independent experiment and condition 70 – 220 cells were imaged for estimating the transfection efficiency. From these cells, and additionally imaged transfected cells, the myc-staining intensity (I_{micr}) was quantified (27-119 cells per construct and per individual experiment). **B** Equal amounts of total protein were analysed by SDS-PAGE and western blotting, using GRP78 or pan-cadherin as loading controls (LC). Myc-band intensities were quantified and normalized to the respective loading control. In addition, values were corrected for the differences in transfection efficiencies to obtain N_{total}. **C** I_{micr} and N_{total} relative to syntaxin-myc, averaged from three independent experiments. **D** For each day, the ratio of I_{micr} and N_{total}, which was corrected for the membrane resident fraction as determined in section 4.1.2.3, was calculated and averaged. Values are shown as mean ± s.e.m. (n = 3).

4.1.3 Lateral mobility of syntaxin in the PM of non neuronal cells - implication of the cytoplasmic domain

Due to the uncertainties described in the previous section, an alternative approach was applied to substantiate the role of the cytoplasmic domain in syntaxin clustering. Therefore, I moved to a dynamic experimental setup by determining the lateral mobility of syntaxin, syx-ΔS and syx-ΔS-Cyt quantitatively.

4.1.3.1 Mobility of syntaxin, syx-ΔS and syx-ΔS-Cyt in HepG2 cells

The link between clustering and mobility of syntaxin in PC12 cells had been drawn in previous studies (Sieber et al. 2007). The authors proposed that the mobility of free molecules deteriorated when molecular interactions attracted them into the clustered state. However, in PC12 cells interaction with SNAP25 or endogenous syntaxin could likewise contribute to the mobility restriction.

Therefore, the aim of the following experiment was to dissect the impact of the cytoplasmic domain explicitly. To do so, syntaxin mobility was studied in HepG2 cells, a cellular system of non-neuronal origin lacking potentially interacting endogenous syntaxin 1A and SNAP25. The diffusion of syntaxin molecules was monitored by means of fluorescence recovery after photobleaching (FRAP) in live cells. Since tracing proteins in FRAP requires fluorescent labeling, the GFP tagged syntaxin variants were used for transfection of HepG2 cells. The visualization of syntaxin-GFP, syx-ΔS–GFP or syx-ΔCyt-GFP in live cells by a confocal laser scanning microscope is displayed in the left image of figure 4.11, panel A. The pinhole of the laser scanning microscope allows to spatially confine the signal to a specific focal plane, in this case the basal PM.

The GFP fluorescence was bleached within a small region of the PM and the fluorescence was recorded at 1 Hz for about 3 min. Lateral diffusion of GFP tagged proteins lead to mixing of bleached and non-bleached molecules resulting in an increase of fluorescence in the bleached ROI (see 4.11, panel A). The increase of fluorescence intensity was followed over time and the resulting recovery traces for each construct were averaged and fitted with a hyperbolic function to determine the half time of recovery $t_{1/2}$ (4.11, panel B) (see 3.2.10 for details on the analysis). $t_{1/2}$ is a key measure for the mobility of the protein and thus constitutes a suitable parameter for the quantitative comparison of the different constructs.

As depicted in 4.11, panel C, the constructs displayed a step wise increase in mobility from syntaxin-GFP with $t_{1/2}$=11.8 s, to syx-ΔS-GFP with $t_{1/2}$=7.6 s, to syx-ΔCyt with

$t_{1/2}$=5.8 s. The maximal fluorescence recovery in the bleached region, indicating the fraction of mobile proteins, increased from syntaxin-GFP to syx-ΔS-GFP to syx-ΔCyt-GFP. To rule out that the increased mobility of syx-ΔS and syx-ΔCyt merely resulted from higher expression levels of those proteins, recovery half times on single cell level were compared as to their intensity (figure 4.11, panel D). Strikingly, only syntaxin-GFP displayed a slight tendency to reduced mobility with rising protein level, while syx-ΔS and syx-ΔCyt were unaffected.

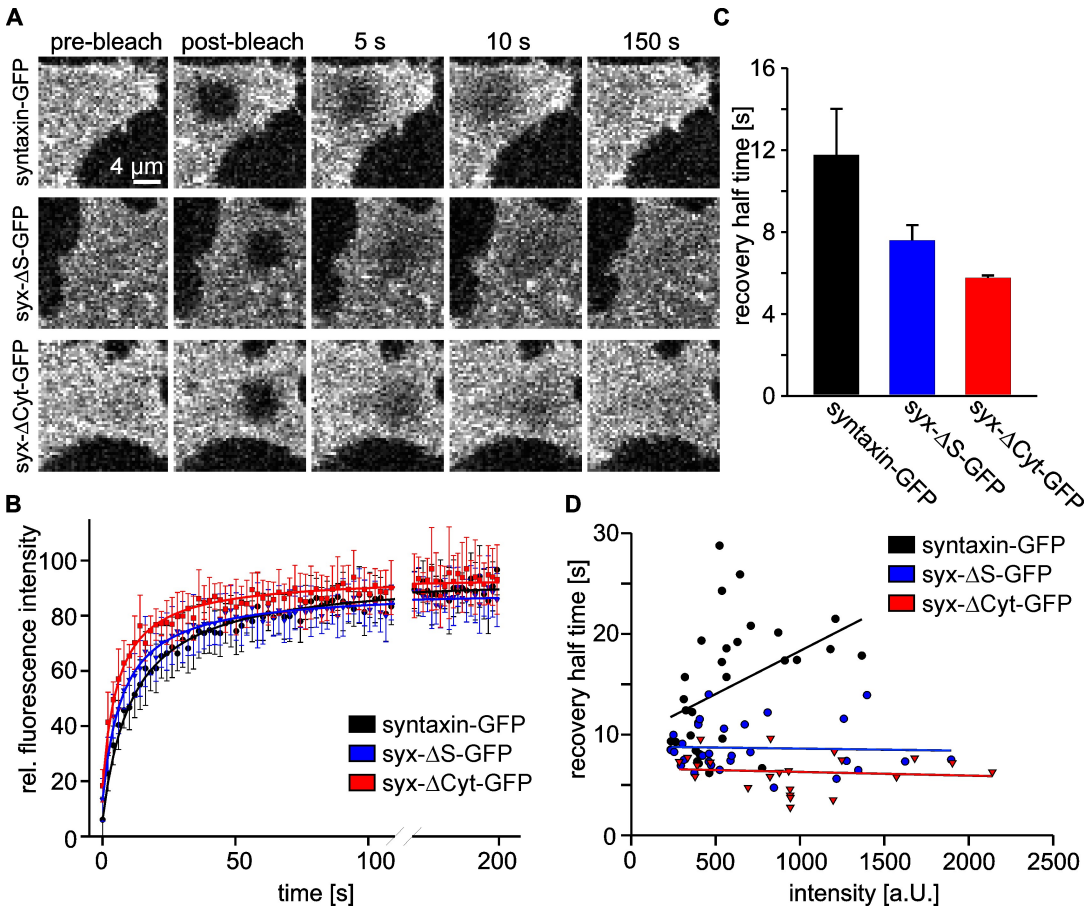

Figure 4.11: **The intact SNARE motif is involved in mobility restriction of syntaxin in non-neuronal cells.** Analysis of fluorescence recovery after photobleaching of syntaxin-GFP and the deletion constructs syx-ΔS-GFP and syx-ΔCyt-GFP in live cells. **A** Live cells expressing the indicated constructs are imaged by confocal microscopy at the basal membrane. For analysis of cells with similar intensities, bright syx-ΔS-GFP and syx-ΔCyt-GFP cells were not selected for imaging. In a squared region of interest (ROI) fluorescence was bleached (compare pre-bleach and post-bleach images). Recovery of fluorescence was monitored at an imaging frequency of 1 Hz. Images are shown at the same scalings. **B** Averaged recovery traces from several cells imaged for one experiment fitted with a hyperbola function (solid line). For clarified view, only every second data point is displayed in the figure. Values are given as mean ± s.d. **C** Half times of recovery obtained by fitting hyperbola functions to traces as shown in **B**. Values are given as mean ± s.e.m. (n = 3 independent experiments with each 8 - 18 cells per construct). **D** For all experiments, half times of recovery were also determined for individual cells and plotted against their pre-bleach intensity (5 - 13 cells per construct).

As reported in section 4.1.2.3 about 20-40% of the visible GFP is located in intracellular structures. Such intracellular fluorescence cannot be excluded entirely in the microscopic setup used. Thus, it is formally possible that the measured differences in mobility of syntaxin-GFP, syx-ΔS-GFP and syx-ΔCyt-GFP are influenced by the intracellular GFP pools. To exclude this, the experiment was repeated on PM sheets.

4.1.3.2 Mobility of syntaxin, syx-ΔS and syx-ΔS-Cyt in HepG2 PM sheets

To determine the mobility of syntaxin, syx-ΔS and syx-ΔS-Cyt in PM sheets, FRAP measurements were carried out as described in 4.1.3.1 except for sheet preparation being conducted shortly before imaging. Figure 4.12, panel A presents exemplary pictures of sheets at the indicated time points of the measurement showing the recovery of fluorescence in the bleached area. As depicted in 4.12, panel B, the recovery traces are similar to the ones obtained in intact cells but with clearer difference among the constructs. With a maximal recovery of about 47% syntaxin-GFP comprised the highest immobile fraction, followed by syx-ΔS-GFP with 26% and syx-ΔCyt-GFP with 12%.

Similar step wise reduction of $t_{1/2}$ could be observed in the order syntaxin-GFP > syx-ΔS-GFP > syx-ΔCyt-GFP when comparing with the values of intact cells (section 4.1.3.1). In absolute terms however, $t_{1/2}$ was increased. Particularly, the $t_{1/2}$ of syntaxin-GFP almost doubled to $t_{1/2}$=26.7 s. Slight changes were measured for syx-ΔS-GFP to $t_{1/2}$=10.8 s, whereas $t_{1/2}$ of syx-ΔCyt-GFP remained with 6.7 s nearly unchanged. As for intact cells, only $t_{1/2}$ of syntaxin-GFP shows slight tendency to rise with increasing fluorescence intensity, whereas syx-ΔS and syx-ΔS-Cyt were unaffected.

One reason for the prolonged recovery half times of syntaxin-GFP in PM sheets could be the formation of cis-SNARE complexes. These complexes are inactive SNARE aggregations and were previously linked to aging effects of sheets (Lang et al. 2002). Along these lines, half times of recovery of syntaxin-GFP within one freshly prepared sample were plotted for the acquisition sequence, which is an indirect measure for the age of the sheet. Note here, that maximal observation time of one sample with freshly prepared sheets was about 25 min. As depicted in 4.12, panel E, recovery half times did not rise generally with the acquisition sequence. Average recovery half time between the first and second acquisition slightly increased, which is in line with a previous study reporting on the formation of a small pool of cis-SNARE complexes within the first minutes after sheeting (Bar-On et al. 2008). However, this pool is not large enough to entirely account for the difference between the constructs.

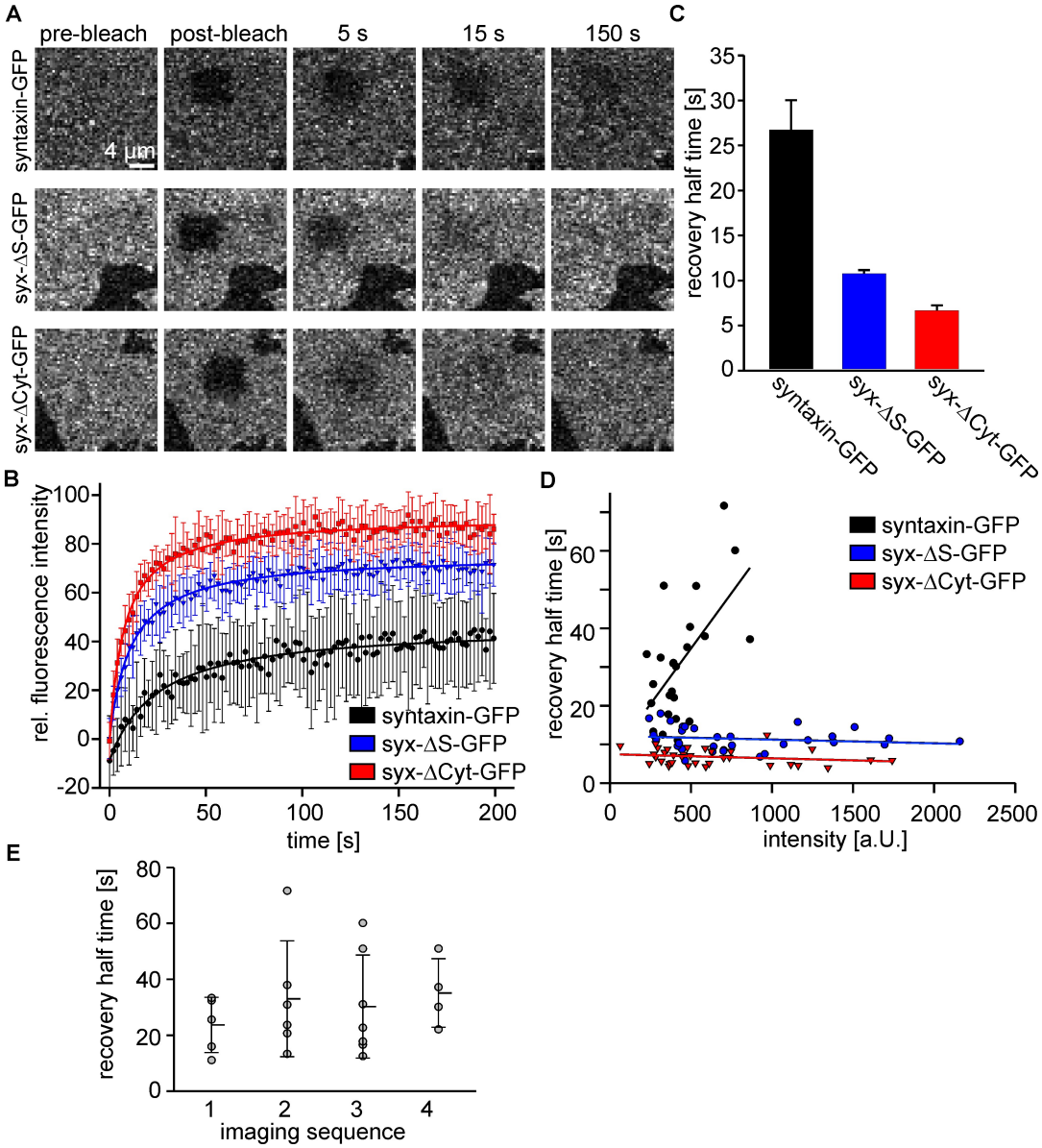

Figure 4.12: **The intact SNARE motif is involved in mobility restriction of syntaxin in PM sheets of non-neuronal cells.** Analysis of fluorescence recovery after photobleaching of syntaxin-GFP and the deletion constructs syx-ΔS-GFP and syx-ΔCyt-GFP in freshly prepared sheets. **A** Sheets of cells expressing the indicated constructs are imaged by confocal microscopy. For analysis of cells with similar intensities, bright syx-ΔS-GFP and syx-ΔCyt-GFP sheets were not selected for imaging. In a squared region of interest (ROI) fluorescence was bleached (compare pre-bleach and post-bleach images). Recovery of fluorescence was monitored at an imaging frequence of 1 Hz. Images are shown at the same scalings. **B** Averaged recovery traces from several cells imaged for one experiment fitted with a hyperbola function (solid line). For clarified view only every second data point is displayed in the figure. Values are given as mean ± s.d. **C** Half times of recovery obtained by fitting hyperbola functions to traces as shown in B. Values are given as mean ± s.e.m. (n = 3 independent experiments with each 9 - 17 PM sheets per construct). **D** For all experiments, half times of recovery were also determined for individual sheets and plotted versus the pre-bleach intensity (24 - 34 PM sheets per construct). **E** Half times of recovery of syntaxin-GFP in individual sheets were plotted against their respective imaging sequence. Mean recovery half times ± s.d. are indicated.

In conclusion, the mobility of syntaxin-GFP is reduced compared to syx-ΔS and syx-ΔCyt independently of interactions with SNAP25. Taken together, these findings indicate that interactions among the cytoplasmic protein domains of syntaxin, in particular the N-terminal SNARE motif, are responsible for stronger attraction into the protein cluster.

4.2 Spontaneous lipid transfer (SLT) at ER-PM membrane contact sites (MCS)

MCS are highly abundant among cellular membranes and are involved in essential cellular functions such as lipid and protein transport and intra- as well as intercellular communication. The tight connections between cellular membranes constitute experimentally challenging structures. It is possible to isolate membrane material containing contact sites using, for example, fractionation via density gradients. However, isolation protocols are time consuming and require large amounts of starting material. Moreover, the purity of the preparation poses a major difficulty, since most organelles exhibit multiple contacts with different organelles. Therefore, it is difficult to distinguish between the different organellar membranes after the isolation and to examine them separately. In particular the ER establishes direct physical contacts with all other cellular membranes including the PM. Apart from these concerns, supra-molecular structures, like MCS, depend on diverse lipid-lipid, lipid-protein and protein-protein interactions at the same time (see section 1.3). Preferred preparations thus demand the maintenance of most possible features of the native system as highlighted in section 1.3.3.

In this study, a novel preparation of ER-PM MCS with tightly tethered ER to the intact PM was developed. The visualization of PC and the lipid composition of ER and PM bilayers regarding PC, cholesterol, PI(4,5)P_2 and PS was examined. Further, it was analyzed if the system contains functional ER and is of physiological relevance. Protease treatment was used to gain information on the stability of the ER tethers. Finally, the system was applied to probe for spontaneous lipid transfer (SLT) of the two different highly abundant membrane lipids, cholesterol and PC.

4.2.1 ER-PM MCS preparation

The intension of the novel approach described here was to remove the bulk of the ER while maintaining tight connection between PM and ER by keeping the tethering complexes and a small piece of ER intact. For that purpose, I made use of the cell unroofing technique. As explained in section 1.3.3 this preparation preserves the basic properties of a PM concerning composition and curvature.

4.2.1.1 Visualization of ER on PM sheets

In order to visualize the ER, HepG2 cells were transfected with either of two different fluorescently tagged ER marker proteins, termed ER-RFP or RFP-Sec61β. ER-RFP refers

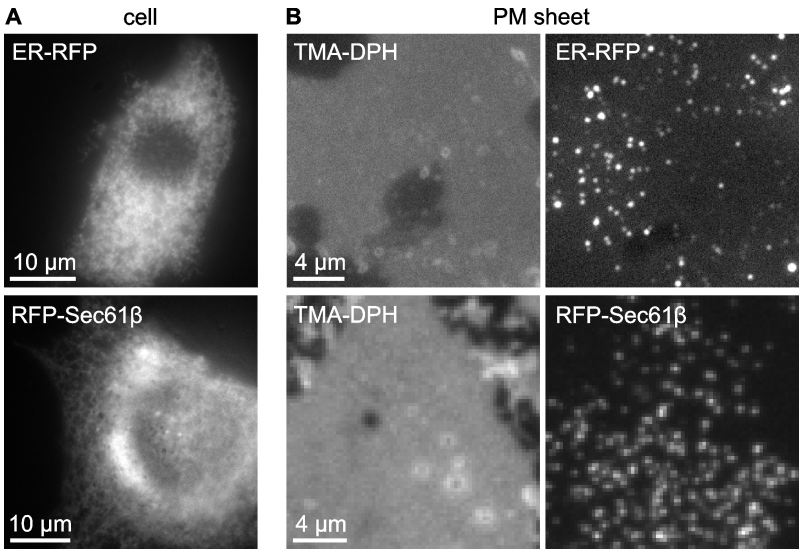

Figure 4.13: **Visualization of ER in whole cells and on PM sheets. A** Epifluorescence images of HepG2 cells overexpressing the ER marker proteins ER-RFP or RFP-Sec61β as indicated. **B** PM sheets of the same cells as in **A** with TMA-DPH used for PM staining (*left images*). Note the spotty fluorescence of the ER marker remnants on the PM sheets (*right images*). Figure and legend modified from Merklinger et al. 2016.

to a RFP fused to the signal sequence of calreticulin and the ER retention signal KDEL. Sec61β is an integral component of the ER membrane. Together with other Sec61 proteins it builds up a complex for protein translocation at the ER.

As expected, overexpression of both proteins resulted in net-shaped staining patterns in whole cells imaged with an epifluorescence microscope (figure 4.13, panel A). The signal surrounded the nucleus and spread throughout the interior of the cell, which is typical for an ER staining pattern. After the application of a short ultrasound pulse the upper part of the cell was removed leaving an intact PM as displayed by the homogenous TMA-DPH membrane staining (figure 4.13, panel B). The major part of the ER marker signal was successfully eliminated during the sheeting process. However, some RFP signals of ER-RFP as well as of RFP-Sec61β were scattered across the entire PM sheet displayed as single spots. This observation indicates strong contact points between the ER and the PM which remain intact even after the application of mechanical forces which removed a substantial part of the ER. Alternatively, the spots represent ER fragments sticking unspecifically to the PM.

4.2.1.2 PC as a marker lipid for the ER membrane

To further test whether the spots actually represented ER membranes, PC was chosen as a marker lipid due to its about twofold enrichment in ER membranes when compared to

the PM (Meer 2011).

A metabolic labeling strategy, developed by Jao et al. 2009, was employed to enable visualization of PC. In brief, the specific cell medium was supplemented by propargyl choline (pC). Choline transporters and the enzymes in the biosynthetic pathway of choline lipids recognize the modified choline as a substrate and process it for the synthesis of propargyl-PC (pPC; illustrated in figure 4.14, left panel) as well as propargyl-lyso-PC, propargyl-ether-PC and propargyl-SM (Jao et al. 2009). In this way, the natural fatty acid chain variation found in PC is preserved. The alkyne group of the pC enables a copper catalyzed cycloaddition of an azide coupled fluorophore yielding a 1,2,3-triazol product. For the first experiments, the dye azido-sulfo-Bodipy (azido-sBP) was used for cycloaddition. The resulting fluorescent PC is illustrated in figure 4.14, right panel.

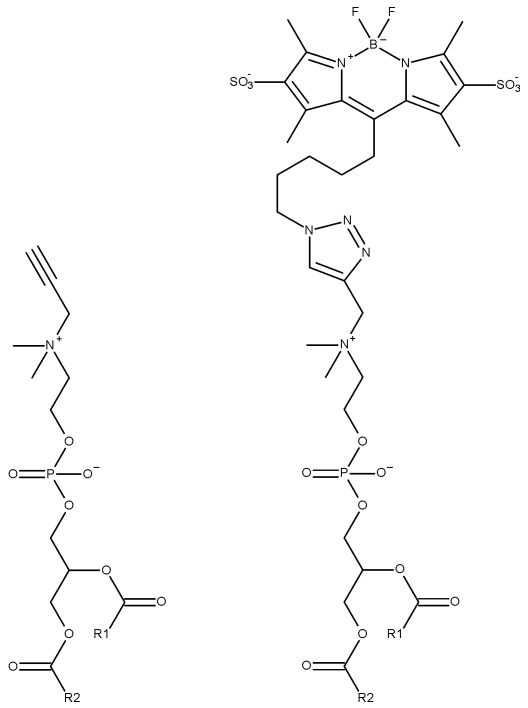

Figure 4.14: **Chemical sketch of pPC and sBP-PC.** pPC (*left*) resulting from metabolic labeling with propargyl choline (pC) differs from natural PC only in the alkyne group linked to tertiary ammonium in the choline headgroup, but not in the fatty acid tail composition (R1 and R2)(Jao et al. 2009. Copper catalyzed cycloaddition of the azido-sulfo-bodipy (azido-sBP) results in the 1,2,3-triazol containing fluorescent sBP-PC (*right*). Figure and legend modified from Merklinger et al. 2016.

Of note, previous evaluation by thin layer chromatography revealed that the major fraction of about 98% pC is incorporated into PC in the experimental system used in this study (Spitta 2012). To further verify the specificity of PC labeling, PM sheets generated from metabolically labeled HepG2 cells were treated with a phospholipase C (PC-LPC) from *Clostridium perfringensis* (EC 3.1.4.3) prior to cycloaddition. This enzyme hydrolyses PC

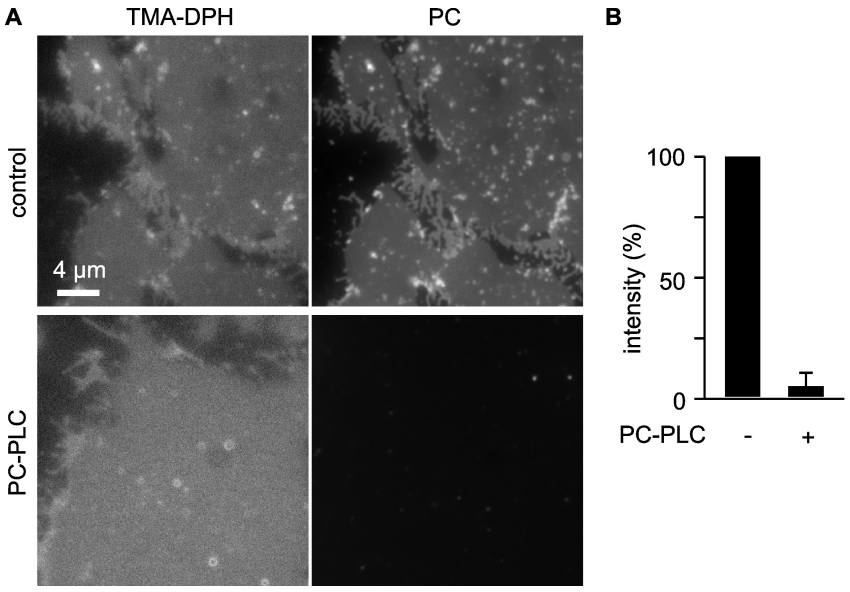

Figure 4.15: **Specificity of metabolic PC labeling. A** Epifluorescence images of PM sheets from HepG2 cells labeled metabolically. Prior to cycloaddition of azido-sBP for PC visualization sheets were incubated with the phospholipase C from *Clostridium perfringens* (EC 3.1.4.3) (PC-PLC; *lower panel*) or with buffer as a control (*upper panel*). Buffer in both conditions contained 50 mM $CaCl_2$ for suppression of SM hydrolyzing activity of the PC-PLC (Pastan et al. 1968), which tended to reduce PC spots on the PM sheets when compared e.g. with figure 4.16, panel B, *left*. **B** ROIs were placed on PM sheets in the TMA-DPH channel for unbiased analysis of average fluorescence intensity of the PC signal. The average values for the PC-PLC condition were related to the averaged control values for each individual experiment. Values are given as mean ± s.e.m. (n = 3 individual experiments). Figure and legend modified from Merklinger et al. 2016

to 1,2-diacyl-sn-glycerol and choline. However, in principle it can also react with other choline lipids such as sphingomyelin. In order to diminish the affinity of the hydrolase to sphingomyelin, 50 mM $CaCl_2$ was added to the incubation buffer (Pastan et al. 1968). As presented in figure 4.15, PC-PLC treatment reduced the cycloaddition signal by more than 90%, confirming that PC is the major lipid observed by metabolic labeling in this current experimental system.

Returning to the assessment of PC as a marker lipid for the ER membrane, the cellular localization of the PC signal in HepG2 cells was examined. To this end pC fed cells were directly fixed with PFA. As PFA causes partial cell ruptures, internal membranes become accessible to subsequent cycloaddition of the dye. Indeed, when imaged with an epifluorescence microscope at the equatorial plane of the cell (figure 4.16, panel A), a net-like structure could be observed similar to the RFP signal of the ER marker proteins in figure 4.13. TIRF microscopy was employed to omit fluorescence from the cytosol and gain a clearer picture of the cytoplasmic periphery of the PM. This technique allows for the selective illumination of the PM and its surrounding within a layer of approximately 100 nm (Steyer et al. 2001) (see 1.3.3). As can be seen in figure 4.16, panel A, the pictures

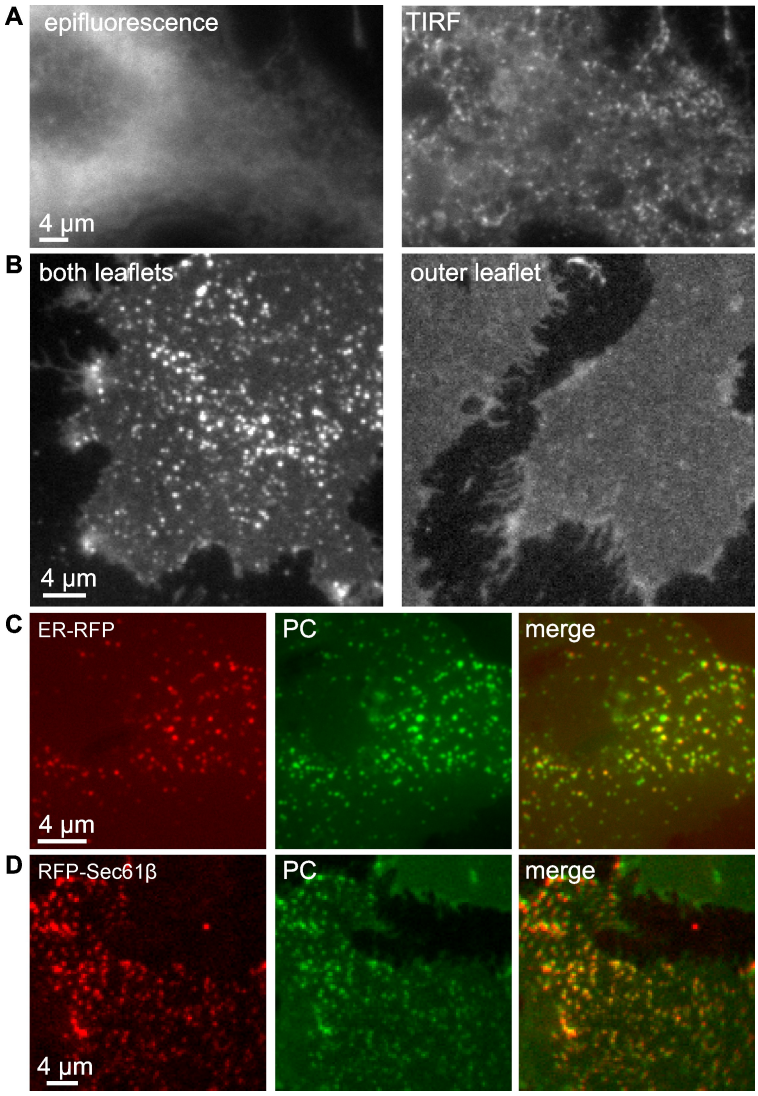

Figure 4.16: **ER membranes visualized by the marker lipid PC. A** Epifluorescence (*left*) and TIRF image for selective illumination of the basal PM (*right*) of HepG2 cells labeled with fluorescent PC. Fixation of cells allowed for intracellular PC labeling. **B** Fluorescent PC signal in PM sheets from metabolically labeled cells. Cycloaddition of sBP was either performed on freshly prepared PM sheets (*left*) or on intact cells for labeling only the outer leaflet at 4 °C (*right*). **C/D** Overlap of ER marker and PC signal on PM sheets. PM sheets from metabolically labeled HepG2 cells expressing ER marker proteins ER-RFP (**C**) or RFP–Sec61β (**D**) were imaged for RFP (*left images*) prior to cycloaddition and imaging of the fluorescent PC (*middle images*). Sheets were aligned based on the TMA-DPH image (not shown). The overlayed images (*right images*) show a high degree of colocalization despite small changes in sheet structure due to the incubation time of about 1 h between the recordings. **A-D** Examples are shown from independent experiments (n $\geq$ 3). Figure and legend modified from Merklinger et al. 2016.

revealed a spotty staining pattern. When comparing this image to the epifluorescence micrograph the intensity peaks near the PM seemed to be connected to the tubular network that spreads throughout the cell.

To asses if these extensions of the ER membrane close to the PM could be retained in the PM sheet preparation, metabolically labeled cells were sheeted prior to the cycloaddition.

Remarkably, the PC-enriched membrane spots remained on the PM sheet (figure 4.16, panel B)). To further confirm that these spots result from intracellular structures, the cycloaddition was performed on live cells at 4 °C prior to sheeting. Under these conditions the hydrophilic dye should not be able to permeate the PM and should only react with alkyne groups at the outer leaflet of the PM. The resulting staining of the PM sheet appeared uniform without any spotty structures (figure 4.16, panel B). Accordingly, the PC enriched membrane fragments were a result of structures at the cytoplasmic side of the PM.

To substantiate the relation of ER marker remnants and the PC enrichments on the PM sheets, a double staining was performed (figure 4.16, C and D). To this end, HepG2 cells were transfected with the ER marker proteins ER-RFP or RFP-Sec61β and additionally fed with pC. RFP signal on the PM sheets was imaged in advance to exclude bleed-through from the PC signal into the RFP channel and to avoid false positive results. The coverslip was then removed from the microscope and membranes subsequently underwent cycloaddition with azido-sBP. Priorly taken TMA-DPH images were used as a reference to enable PC imaging of the same sheets during the second round of imaging. The shape of PM sheets slightly changed between the two imaging steps as a consequence of the in-between incubation time. Accordingly, perfect alignment between the RFP and PC images could not be attained, preventing quantitative analysis of colocalization. Nevertheless, nearly 100% of the ER-RFP and RFP-Sec61β spots had a corresponding spot in the PC image. This strong overlap between the spots arising from the ER marker proteins and the PC spots indicates that the PC spots indeed represent ER membranes.

Since PC is as well a general membrane marker, it is important to ask to what extent the locally enriched PC signal may reflect membrane invaginations. To answer this question, metabolically labeled HepG2 cells were sheeted, fixed and after the cycloaddition reaction immunostained for clathrin or caveolin, markers for endocytic invaginations. Two approaches were used to analyze the amount of colocalization between PC spots and either caveolin or clathrin, the Pearson correlation coefficient (PCC) and a spot-wise colocalization. The PCC is a common method to quantify interrelation between two variables. In image analysis, it is used to analyze colocalization of fluorescence intensity peaks in two different channels. The PCC ranges from -1 to 1, where 1 reflects perfect colocalization and -1 perfect negative colocalization. In a second analysis, a spot wise overlap was analyzed. To this end spots in one channel were surrounded by a circular ROI and transferred to the aligned second channel and overlapping spots were quantified (for detailed descrip-

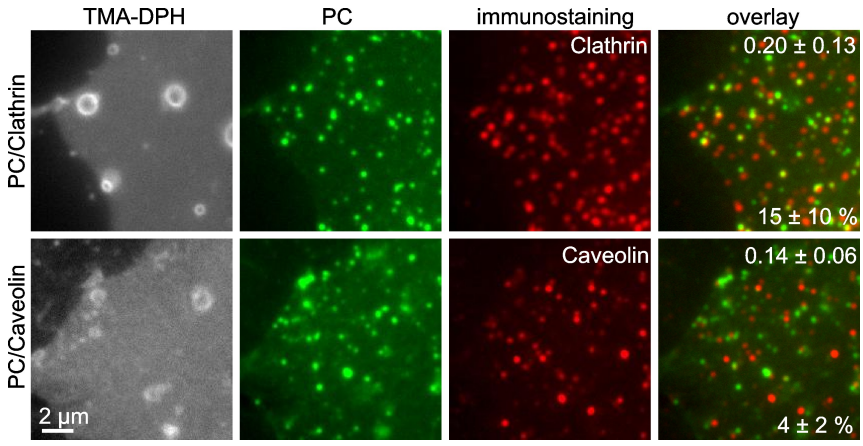

Figure 4.17: **Overlay of clathrin and caveolin with PC spots.** Epifluorescent micrographs of HepG2 PM sheets with fluorescently labeled PC and immunostaining for clathrin (*upper panel*) or caveolin (*lower panel*). Colocalization of PC and immunostaining was analyzed calculating the Pearson correlation coefficient (PCC) (top value in the overlay image) or based on analysis of individual PC spots (percentage of overlapping spots; indicated by the bottom values in the overlay image). Values are given as mean ± s.e.m. (n = 3 independent experiments). Figure and legend modified from Merklinger et al. 2016.

tion see 3.2.15). As depicted in figure 4.17, only 15% of the PC spots overlapped with clathrin and 4% with caveolin, supported by the relatively low value for PCC of 0.2 and 0.14, respectively. Thus the large majority of spots do not arise from an increase in local membrane area due to invaginations.

Taken together, these results suggest that pPC is a suitable marker lipid for the ER membrane localized at the tight association between the PM and ER, that can be preserved on the PM sheets.

4.2.1.3 Lipid composition of ER-PM contact sites

Preserving the lipid composition of the two compartments is of great interest when investigating lipid transfer at the contact sites. Assessing this issue in more detail, I stained PM sheets with two general membrane dyes, R18 and CellMask and analyzed their correlation with the PC signal. Both general membrane dyes exhibit amphiphilic structure with a hydrophobic membrane anchor attached to a hydrophilic fluorescent dye. In principle, they should be able to stain the ER membranes equally well. Interestingly, R18 and CellMask showed only 30% and 63% spot-wise overlap with the PC signal, respectively (figure 4.18, panel A). The spot intensity above background was measured to quantify the enrichment of the dyes in the ER spots (figure 4.18, panel B). While a 150% increase over the PM staining was observed for PC labeling, R18 and CellMask increased only to 10 and 16%, respectively. Thus, the used membrane dyes differ in their ability to stain the

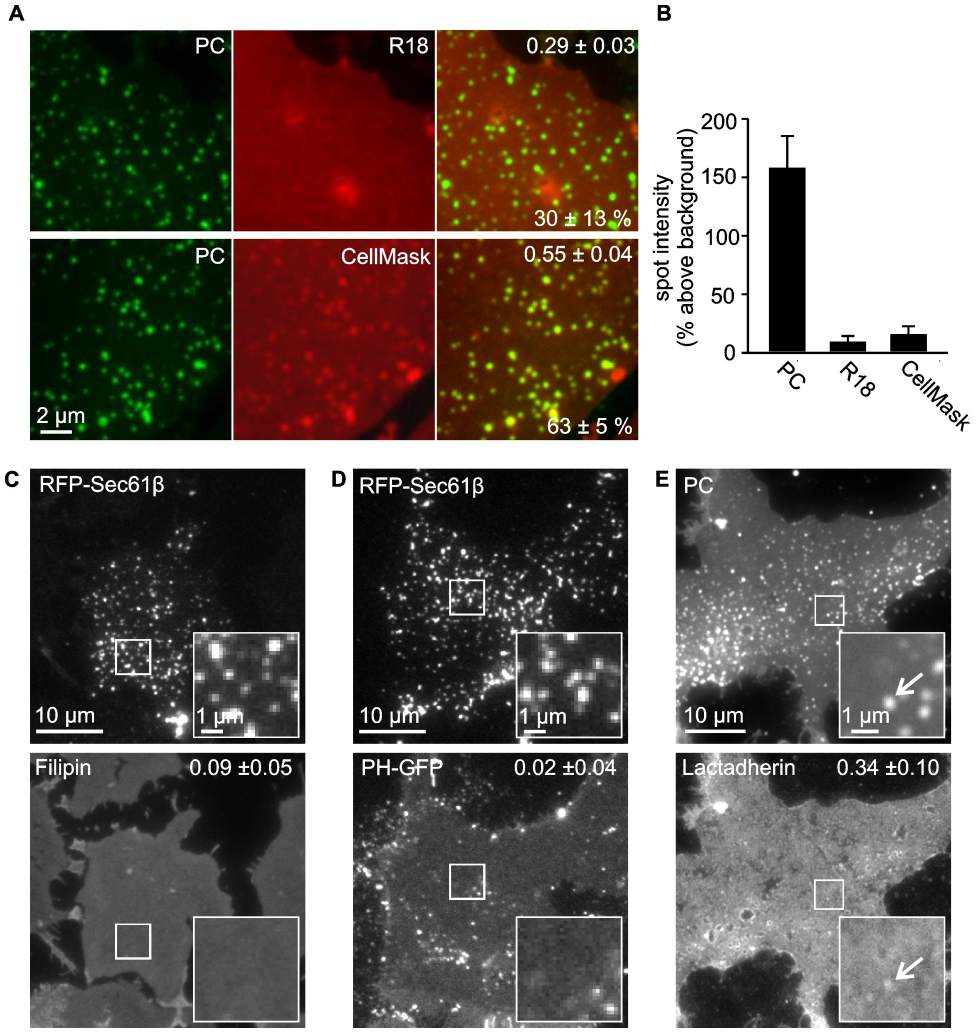

Figure 4.18: **Overlap of ER spots with membrane dyes and markers for cholesterol, PI(4,5)P_2 and PS. A** Counterstaining of PC spots with general membrane dyes. PM sheets with fluorescent PC were stained with TMA-DPH (not displayed) and either R18 (*upper panel*) or CellMask (*lower panel*). Images were analyzed for overlap by PCC (top value in overlay image) and at the level of individual spots (lower value in overlay image). **B** For ER spots, identified in the PC channel in PM sheets from **A** the increase of intensity over background was measured for PC, R18 and CellMask. **C-E** Counterstaining of PC spots with specific lipid dyes for cholesterol (**C**), PI(4,5)P_2 (**D**) or PS (**E**). ER remnants in HepG2 PM sheets were either visualized by overexpression of RFP-Sec61β or by metabolic PC labeling followed by cycloaddition of azido-Atto647N. Squares in lower right: magnified views from picture details indicated by small white boxes. Arrows indicate overlapping spots. PCC values are given in the upper right corner in the *lower panel*. **C** Cholesterol was stained with filipin (images from experiment shown in figure 4.25, panel A); **D**, PI(4,5)P_2 was labeled by co-expression of a PH domain of PLC1delta tagged with GFP (PH-GFP) (Stauffer et al. 1998). **E** FITC-labeled lactadherin was used for PS staining on the PM sheets after the cycloaddition reaction. All values are given as mean ± s.e.m. (n = 3 individual experiments with each 24-44 PM sheets for **A**/**B** and 11-90 PM sheets for **C**-**E**). Figure and legend modified from Merklinger et al. 2016.

ER membranes, indicating a potential difference in membrane properties of ER and PM.

The measured enrichment of PC in the ER membranes fits the common knowledge of PC distribution between the ER and the PM (Meer et al. 2011, Zambrano et al. 1975),

where there is about two times more PC in the ER. If the ER membrane spots were indeed ER membranes, the difference in lipid distribution should also hold true for other lipids. For a more specific evaluation, specific lipid probes were employed for three different lipids: cholesterol and PI(4,5)P_2 which mostly resides in the cytoplasmic leaflet of the PM (Watt et al. 2002) and PS, which is partly present in ER due to its synthesis in this compartment (Fairn et al. 2011).

PM sheets of HepG2 cells expressing RFP-Sec61β as an ER marker were stained with filipin, an autofluorescent antibiotic from *Streptomyces filipensis* which binds specifically to cholesterol (Elias et al. 1979). Epifluorescence imaging of the filipin revealed a homogenous staining (figure 4.18, panel C, bottom). No notable increase of fluorescence at the sites of ER signal could be observed. Accordingly, colocalization with the ER signal measured by Pearson correlation coefficient yielded a low value of about 0.09.

In order to attain PI(4,5)P_2 staining, the pleckstrin homology (PH) domain of phospholipase C delta (PLCδ) fused to a GFP was cotransfected with RFP-Sec61β in HepG2 cells. The PH domain is known to bind highly specific to PIPs headgroups (see section 1.3.2.1) and thus provides a suitable tool for the targeting of PI(4,5)P_2 (Lemmon et al. 2000). PH-GFP staining on PM sheets appeared less homogenously than the filipin staining. More precisely, the edges of sheets were speckled with PH-GFP accumulations while the fluorescence in the center of the sheets was rather uniform (figure 4.18, panel D, bottom). The fluorescent peaks did not correlate with the signal arising from the ER spots as indicated by a low PCC of 0.02.

Lastly, a lactadherin probe was used to test for the PS content of the ER membranes. The C2 domain of lactadherin specifically binds to PS (Yeung et al. 2008). In this assay, sheets from metabolically labeled cells were subjected to cycloaddition with azido-Atto647N for the visualization of PC, followed by staining with a FITC-labeled bovine lactadherin. As expected, a homogeneous staining of the PM was observed interspersed with spots of higher labeling density, which occasionally overlapped with the PC spots, yielding a PCC of 0.34 (figure 4.18, panel E, bottom). In summary, no PI(4,5)P_2 or cholesterol could be detected in the ER spots, while there was a slight increase in fluorescence for PS at ER membrane patches. This result broadly complies with the known lipid distribution between ER and PM.

Taken together, the results indicate that the lipid composition of the ER remnants largely reflects the lipid composition of the ER and clearly differs from the PM. The next section moves on to investigate the applicability and biological relevance of the preparation.

4.2.2 Application and biological relevance of ER-PM contact preparation

So far, the preparation method of ER-PM contacts was tested only in HepG2 cells, a liver epithelial cell line derived from a hepatocellular carcinoma. A more universal application of the method, however, is preferable. Therefore, I tested the method for two additional cell lines from different origins, PC12 cells and Jurkat cells. PC12 cells are rat pheochromocytoma cells that are often used as a model for neuronal differentiation, secretion of neurotransmitters or neurotoxicity. In contrast to the adherent cultures of HepG2 and PC12 cells, Jurkat cells, human T lymphocytes, grow in suspension. For the experiment, HepG2, PC12 and Jurkat were fed with pC. The next day all three cell lines were subjected to an ultrasound pulse to obtain PM sheets. In the case of Jurkat cells, cells were adhered to coverslips in Ringer solution before cell unroofing. Subsequent to the cycloaddition reaction with azido-sBP, the PM sheets were imaged with an epifluorescence microscope. In all three cell lines PC signal accumulated in spots on the homogeneous staining on the PM (figure 4.19). Size and distribution of the PC spots appeared similar amongst HepG2 and PC12 cells with minor differences observed for the Jurkat cell line, where some of the spots exhibited trapezoid shape. Thus, it can be inferred that the preparation method of ER contacts on PM sheets is applicable to a diverse range of cells.

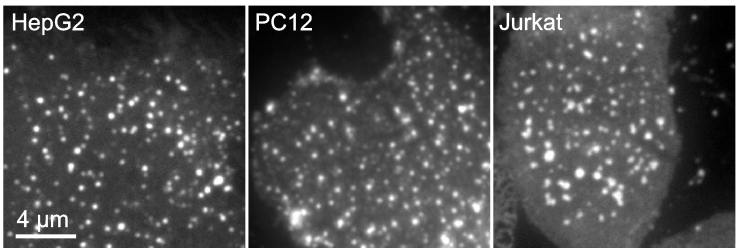

Figure 4.19: **Application of ER-PM MCS preparation in different cell lines.** Epifluorescence images of PM sheets from HepG2, PC12 or Jurkat cells as indicated. Visualization of ER remnants was achieved by metabolic PC labeling and cycloaddition on PM sheets as in 4.16. Jurkat cells were incubated in Ringer solution prior to cell unroofing. Figure and legend modified from Merklinger et al. 2016.

4.2.2.1 Functional ER-PM MCS

As pointed out in the previous sections, the contacts between ER and PM apparently resist high mechanical forces during the sonication pulse. Furthermore, incubation times of fixed samples up to five hours during immunostaining of clathrin and caveolin did not lead to an apparent reduction of ER spots (figure 4.17). Together with the similar occurrence in cell lines of different species and tissues, these findings are strong hints that ER spots

on PM sheets represent actual ER-PM MCS and not dispersed membrane remnants. To further substantiate this assumption I made use of a well documented phenomenon specific for ER-PM MCS, the STIM1 recruitment to ER-PM MCS upon calcium release from the ER. STIM1 is an integral protein of the ER membrane with the ability to sense calcium concentration by a luminal EF hand Ca^{2+} binding site (Williams et al. 2001). As explained in section 1.3.2.2, low calcium concentrations in response to cellular signaling or exogenous drugs such as thapsigargin (TG), promote the oligomeric state of the protein and subsequent migration towards the MCS with the PM to participate in the activation of calcium channels in the PM.

Before turning to the PM sheet preparation, the biological process was monitored by TIRF microscopy. Transient transfection of HepG2 cells with a YFP tagged STIM1 enabled the tracking of STIM1 in the subplasmalemmal area. In unstimulated cells the YFP signal of STIM1 was hardly visible as an indistinct signal with some bright spots (figure 4.20, panel A). The intensity of YFP-STIM1 spots increased clearly after about 100 s after TG treatment, but not in the control condition (figure 4.20, panel B and C). This result matches previous studies (Wu et al. 2006) and confirms the suitability of the experimental setup for observing ER-PM MCS using YFP-STIM1 as a marker.

If the observed ER spots on PM sheets were indeed authentic ER-PM MCS, they should be likewise able to recruit YFP-STIM1. To test this hypothesis, YFP-STIM1 transfected cells were labeled metabolically with pC and PM sheets were obtained after control or TG treatment. Sheets of activated and control cells underwent cycloaddition with an azido-Atto647N. The colocalization of PC and YFP-STIM1 was determined using the PCC, as well as the manual point-wise colocalization (for description see 3.2.15). As depicted in figure 4.20, panel D, a slight YFP-STIM1 fluorescence signal was already visible on the PM sheets of the control condition. The spotty pattern was similar to the one observed for the other ER marker proteins, RFP-Sec61β and ER-RFP (figure 4.13) and overlapped with PC. The application of TG yielded a considerable increase of YFP-STIM1 signal on the PM sheets (figure 4.20, panel D). More precisely, the YFP-STIM1 spots became larger and brighter upon TG treatment. Interestingly, a high colocalization of about 74.1% (spot wise) with a PCC of 0.68 was observed already in the control condition (figure 4.20 panel E, upper lane) and increased sparsely to 87.1% (spot wise) with a PCC of 0.76 upon TG treatment of the cells. Overall, significant portions of PC spots matched with YFP-STIM1 spots. The most surprising aspect was that PC spots differed in their size after incubation with TG in the YFP-STIM1 transfected cells, but not in the untransfected

cells. Sometimes spots even created trapezoid shape and connected to each other on the sheets. As this behavior was also observed for the PC labeled structures, this experiment indicates that ER on PM sheets represents the proximal parts of the ER that are able to recruit STIM1 in a calcium dependent manner. Thus, the preparation yields functionally relevant ER-PM MCS.

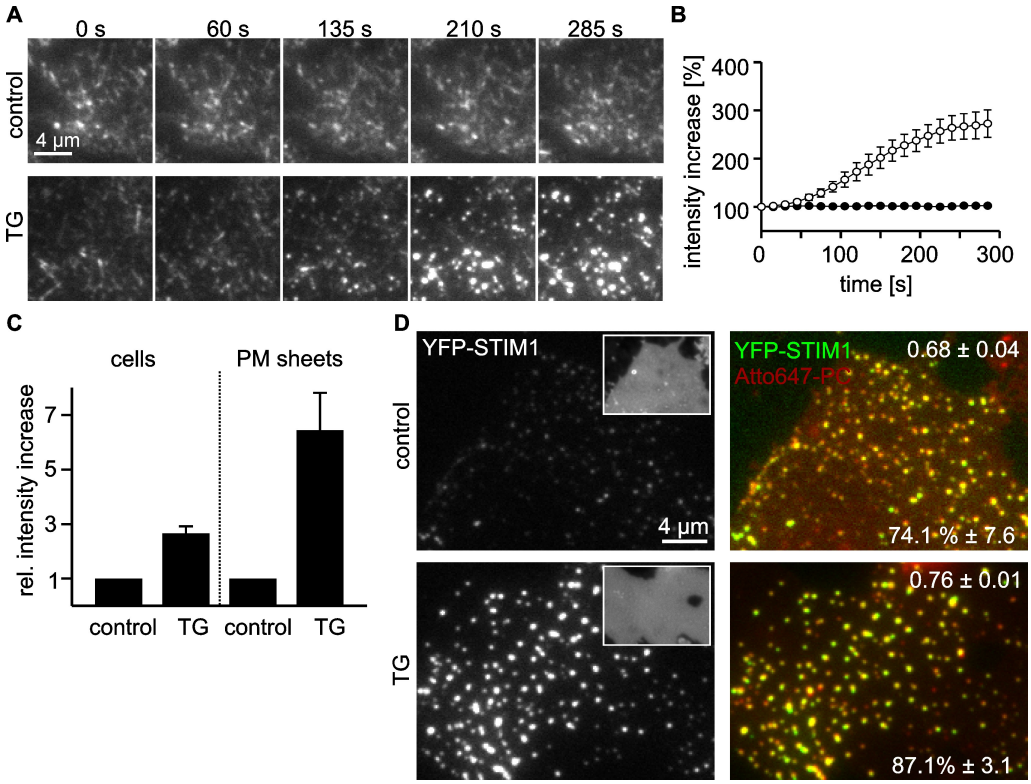

Figure 4.20: **STIM1 enrichment upon stimulation at PC spots on PM sheets. A** HepG2 cells overexpressing YFP-STIM1 were treated with 1 µM thapsigargin (TG) (lower panel) or incubated in buffer as a control (upper panel) as described previously (Wu et al. 2006). The fluorescence was recorded every 15 s for about 5 min by TIRF imaging. Time after stimulation is indicated in the example images. **B** Fluorescence intensity was quantified at each time point after stimulation and the values were related to the intensity of the first image. Each individual experiment resulted in averaged traces for control (closed circles) and TG stimulated cells (open circles), which were averaged for the graph in **B** (5 - 8 cells per independent experiment, n = 3; values are shown as mean ± s.e.m.). **C/D** Metabolically labeled cells expressing YFP-STIM1 were treated as in **A** followed by cell unroofing and fixation. pPC was visualized by cycloaddition of azido-Atto647N. **D** *upper panel*: control condition; *lower panel*: TG stimulation; insets in left images: TMA-DPH staining indicates integrity of the PM sheets. Images of YFP-STIM1 (*left*) are shown at same scaling. For better visualization overlay images of YFP-STIM1 and fluorescent PC (*right*) are presented at arbitrary scaling. Top values in the overlays indicate PCC and bottom values the spot wise colocalization (31-61 sheets per independent experiment). **C** YFP-STIM1 intensity was analyzed on PM sheets from **D**, averaged and related to the control condition. Values are given as mean ± s.e.m. (n = 3; with 53–85 PM sheets per independent experiment). Stimulation induced increase in YFP-STIM1 fluorescence in cells from **A** (after about 5 min) was plotted for comparison. Figure and legend modified from Merklinger et al. 2016.

4.2.2.2 Tethering of ER-PM MCS

A considerable amount of literature has been published on tethering between the PM and the ER in recent years (section 1.3.2.1) and it is commonly accepted that interactions are mostly mediated by integral ER proteins, which interact with lipids of the opposing PM (Helle et al. 2013, see also section 1.3.2.1). In this context, I further tested if the prepared ER-PM MCS on the sheets corroborate the known protein dependency by protease treatment. To this end, PM sheets from metabolically labeled cells were generated and PC was visualized via cycloaddition of azido-sBP. The PM sheets were either treated for 45 min with the serine endopeptidase trypsin or with a mixture of trypsin and trypsin inhibitor (type II-O, see section 3.2.14) as a negative control. During the incubation time, sheets rounded up slightly at the edges, but the staining intensity of PC in the uniform background of the PM did not change (figure 4.21, panel A). Compared to the control condition, the trypsin treatment strongly diminished the number of MCS (figure 4.21, panel A). Even though a small population resided on the sheets even after 45 min of protein digestion, the majority of ER-PM MCS were indeed susceptible to protein digestion. This provides further evidence for the involvement of protein interactions in the formation of ER-PM MCS.

Protease treatment for 45 min probably leads to an almost complete disintegration of protein complexes surrounding and stabilizing the membrane as can be seen from the transformation in shape of PM sheets during incubation with trypsin. For more refined information on stability, the protease effect of detachment and disintegration of ER contact sites was dissolved temporally. To this end trypsin or inhibited trypsin were applied to the PM sheets stained for PC directly on the microscope and fluorescence was monitored subsequently for several minutes (figure 4.21). Surprisingly, the spots started moving laterally immediately after the application of trypsin, but not in the control condition. This movement seemed to occur in random directions while it was restricted to the area of the sheet. The mean square displacement (MSD), that describes the average distance a particle travels in a defined time window, was calculated. The almost linear increase of MSD with the time interval (figure 4.21, panel C) hints to a normal diffusion. Diffusion constant could be calculated by linear regression of the averaged MSD plots yielding 8.56 x 10^{-4} µm^2/s for trypsin treatment, while diffusion of the spots in the control condition was negligible. The stability of the control PC spots was accompanied by similar fluorescence intensities calculated over the tracking period (figure 4.21, panel D) indicating a persistent PC gradient between ER and PM.

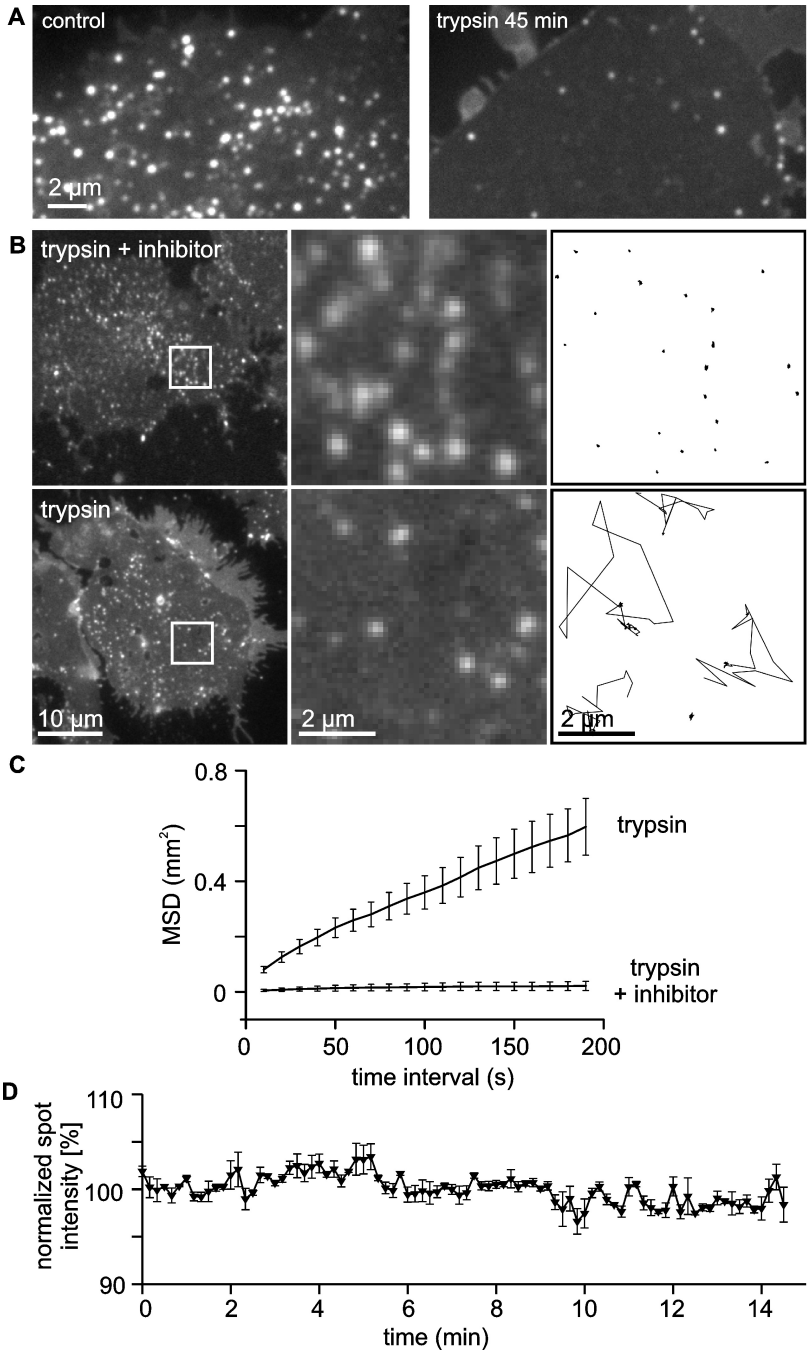

Figure 4.21: **Tethering of the ER contact sites mediated by proteins.** Epifluorescence microscopy of HepG2 PM sheets with fluorescent PC upon treatment with trypsin or trypsin in presence of an inhibitor as a control. In **A** PM sheets were treated for 45 min prior to imaging. **B** Treatments were performed directly on the microscope and images were acquired every 10 s after an initial 1 min incubation time with the protease for 200 s after treatment. *Left*, Images 60 - 70 s after treatment, insets displayed in magnified view in the *middle image*. *Right*, illustration of spot tracks over 200 s observation. **C** The mean-square displacement (MSD) was calculated in increasing time intervals from tracks of 141 - 143 spots on 3 - 5 PM sheets per condition and independent experiment (n = 3; values given as mean ± s.e.m.). Linear regression yielded diffusion coefficients of 8.56 x 10^{-4} µm^2/s and 0.311 x 10^{-4} µm^2/s for trypsin and control condition, respectively. **D** Deviation of fluorescence intensity of PC spots in the control condition during the tracking (28 - 47 spots per independent experiment, n=3, values given as mean ± s.e.m.). Tracking analysis was performed by Dr. Jan-Gero Schlötel. Parts of the figure and legend modified from Merklinger et al. 2016.

In summary, this experiment suggests that there are two different mechanisms how ER contact sites are stabilized at the PM. One anchors the ER membrane vertically to the PM. The second one, however, controls lateral movement of the anchored contact sites. The latter protein mediated connection is more susceptible to trypsin while the former needs harsh treatment for disruption.

4.2.3 Spontaneous lipid transfer at ER-PM MCS

Genes involved in the sophisticated network of lipid biosynthesis make up nearly 5% of all cellular genes (Meer et al. 2008) and produce about 1000 different membrane lipid species in mammalian cells (Coskun et al. 2011). However, most of the lipids are not synthesized at their cellular destination but instead at the ER (Fagone et al. 2009). From their place of synthesis they need to be transported to other locations. Lipid transfer in cells occurs mainly via vesicular trafficking. Additionally, lipid transfer proteins (LTPs) can mediate the exchange of lipids between cellular compartments.

Another possible mechanism for monomeric lipid exchange is the spontaneous lipid transfer (SLT). In this process, a lipid desorbs from the membrane spontaneously, without the specific interaction of a LTP, transfers through the aqueous milieu to another membrane, where it inserts. SLT has been suggested for PC in experiments on lipid vesicles at high concentration (Jones et al. 1989) and for phosphatidic acid between vesicles and cells (Longmuir et al. 1989). One major obstacle for such mechanism is to overcome the thermodynamic barrier for desorption of the lipid from the donor membrane, which could in principle be facilitated by close proximity of donor and acceptor membranes either by a transient collision or a permanent contact (Lev 2010, R. E. Brown 1992). Direct physical contact between membranes could allow lipids to desorb from membranes and enter the other membrane without changing the hydrophobicity of its surrounding. Therefore, the question arose if at MCS such close proximity is given, sufficient for SLT to occur (Lev 2010).

The preparation of ER contact sites on PM sheets seems to be a suitable system to test for SLT. Firstly, it provides close and highly stable contacts between the two membranes (see 4.2.2.2). Secondly, the reservoir of ER lipids is defined and cannot be replenished by cisternal ER membrane parts, which would complicate the analysis of SLT. Hence, the PC gradient dissipation should be visible by a reduction in PC intensity over time, when PC is transported from the ER membrane remnants to the PM.

4.2.3.1 Spontaneous transfer of PC

I aimed to test for SLT of PC as a marker lipid, since a concentration gradient between ER and the PM (see section 4.2.1.3) is observed and PC can be labeled metabolically preserving its natural fatty acid distribution (see section 4.2.1.2).

Accelerated PC transfer along the concentration gradient

In a first step, I asked whether the ER/PM concentration gradient of PC could in principle be attenuated and more importantly, if the system was sensitive enough to monitor such diminishment of PC in the ER spots. To this end, I made use of the cyclodextrin HPαCD as a catalyst for lipid transfer. In general, the surface of cyclodextrins is hydrophilic, but they can build inclusion complexes with apolar substances within their hydrophobic cavity (Zidovetzki et al. 2007). The cavity of HPαCD is rather small compared to other species of cyclodextrins. Therefore, it is deemed to posses, albeit on a restricted basis, specificity for phospholipids (Irie et al. 1992). Cyclodextrins are able to extract lipids from membranes as well as insert them back in a concentration gradient-dependent manner (Christian et al. 1997).

In order to proof that HPαCD is capable of extracting and releasing pPC, PM donor sheets from metabolically labeled cells were incubated with buffer containing HPαCD or only buffer as a control. After 30 min the supernatant was removed from the donor sheets and was added to acceptor sheets from unlabeled cells for another 30 min. These acceptor sheets were washed and cycloaddition for the visualization of pPC was performed. Figure 4.22, panel A, displays acceptor sheets imaged with an epifluorescence microscope. The sheets treated with the preincubated cyclodextrin exhibited a uniform PC staining of the PM sheet. As expected, no fluorescent PC signal was noticed in the control condition. Thus, HPαCD is capable of extracting as well as inserting pPC.

For analysis of the transfer between ER remnants and the PM, PM sheets of pPC labeled cells were incubated for 30 min with HPαCD or only buffer as a control and subsequently stained by cycloaddition of the dye. While the spots of fluorescent PC are clearly distinguishable from the uniform background of the PM in the control condition, the intensity difference between the two compartmental membranes is clearly reduced upon HPαCD treatment (figure 4.22, panel B). This observation could be affirmed by the analysis of spot intensity above background (analysis see section 3.2.15) revealing a decrease of about 60% in the case of cyclodextrin treatment compared to the control condition. The mean signal intensity of the sheets was not affected by cyclodextrin (figure

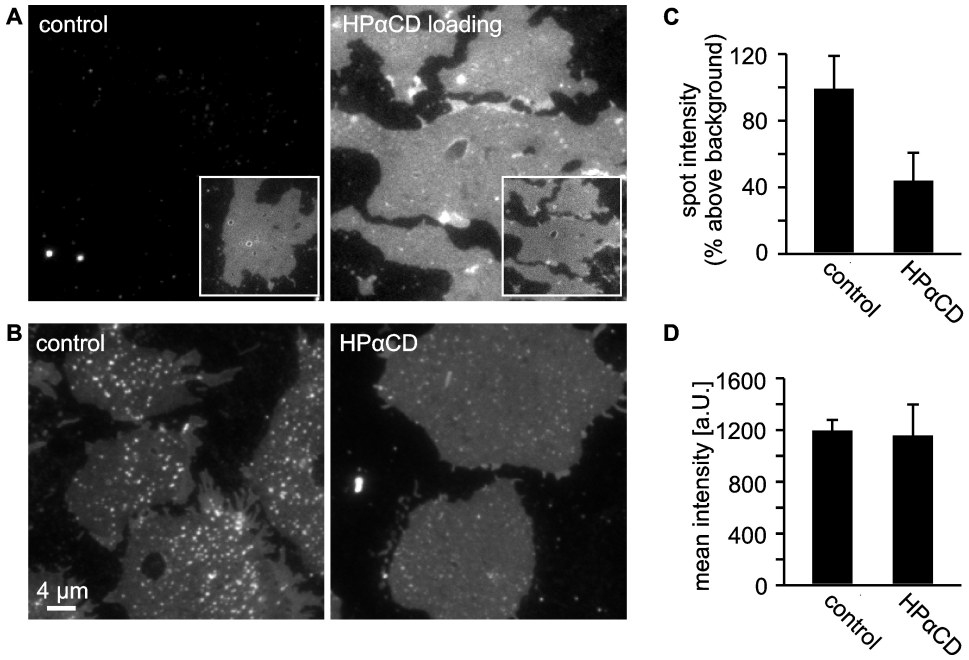

Figure 4.22: **The lipid carrier HPαCD mediates PC transfer at ER-PM MCS. A** PM sheets from metabolically labeled HepG2 cells were incubated with buffer containing 50 mM hydroxypropyl-α-cyclodextrin (HPαCD) or buffer as a control. The supernatants from this incubation were applied to PM sheets from unlabeled cells as a control for the pPC transfer capability of HPαCD. After incubation for 30 min, cycloaddition was performed with a fluorescent dye (sBP) for visualization of pPC. Large images show sBP-PC fluorescence, insets indicate the staining of the same membranes with TMA-DPH at smaller magnification. Images are shown at same scaling. Due to lower staining intensities, scaling largely differs from **B**. **B** Epifluorescence micrographs of PM sheets from metabolically labeled HepG2 cells incubated for 30 min with buffer (control) or buffer supplemented with 50 mM hydroxypropyl-α-cyclodextrin (HPαCD). Staining of pPC was performed as in **A**. **C** Spot intensity above background was quantified for images in **B**. Note here, that in comparison to figure 4.18 values are lower due to twofold larger ROIs for analysis. **D** Average fluorescence intensity from images in **B**. The fraction of the signal arising from spots was 12.4% ± 2.1 and 3.5% ± 2.1 without or with HPαCD, respectively (see section 3.2.15). Images within one row are shown at same scaling. All values are given as mean ± s.e.m. (n = 3 independent experiments) Figure and legend modified from Merklinger et al. 2016.

4.22, panel D). This is important, since it confirms that the diminishment of spot intensity does not result from mere uptake of pPC, but rather from redistribution of the lipid. The results permit the conclusion that the concentration gradient indeed was diminished by promoting desorption / absorption via HPαCD. Furthermore, it can be deduced that the system is sensitive enough to resolve such a reaction.

SLT of pPC

Knowing that the PC gradient is sufficient to drive lipid redistribution in the presence of a carrier, I intended to test whether transfer is possible without a facilitator. In a simple experimental setup, PM sheets from metabolically labeled cells were incubated at 37 °C for 1 or 2 h in buffer. After each of the time points fresh sheets from metabolically labeled cells were prepared as a reference. All samples were stained by cycloaddition of azido-sBP and imaged with an epifluorescence microscope (figure 4.23, panel A). Spot to background intensity was analyzed as a measurement of PC gradient dissipation (for analysis see section 3.2.15). Decrease in signal intensity over background would hereby indicate lipid transfer from the ER to the PM, whereas a consistent value would indicate no PC transfer. Surprisingly, the spot intensity over background raised during the incubation (figure 4.23, panel B). This was due to a slight decrease in PM intensity in the incubated samples when compared to the freshly prepared ones (figure 4.23, panel A). Phospholipase mediated head group cleavage during the incubation may have caused specifically in the PM the reduction of propargyl groups for cycloaddition. Albeit, it cannot be ruled out entirely that LTPs moved lipids from the PM to the ER, SLT from the PM into the ER is thermodynamically highly unlikely, because in this scenario lipid flux would have to occur against the concentration gradient.

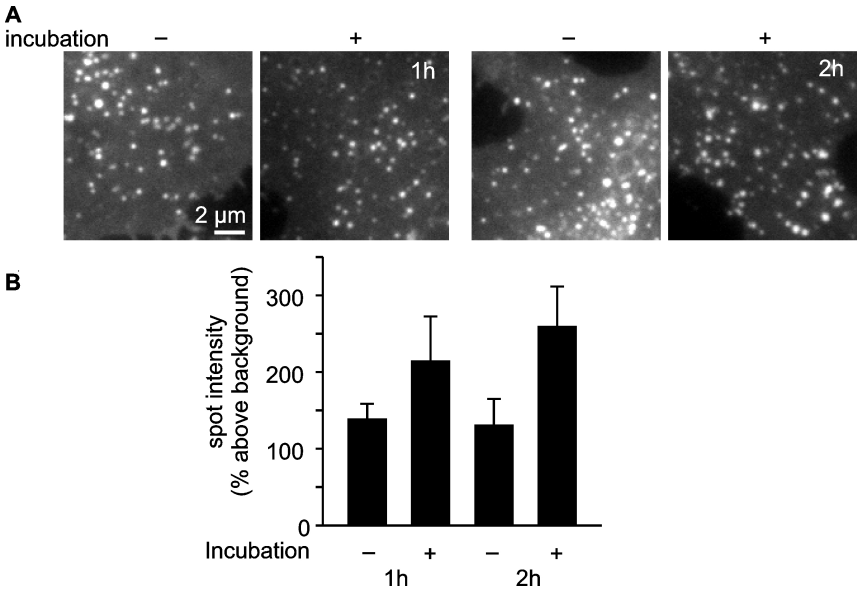

Figure 4.23: **Probing loss of pPC from ER membranes after long incubations. A** Epifluorescence micrographs of PM sheets from metabolically labeled HepG2 cells that were either freshly prepared or incubated in buffer for 1 h or 2 h (as indicated) at 37 °C prior to cycloaddition for visualization of pPC. As a control, cells were sonicated and directly underwent cycloaddition. PM sheets were imaged in sonication buffer. **B** Spot intensity above background was quantified for the conditions depicted in **A**. Values are given as mean ± s.e.m. (n = 3 independent experiments). Parts of figure and legend modified from Merklinger et al. 2016.

SLT of sBP-PC

The previous experiment provided evidence for a lack of SLT of pPC at ER-PM contact sites along the concentration gradient of the lipid. To solidify this finding, I turned to the labeled lipid sBP-PC. Its charged fluorophore headgroup is more hydrophilic and thus should even facilitate desorption from membranes compared to the non labeled pPC. For testing the sBP-PCs ability to pass from the ER membrane to the PM, fluorescence loss after photobleaching (FLAP) was employed. For this approach sheets were generated from metabolically labeled cells and cycloaddition was performed to label pPC with azido-BP. Instantly after labeling, sheets were imaged with a confocal laser scanning microscope. Figure 4.24, panel A, upper image, shows the characteristic spotty pattern of the ER contact sites on a uniform distributed PM signal.

The fluorescence on one half of the sheet was bleached using high laser intensity (figure 4.24, panel A, middle image). 20 min after bleaching, another picture of the respective

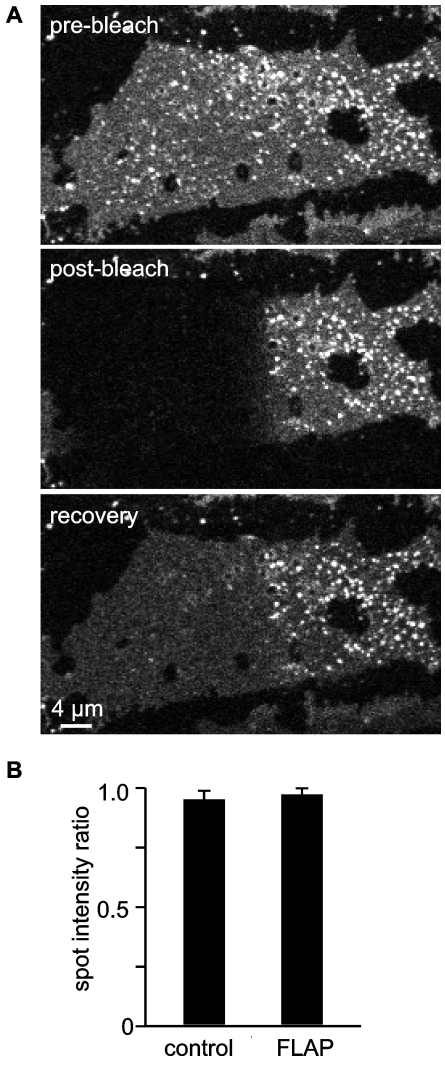

Figure 4.24: **No evidence for SLT when probed by FLAP. A** Confocal images of HepG2 PM sheets with fluorescent PC (sBP-PC, as in 4.16). Fluorescence was bleached in one half of the PM sheet (compare pre-bleach image (*upper*) with post-bleach image (*middle*)). The sheets were incubated for 20 min for re-equilibration of the signal and another image was taken (*lower image*). Additionally, control sheets were imaged in the same sequence without bleaching (not shown). **B** Intensity of individual ER membranes on the non-bleached half of the sheet or on control sheets were measured in the pre-bleach and the recovery image. Values were corrected for changes in the uniform background of the PM and the ratio between pre-bleach and recovery was calculated. Values are given as mean ± s.e.m. (n = 3 independent experiments). Figure and legend modified from Merklinger et al. 2016.

sheet was taken (Figure 4.24, panel A, lower image). While the uniform background of the PM recovered on the bleached site of the sheet, the spotty pattern did not. Only occasionally spots regained fluorescence probably due to impaired self-quenching of the dye (for further discussion see section 5.2.4). Turning to the spots on the non bleached half, ratio between spot intensity in prebleach and postbleach images were calculated (for analysis see 3.2.11)(figure 4.24, panel B). In the case of SLT along the concentration gradient of sBP-PC, the absolute fluorescence signal in the ER spots should be diminished. This is because fluorescent molecules move to the PM, resulting in a ratio below one. Indeed, there was a marginal reduction of the ratio. However, this reduction was in the same range as for control spots measured on non-bleached PM sheets, pointing to a minor extend of bleaching rather than SLT.

Accordingly, the intensity of PC in ER membranes was not affected by the loss of fluorescence in the PM. It can be deduced that there is no lipid exchange between the PM and the ER at the contact site in this experimental setup, even upon augmented hydrophilicity of the observed lipid.

4.2.3.2 Spontaneous transfer of cholesterol

Having investigated SLT of PC for potential SLT at the ER-PM MCS, a second lipid class was examined, the sterols. In an experimental setup using artificial lipid vesicles, cholesterol had been shown previously to exchange between lipid bilayers independent from membrane fusion or transport proteins (Fugler et al. 1985). As mentioned in the previous section, SLT depends on the concentration of the respective lipid in the donor and acceptor membrane. Given the excess of cholesterol in the PM over the ER membrane, SLT should be promoted from the PM to the ER. However, it is important to consider the difference between absolute concentration and concentration of free lipid. SM is known to reduce the amount of free cholesterol by complexing it (section 1.3.1). ER and PM content of free cholesterol, relevant for SLT, could therefore be even similar (Baumann et al. 2005). Thus, elevation of cholesterol level in the ER would lead to cholesterol flux into the PM, if SLT was possible.

To test for this, sheets from RFP-Sec61β transfected cells were incubated with a cholesterol-MβCD complex for cholesterol loading of the membranes (see section 3.2.4.2) and cholesterol was stained for 45 min using filipin. As depicted in figure 4.25, panel A, for the control condition the characteristic spotty pattern of the ER contact sites was observed in the RFP channel in contrast to the rather even filipin staining of the PM. Strikingly,

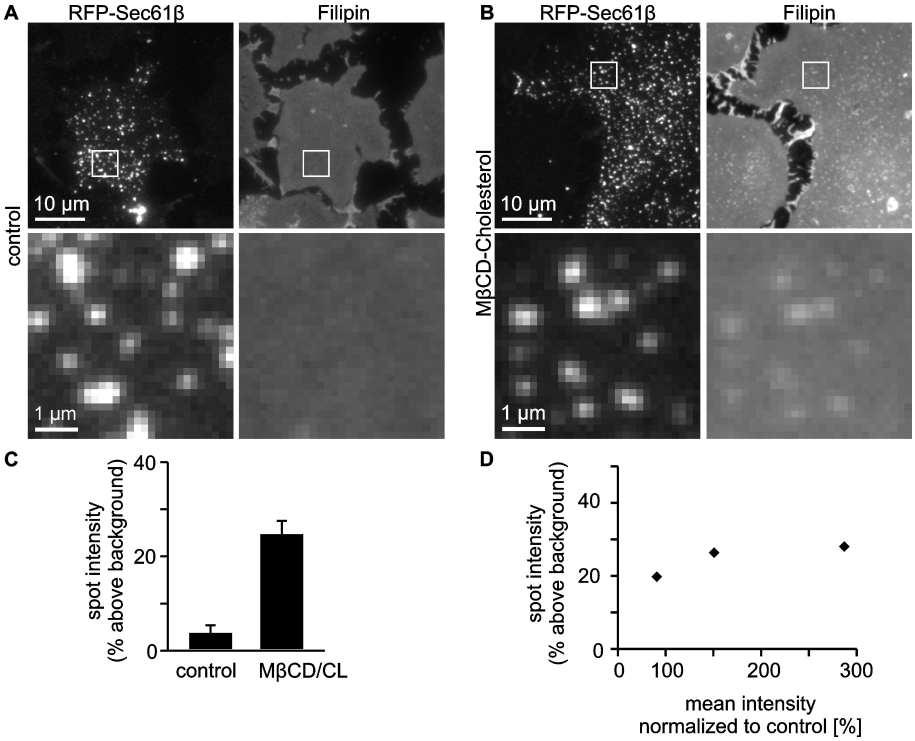

Figure 4.25: **Cholesterol loading of ER membranes.** Epifluorescence images of PM sheets from HepG2 cells expressing the ER marker RFP-Sec61β, incubated for 10 min at 37 °C with buffer (**A**) or buffer containing 1.5 mM cholesterol-β-methyl-cyclodextrin complex (MβCD/CL) (Klein et al. 1995) (**B**). After the incubation cholesterol was stained with the autofluorescent filipin for 45 min at RT. *Upper panels*, overview images of sheets; *lower panel*, magnified view of squares indicated in the overview images. **C** ER membranes were identified based on the RFP signal and marked with ROIs. The ROIs were transferred to the filipin channel, which occasionally required recentering due to lateral shift between the two images. The spot intensity over background was calculated in the filipin channel. Values are given as mean ± s.e.m. (n = 3 independent experiments). **D** Spot intensity above background was plotted against the mean filipin staining intensity for the MβCD/CL condition (normalized to the control) for each independent experiment. Figure and legend modified from Merklinger et al. 2016.

in the MβCD condition the filipin staining was interspersed with spots corresponding to the RFP signal of the ER marker protein. Intensity of spots above background in the filipin channel, that overlapped with the Sec61β signal, increased clearly upon treatment with cholesterol-MβCD (figure 4.25, panel C). This increase was independent from the degree of PM cholesterol saturation as demonstrated from the comparison of spot intensity above background and normalized cholesterol staining intensities in the single experiments (figure 4.25, panel D). This is important, because high cholesterol loading of the PM could diminish the capacity of the PM to complex cholesterol.

In summary, a cholesterol-MβCD complex can be used to load ER membranes at ER-PM contact sites with cholesterol. Since the artificial cholesterol gradient is retained, there is no evidence for SLT of cholesterol along the concentration gradient in this experimental setup.

5 Discussion

In this study, structural and functional aspects of two supra-molecular structures were investigated. Both structures, the syntaxin clusters and ER-PM MCS, rely on a sophisticated network of interactions at the cytoplasmic periphery of the PM. The factors influencing syntaxin clustering include the cholesterol content of the PM (Lang et al. 2001), electrostatic interactions with phosphoinositides (section 1.3.2.1), hydrophobic mismatch between TM domains (Milovanovic et al. 2015) and cytoplasmic protein-protein interactions (Sieber et al. 2006, Sieber et al. 2007). Similarly, the ER-PM MCS structure relies on protein-phosphoinositide interactions (section 1.3.2.1) and protein-protein assemblies (section 1.3.2.2), that are susceptible to changes in their surrounding such as e.g. high salt concentrations (section 4.2.1.2) or alteration of stoichiometry between the interacting components (Derler et al. 2016).

Investigation of such structures requires minimally invasive methods. Therefore, fluorescence microscopy in combination with the sheeting technique was chosen to examine syntaxin cluster and ER-PM MCS. This approach enabled observation of both structures with high signal-to-noise ratios (see for example figure 4.2 or figure 4.13). It further allowed for the observation of protein (figure 4.11) and lipid dynamics (figure 4.22). Furthermore, the physical dissection of the PM and its direct periphery by the sheeting technique made it possible to co-isolate functional ER-PM MCS without the usage of bilayer disturbing detergents thus preserving lipid contents of ER and PM (section 4.2.1.3). Importantly, PM sheets were previously shown to maintain important PM features such as protein dynamics (Sieber et al. 2007). This was largely corroborated by comparative measurements of syntaxin mobility in cells and PM sheets (section 4.1.3).

Despite some limitations such as the need for specific labeling or eliminating the difference between intra- and extracellular environments in the PM sheet preparation, the methods used in this study allowed to assess important aspects of both structures, which will be discussed in the following.

5.1 Inner architecture of the supra-molecular syntaxin cluster at the cytoplasmic periphery of the PM

Syntaxins segregate into clusters, protein-dense nano-domains that contain dozens of molecules in a small patch of the membrane. The syntaxin cluster is not only a paradigm to study protein clustering, but also represents a perfect example for the mutual dependencies of hydrophobic and hydrophilic interactions (see section 1.3) that influence supra-molecular structures at the cytoplasmic periphery of the PM. Within this scope, the present work focused on the impact of cytoplasmic protein-protein interactions on the architecture of syntaxin clusters.

5.1.1 Physical properties of syntaxin clusters

The assembly of proteins into clusters can principally be regarded as a type of higher order protein structure. In contrast to defined protein complexes, however, clusters are held together by short-lived transient interactions as revealed by the constant exchange of clustered syntaxin molecules in the PM environment (Sieber et al. 2007 and section 4.1.3). This renders purification and subsequent structural analysis of clusters by e.g. electron microscopy or crystallography to be inherently difficult. Nevertheless, to obtain information on such structural level, the physical appearance in fluorescence microscopy, size, shape and packing density are useful means for cluster characterization.

Determination of cluster size - a technical limitation in absolute size measurements

Dimensions of clusters were measured by super-resolution microscopy and revealed an average size for full-length syntaxin clusters of about 70 - 80 nm (see section 4.1.1.1). Prior studies reported a cluster size of 50 - 60 nm (Rickman et al. 2010, Sieber et al. 2007). This slight discrepancy can be explained by the general technical limitation in obtaining absolute values on cluster size as will be outlined in the following.

Cluster size determination by high resolution microscopy can be divided into three technical steps: staining, image acquisition and analysis. The STED microscopy applied here requires high staining intensities for proper image acquisition. For this reason, I chose a standard labeling approach to stain the tagged proteins with a first and secondary antibody. One drawback of this method is that multivalent antibodies could potentially form an "umbrella" around the cluster. Due to the large size of the antibodies (see figure 4.4), the "umbrellas" are larger than the clusters themselves, thereby increasing actual cluster sizes. To minimize or circumvent probe-induced enlargement the usage of nanobodies or

cycloaddition of fluorophores to genetically encoded unnatural amino acids (Vreja et al. 2015) could be beneficial. However, this approach results in fewer fluorophores per epitope and the resulting signal reduction may entail problems in image acquisition.

As mentioned in section 4.1.1.1, the absolute cluster size measured for myc-tagged syntaxin and syx-ΔS decreased with higher deexcitation laser power (see figure 4.2). Resolution in the range of cluster sizes is a likely cause for this effect. On principle, the resolution potential of the STED beam directly depends on the beam intensity (Klar et al. 2001). On the other hand, the increased laser power was also accompanied by a general reduction in signal intensity. This results in a higher signal offset and may conceal existing edge regions of the cluster accounting for the observation of smaller clusters.

Another challenge is the analysis of the microscopy data. In this study, I employed a widely used approach, which involves image segmentation, line scan analysis and subsequent fitting with a Gaussian function to obtain the FWHM (see section 4.1.1). This single object-based analysis is biased by the preferential inclusion of round clusters that are clearly separated from other clusters. The method reaches its limits when clusters adopt irregular elongated shapes or are in close proximity to each other as occasionally observed in this study upon high overexpression of the constructs (section 4.1.1.1). Limitation to round clusters could be evaded by the application of segmentation free methods that are pixel-based (Hermann et al. 2014). However, such methods cannot obtain information on the level of single clusters in contrast to the segmentation approach. Automated delineation of cluster area by a combination of object-based segmentation and image restoration (Paul et al. 2013, Rizk et al. 2014) may be useful to gather information on size independent of shape on single cluster level.

Despite the described technical limitation, a robust tendency to bigger clusters in syx-ΔS could be observed when compared to the full length construct (see figure 4.2). Therefore, even if absolute measurements depend on staining, analysis and the deexcitation energy, relative differences between constructs are still detectable.

What defines and limits cluster size?

As outlined above, the deletion of cytoplasmic protein parts (syx-ΔS) slightly increased the cluster size, whereas cluster sizes did not depend on expression level (see figure 4.2). This is in line with previous studies reporting on the limited sizes of protein clusters (Sieber et al. 2006, Homsi et al. 2014). Interestingly, if syntaxin was anchored to the PM via prenylation, instead of its natural TM domain, cluster size slightly increased with expression level (see figure 4.3).

This points to hydrophobic core interactions restraining cluster size. It could be explained by the non-linear increase of repulsive forces upon high local concentration of TM domains. Embedding of proteins in membranes impinges on lipid behavior (see section 1.3.1) and can result in elastic membrane deformation. Accompanied high energetic costs thus counteract cluster promoting forces (Weitz et al. 2013). Such effects should be particularly pronounced if the embedded protein parts exhibit low structural flexibility. For syntaxin, a rigid helical structure beyond the SNARE motif into the hydrophobic core of the membrane has been proposed (Stein et al. 2009). In fact, membrane deformation upon crowding of the syntaxin TM domains has been observed in molecular dynamics simulations (Bogaart et al. 2011). In contrast to the stiff TM domains, the lipidic prenyl anchor might be less capable of transmitting bending force and therefore might allow for higher order assemblies.

Alternatively, it could be argued that the lacking poly basic stretch (pbs) in the prenylated constructs abolishes size limitation. This is, however, less likely since the constructs still contain clusters of positive amino acids in close proximity to the lipid headgroups. These are capable to interact with negatively charged lipids at the PM such as $PI(4,5)P_2$ (Heo et al. 2006) similarly to the pbs of syntaxin (Bogaart et al. 2011).

Attraction in conjunction with complete absence of repulsive forces would lead to the formation of a single gigantic protein domain in the PM. Since this was not even observed for the prenylated mutant of syntaxin even at high expression levels, it can be assumed that further factors play a role in the separation into single clusters. Sterical hindrance of large protein domains or accumulation of electrostatic charges could produce a repulsive force increasing with the number of molecules per cluster. Future research could involve the combination of prenyl-anchoring with step-wise deletion of cytoplasmic protein domains to get further insight into the limitation of protein cluster size.

How is the shape of clusters influenced?

Another interesting observation was the occasional occurrence of elongated cluster structures. This phenomenon could be observed only for the constructs less attracted to the clustered state, syx-ΔS and syx-ΔCyt (see figure 4.2) and more often at higher concentrations of the respective proteins.

An explanation for this effect could be the destabilization of cluster boundaries. Elevated distance between TM domains (see section 4.1.2.3) accompanied by the reduced attraction into the clustered state (4.1.3) may decrease line tension of the cluster for syx-ΔS and syx-ΔCyt entailing the deformation. This hypothesis is based on theoretical calculations, in

which shape alterations of phases were found to depend on a balance between line tension and repulsive forces between the components (Seul et al. 1995).

Intriguingly, rising concentrations of the syntaxin constructs entailed coverage of large and connected membrane areas spaced by protein free stripes. Similar patterns have been observed previously when imaging general protein distribution in the PM (Lillemeier et al. 2006, Saka et al. 2014). It is therefore tempting to speculate that upon stark overexpression cluster fill up the PM restricted to the areas that are defined by a superordinate organization pattern (Saka et al. 2014). The question remains whether these enlarged areas still consist of separated single clusters at close proximities, or the clusters merge to form large aggregates.

Addressing packing densities of supra-molecular structures in the PM

Despite its standing as the most detailed described protein cluster, little is known about the actual packing of the syntaxin cluster. As to that, different scenarios were suggested: i) the syntaxin molecules distribute evenly among the cluster area spaced by a distance of a few nanometers (Sieber et al. 2007) or ii) TM and SNARE motifs are in direct contact with the N-terminal H_{abc} domains tilting outwards from the center of the cluster (Sieber et al. 2007) or iii) there is a density gradient of syntaxin molecules towards the outer cluster periphery (Bar-On et al. 2012).

Distinguishing between these different arrangements requires resolution in the range of a few nanometers, which is technically not realizable as yet. However, even if it were possible to accurately localize single molecules to 1 - 2 nm, all proteins would have to be labeled with small probes that do not interfere with clustering.

An option for such a labeling is the application of non-conventional amino acids with groups for cycloaddition of fluorescent dyes. While this labeling method interferes only minimally with protein structure, it is highly unlikely that the efficiency of the cycloaddition reaction would reach 100% in the aqueous solution. The only method to obtain true 1:1 protein to fluorophore labeling is the usage of genetically encoded tags such as fluorescent proteins, SNAP or CLIP tags. However, those might interfere with dense cluster packing due to their large dimensions.

Due to these difficulties, I aimed for a different approach and developed a systematic experimental assay to study packing density of clusters in native PMs by the application of antibodies as packing sensors (see section 4.1.2.3). The results indicated an impact of cytoplasmic protein-protein interactions on packing density (section 4.1.2). However, high variability was observed between individual experiments (see figure 4.10) calling for the

discussion about possible limitations and improvements of this approach.

The experimental approach used in this study involves a comparative quantification of antibody labeling in the PM and the absolute amount of the protein of interest. As described in section 4.1.2.3 the relation can be described according to equation 4.1.

Firstly, it has to be mentioned that the accessibility factor (f_{access}) could be formally divided into two factors for first and secondary antibody, respectively. Those two factors could in principle act antagonistic: sparse occupation with first antibody could facilitate secondary antibody binding, while dense first antibody labeling on a cluster would impair accessibility for secondary antibodies. Such an effect would obscure different packing densities and could be circumvented by the usage of directly labeled first antibodies.

Secondly, the above mentioned equation is based on the assumption that the population subset for determination of I_{micr} is identical to the population underlying N_{total}. However, as occasionally observed for cells overexpressing GFP tagged syntaxin, there could be a population of strongly overexpressing cells that are only loosely attached to the glass after transfection. Those cells usually contain high amounts of overexpressed protein and could, in theory, be washed off during antibody staining. In this case they would contribute to N_{total} but not I_{micr}. Preliminary experiments suggest, however, that these high expressing cells are present in both experimental parts, epifluorescence microscopy and western blot, at similar proportions (personal communication with Sarah Holz and Thorsten Lang). Thus, it is unlikely that these cells will substantially influence the experiment, although it cannot be fully excluded.

Another challenge in this experimental approach is to precisely determine the subcellular distribution (see f_{sort} in equation 4.1) of syntaxin and its variants. In this study I employed two different approaches, microscopical dissection by 3D-STED and pH quenching of the GFP tag, the latter proved to be more reliable in view of the control proteins (see section 4.1.2.3). However, the actual packing density experiment was conducted with the myc tagged constructs and for a reference it has to be assumed that myc- and GFP tagged proteins are sorted equally. In favor of this hypothesis, protein domains known to determine sorting of tail-anchored proteins such as syntaxin (Bulbarelli et al. 2002, X. Yang et al. 2006) are similar between the GFP and myc tagged constructs. Nevertheless, sorting was clearly affected by the expression level of the constructs (data not shown). Therefore, slight changes in transfection efficiencies could have had a substantial impact on the subcellular distributions and thus contribute to the large deviations in the experiment (figure 4.10).

In summary, two changes could further improve the reliability of the approach: Firstly, the calculation could be simplified by circumventing f_{sort}. To do so, staining of permeabilized cells for epifluorescence microscopy would directly include the intracellular signal, rendering a correction unnecessary. In fact, preliminary data on such an experiment indeed show less variation and confirm the results obtained in section 4.1.2.3 (personal communication with Sarah Holz and Thorsten Lang). Alternatively, a proximity based approach, such as Foerster resonance energy transfer (FRET), could be helpful to obtain information on packing density uncoupled from differential expression of the constructs.

5.1.2 Correlation between cluster packing density and attraction into the clustered state

So far the discussion has focused on static physical properties of the clusters measured in fixed samples. Tendencies to enlarged and less tightly packed clusters upon deletion of cytoplasmic protein domains were observed. This begs the question as to whether those characteristics correlate with dynamic properties of the proteins.

Cytoplasmic protein domains mediate attraction into the cluster

Evidence for enhanced clustering via the cytoplasmic protein domains is provided by the different mobilities of the syntaxin variants (see figure 4.11 and figure 4.12). Diffusion based analysis has been used widely as a measure for protein confinement in the PM (Kusumi et al. 1993) linking diminished protein mobility to the clustering state of several membrane proteins (Zilly et al. 2011, Schreiber et al. 2012) including syntaxin (Sieber et al. 2007). The relationship between membrane diffusion and clustering could be explained by a balance between the clustered and the free state of the proteins, where clustered molecules are less mobile than the free population. Consequently, the larger the pool of free molecules or the faster the molecules exchange from clustered into the free state, the higher the mobility as it is determined by FRAP.

Based on these considerations, the full length syntaxin shows the highest clustered fraction, while the two variants lacking cytoplasmic protein parts were less trapped in the clustered state (see section 4.1.3). Note here, that syx-ΔCyt and syx-ΔS behave very similarly and the minor decrease in mobility of syx-ΔS in comparison to syx-ΔCyt could in principle be attributed to differences in physical size and/or shape of the proteins. This small difference is surprising, since syx-ΔCyt lacks almost the entire cytoplasmic part of syntaxin and therefore differs considerably from syx-ΔS in terms of possible interaction surface or steric hindrance. This finding is of conceptual importance, since it identifies the

N-terminal part of the SNARE-motif of syntaxin as the major player in terms of mobility restriction. This is in line with previous studies of Sieber et al. 2007 and the tendencies observed for cluster density (see figure 4.10).

The experiments in the system used are interpreted in the light of homomeric interactions of syntaxins. The putative interaction partner SNAP25 can be ruled out, because it is not expressed in the cell type used (HepG2). Nevertheless, the results could be influenced by other interactions of syntaxin. However, different motifs of syntaxin such as the SNARE domain and the TM region are known to convey specificity for clustering (Sieber et al. 2006, Milovanovic et al. 2015). This does not entirely exclude heterologous interactions, but renders it less likely especially for the full length construct. On the other hand, the slight tendency towards higher recovery half times at elevated syntaxin concentration argues for homomeric interactions as the cause for decreased mobility (see figure 4.12).

Theoretic relation between attraction into the cluster and packing density

As laid out above, higher mobility in the PM (see section 4.1.3) correlates with a trend towards enlarged intermolecular distance within the clusters (see section 4.1.2.3). A relation between attraction into the clustered state and cluster density has been addressed by physical models on micro patterning of proteins in membranes. In this context, the balance between short-range attractive and long range repulsive forces were found to control the number of proteins attracted to one cluster (Meilhac et al. 2011).

Of note, the number of proteins in these models is often referred to as "size" of the cluster (Meilhac et al. 2011). This should not be confused with the size definition in this thesis (see e.g. figure 4.2), which describes the physical dimension of the cluster.

According to the theoretical model of Meilhac et al. 2011 the reduction in attractive forces, in this case via deleting the n-SNARE domain of syntaxin, would reduce the number of molecules per cluster. Considering the slightly enlarged cluster area in those constructs lacking the n-SNARE part (see section 4.1.1.1), intermolecular distances have to be increased, further supporting the results obtained in section 4.1.2.3.

5.1.3 Putative mechanism of protein-protein interaction mediated cluster density

Although it proved difficult to obtain absolute figures, the antibody based approach in the current study hints to elevated intermolecular distances within the clusters upon deletion of cytoplasmic protein domains (see section 4.1.2.2 and 4.1.2.3). In principle, this could be mediated by the loss of cluster specificity, mediated by the SNARE domain (Sieber et al. 2006). Thus, the deletion of these very parts could promote the formation of heteromeric

clusters with other proteins (see above). Those proteins could act as spacers between the syntaxins and thereby lead to elevated intermolecular distances.

A strong argument against this hypothesis is provided by the fact that increased intermolecular distances correlates with enhanced mobility in the PM (see section 4.1.3). Such phenomenon points to the general reduction of intermolecular interaction within the clusters. Therefore, it is more likely that the elevated distances are based rather on loosening of the cluster than on the assembly into heteromeric clusters.

Clearly, the here conducted experiments cannot reveal a detailed molecular mechanism for a dense packing mechanism. However, they allow for a few speculations on the question as to how this finding could be explained on a molecular basis:

The most prominent structurally resolved complex with syntaxin is the four-helix SNARE bundle that is important for the fusion of vesicles in neuronal exocytosis. In this complex of SNAP25, synaptobrevin and syntaxin, the SNARE motifs form intertwined helices in close contact, which are stabilized through several layers of interaction (Sutton et al. 1998). The N-terminal part of the SNARE motif was identified to initialize this contact (Sørensen et al. 2006) and N to C terminal zippering of the helical SNARE motifs was suggested to proceed beyond the SNARE motif into the PM (Stein et al. 2009).

Intriguingly, close physical contact of SNARE motifs is not restricted to the heteromeric four-helical bundle, but can also occur between two SNARE domains of syntaxin (Misura et al. 2001, in this study the SNARE motif is called "H3"). Such self-association to tightly packed dimers as observed in Misura et al. 2001 highlights the feasibility of SNARE interactions conveying homomeric assemblies of syntaxin. The dimers could constitute the basic structural entity from which higher order oligomers are formed.

In respect of the current study, the N-terminus of the SNARE motif could initiate the helical extension and therefore assure the tight packing within the cluster. Clearly, the results obtained from *in vitro* studies of the four-helix bundle or the syntaxin SNARE dimer are not entirely transferrable to the syntaxin cluster. The question remains why the putatively similar interaction mechanism results in an assembly of maximal four helices *in vitro* (Sutton et al. 1998) but clusters of roughly 75 molecules in the PM (Sieber et al. 2007). Certainly, other clustering promoting forces have to be responsible for this difference.

5.1.4 Sketching an integrative view on syntaxin clustering factors

Syntaxin exhibits the propensity to cluster even without major cytoplasmic parts (see syx-ΔCyt in figure 4.2). Stunningly, exactly those cytoplasmic protein domains are able to cluster on their own without the TM domain and the polybasic stretch (see figure 4.3). Therefore, clustering has to be mediated via different layers of interaction. This finding is in line with previous studies reporting on the influence of several different factors for syntaxin clustering residing in the hydrophobic core of the PM as well as in the cytoplasmic periphery.

Certain interactions mediate qualitatively different clusters. An example is the SNARE domain-mediated specificity for the attraction into either syntaxin 4 or syntaxin 1 clusters (Sieber et al. 2006). In the same context, the here presented results point towards the importance of specific protein-protein interactions for packing density of the protein cluster.

Therefore, it could be speculated that there is a basic framework for clustering mediated, for instance, by electrostatic interactions (Bogaart et al. 2011, Khuong et al. 2013), hydrophobic mismatch (Milovanovic et al. 2015), the embedding in superimposed protein networks (Saka et al. 2014) and confinement through cytoskeleton interactions (Lillemeier et al. 2006, Kusumi et al. 2011).

Beyond this, there may be further mechanisms for the manifestation of specific cluster characteristics such as composition or packing density. Protein-protein interactions constitute perfect candidates for mediating such fine tuning, since they could be readily regulated by e.g. binding of adaptor proteins or phosphorylation without the necessity to amend overall membrane properties as, for instance, cholesterol or phosphoinositol content.

To assemble the pieces of this puzzle, further work has to be done. Experiments on this matter should not only include outer cluster dimensions but should further concentrate on the inner architecture of the cluster such as packing density. Of general interest could be the implication of structure for clustering. From a more general perspective on the relationship of secondary structure and homomeric protein assemblies, interactions between helical protein domains allow for dense assembly with theoretically unlimited extensions (J. A. Marsh et al. 2015). This correlation applies for soluble proteins and it would be exciting to extend it to membrane embedded proteins. Future experiments could therefore involve the insertion of helix breakers in the SNARE motif and the linker region with the TM domain and subsequent testing of mobility or packing density.

5.2 Functional aspects of a supra-molecular structure at the cytoplasmic periphery of the PM - ER-PM MCS

Membrane contact sites between the PM and the ER are ubiquitously present in eukaryotic cells at high copy numbers (Helle et al. 2013). Despite their universal occurrence, research on ER-PM MCS was neglected for decades due to technical difficulties limiting the investigation of their composition and function. Recent technical innovations helped to gain knowledge particularly with respect to the tethering architecture mediated by lipid-protein and protein-protein interactions. However, there is still room for improvement. The presence of putative lipid transfer proteins (LTP) that are able to bind to both opposing membranes at MCS point towards an important involvement of MCS in vesicle independent lipid transfer (Levine 2004, Prinz 2014). To address this issue, the present study established a cell-free ER-PM MCS preparation, which enables the analysis of lipid transfer allowing for differentiation between LTP-mediated and spontaneous lipid transfer (SLT) at those sites.

5.2.1 Relevance of the ER-PM preparation

This study revealed that the sheeting technique can be applied to dissect ER-PM MCS (section 4.2.1). Those sites were highly abundant on PM sheets of diverse cell lines (section 4.2.2), which is consistent with electron microscopy studies of ER-PM MCS (Pichler et al. 2001, Giordano et al. 2013).

Although the sheeting technique has been used for decades, remaining ER membranes on PM sheets have not attracted attention before. One possible reason can be found in the difficulty to visualize the ER fragments on PM sheets (Luis Spitta and Thorsten Lang, personal communication). Presumably, when the bulk of the ER is removed, the ER membranes partly reseal to prevent lipid perturbation at the edges. Detection of luminal ER epitopes by antibodies could hence be restricted. Furthermore, the contact sites of the ER are highly specialized micro-environments with a defined protein content that likely differs from the rest of the peripheral ER (Shibata et al. 2010). This renders it difficult to identify the MCS by immunostaining of general ER marker proteins. Thus, only the overexpression of intrinsically fluorescent ER resident proteins, in case of this study RFP-Sec61β and ER-RFP, or the staining of marker lipids by click-chemistry enabled the detection of ER on the PM sheets (section 4.2.1.1).

In principle, it is conceivable that high mechanical forces of the sonication pulse produces small fragments of the ER, which are pushed to the PM sheets. In this case, the preparation

would consist of artificial ER remnants not related to physiological ER contact sites. There are three major arguments, however, which contradict this hypothesis. First, the ER spot pattern near the PM was also present in unsonicated cells (section 4.2.1.2). Second, the stable attachment of ER to the PM was mediated by proteins (section 4.2.2.2). Finally, the strongest evidence for functional ER-PM MCS is the translocation of the integral ER membrane protein STIM1 into the ER spots on PM sheets upon ER calcium depletion (section 4.2.2.1). Collectively, the data strongly argue in favor of the ER spots on the PM sheets presenting actual MCS.

It should be noted, that at this point an increased distance between PM and ER in the preparation compared to intact cells cannot be ruled out. However, the stability over long times and the proteinaceous anchoring at the PM are in line with the finding that close apposition of the two membranes is mainly mediated by tethering proteins (Manford et al. 2012) and thus do not support this notion. Quantitative and comparative analysis of EM images in cells and on PM sheets could provide more information on this matter.

One major limitation of the established cell-free MCS dissection is the reduction in cytoskeleton elements. While single elements, as e.g. actin stress fibers, partially remain attached to the PM sheets, major anchoring points are lost during the preparation. The tension necessary for remodeling and restructuration of the peripheral ER is lost. However, this does presumably not change the micro-environment of the contact site itself, since direct tethering of ER and PM is mediated by separate, specific protein-lipid interactions (see section 1.3.2.1).

In summary, this study provides a detergent free technique for preparing *bona fide* ER-PM MCS suitable for the investigation of lipid transfer at these sites. The removal of the bulk of the ER as well as other intracellular structures enables fluorescence microscopy with high signal-to-noise ratio. Consequently, nano-anatomical aspects of MCS diameter and shape, for example by high resolution microscopy, can be investigated. Moreover, the preparation could be used to perform protein composition analysis, e.g. by double stainings, to identify MCS associated proteins.

5.2.2 Advantages and insights from the novel ER-PM MCS preparation

Before turning to the main issue of spontaneous lipid transfer, a few side issues should be discussed to illustrate the potential of the preparation in further research on ER-PM MCS.

Definition and identification of ER-PM MCS

What is the exact definition of an ER-PM MCS? First and foremost, tethering via specific proteins is a commonly accepted idea. There are several proteins identified that link the two membranes together via lipid-protein or lipid-lipid interactions. However, a number of proteins are yet to be identified. Second, the distance between ER and PM, measured by EM, provides an option for MCS classification. Values ranging between 7 and 30 nm have been proposed (Carrasco et al. 2011). However, obtaining accurate membrane distances is difficult and largely depends on the methods used for the preparation of EM samples. Moreover, extended peripheral ER sheets adjacent to the PM, which are distinct from MCS, further complicate the analysis. Furthermore, the preparation and imaging of EM samples is time consuming and expensive.

In contrast, the preparation used in this study offers a fast, simple and cheap identification method for ER-PM MCS that allows high throughput screening and statistical analysis based on high numbers. According to the results presented in section 4.2, ER-PM MCS could be defined as the parts of the peripheral ER, that (i) remain attached to the PM after the application of a defined mechanical force for generation of PM sheets (section 4.2.1) and (ii) are tethered via proteins to the PM (section 4.2.2.2). This definition essentially matches those proposed by others (Carrasco et al. 2011). Additionally, staining for specific proteins could allow for fast discrimination of MCS subpopulations with different compositions.

Structural aspects of SOCE at ER-PM MCS

One of the best established functions of ER-PM MCS is the store activated calcium release (SOCE), which is the calcium depletion-induced opening of PM localized calcium channels. The concomitant STIM1 relocation to the MCS was used in the current study to confirm that the ER spots on PM sheets indeed are MCS (section 4.2.2.1). In this context, the colocalization of STIM1 and PC spots was calculated, revealing a high overlap of 87% upon activation with TG. PC spots nearly exclusively represent ER membranes (see figure 4.16), with the exception of a few vesicles (see figure 4.17), and the number of MCS did not evidently increase after activation with TG (see figure 4.20). Thus, STIM1 appears to be mainly recruited into preexisting contact sites, which are kept in place by other tethering proteins.

This finding is in contrast to a study of Wu et al. 2006, who reported on a substantial portion of new contact sites upon store depletion. The difference could be explained by the different parameters used for the identification of the MCS: while Wu et al. 2006 measured

the distance between ER and the PM by electron microscopy, this present study identified MCS by the fluorescence signal of ER markers after generation of PM sheets. Interestingly, TG treatment entailed the enlargement of the ER spots on the sheets without influencing the number of spots (see figure 4.20). This matches the study of Orci et al. 2009 reporting on the formation of cisternal ER stacks near the PM upon calcium depletion from the ER.

In any case, the present study corroborates the idea that in a resting cell state ER-PM MCS are mediated by basic tethering proteins into which STIM1 is recruited upon calcium depletion from the ER. Hence, it could be hypothesized that the extensive remodeling proposed for the process of SOCE (Shen et al. 2011) mainly affects the morphology of the MCS, but not its initial formation. Therefore, the system used in this study conceivably reflects changes in the structure of the cortical ER with the advantage of simple identification of proteinaceous ER anchoring to the PM. The preparation can thus be used as a tool to investigate structural remodeling of the ER in the cytoplasmic periphery of the PM, for instance during SOCE.

Bidirectional tethering of the ER to the PM

The dissected ER contacts remained stable on the PM sheets even after long incubation times up to three hours (see for example figure 4.17). Two factors were found to destabilize them: exposure to high (50 mM) $CaCl_2$ (section 4.2.1.2) and protein digestion with trypsin (section 4.2.2.2).

A possible explanation for calcium sensitivity lies in the known features of tethering proteins at MCS: As introduced in section 1.3.2.1 all of the so far identified tethering proteins depend on interaction with negatively charged proteins at the PM such as $PI(4,5)P_2$ (Henne et al. 2015). Calcium is known to interact with these lipids (Carvalho et al. 2008) and to inhibit their recognition by specific protein domains (Bilkova et al. 2017). The interference of high calcium concentrations with tethering of ER-PM MCS is therefore not surprising. Further studies on this issue could involve calcium concentration series to refine the picture of calcium dependent tethering and to dissect the interaction in greater molecular detail.

Protein digestion by trypsin readily mobilized the ER-PM MCS on PM sheets and they started moving laterally on the sheet (section 4.2.2.2). Only after long trypsin incubations of 45 min ER spots completely detached from the PM sheets. This finding is unexpected and suggests that there are two types of ER-PM anchoring: a focal attachment that determines the direct binding and a second type that causes lateral stability and is more susceptible to trypsin. Possible underlying candidates for the later type are elements of

the cytoskeleton, that are known to restrain protein diffusion within membranes (Lenne et al. 2006). Still, at this point we can only speculate about the nature of the lateral tether. Analyzing colocalization of the ER spots and cytoskeleton markers or testing the susceptibility of the contact sites to cytoskeletal drugs could help to develop a more refined picture.

There are two possible scenarios that would allow for uncaged movement along the membrane plane upon trypsin treatment. Firstly, it could be mediated by a lipid induced haptotactic motion due to charge differences between the cytoplasmic leaflets of PM and ER. This "surfing" of lipid vesicles was shown in a protein free environment on a supported bilayer (Solon et al. 2006). The study revealed an exchange of lipids at the contact zone between GUV and planar lipid bilayer, which is in contrast to our finding of a rather stable PC spot intensity (section 4.2.2.2), rendering this mechanism unlikely. Secondly, lateral movement could be possible via a protein anchor inserted into the PM. This is the more likely scenario, since the final detachment of the PC spots was shown to depend on protease activity.

To sum up, the dissection method for the production of ER-PM MCS developed in this study offers a fast, cheap and simple approach to investigate diverse questions related to structure and function of these supra-molecular assemblies.

5.2.3 Revisiting spontaneous lipid transfer at MCS

The major site of lipid biosynthesis is the ER. In order to supply other cellular membranes with lipids there have to be efficient lipid export mechanisms such as vesicular transfer or LTPs. The simplest way, however, for lipids to switch from one membrane to another is spontaneous transfer, during which a lipid desorbs from the donor bilayer and transfers through the aqueous surroundings followed by subsequent adsorption into the acceptor bilayer, independent of carrier proteins. So far, SLT is considered a possible mechanism of cellular lipid transport (Lev 2010, Lev 2012, Stiban et al. 2008, Somerharju 2015). However, with some exceptions (Stiban et al. 2008, Kunze et al. 2009), the vast majority of experimental evidence for SLT is derived from *in vitro* studies on artificial or partly artificial membrane systems, mostly deprived of proteins (Jones et al. 1989, Longmuir et al. 1989). Transfer half times of hours to days in these systems lead to the assumption that SLT is physiologically irrelevant for cellular lipid transfer (Holthuis et al. 2014). However, *in vitro* studies revealed that SLT is influenced by the donor-acceptor membrane distance

(Jones et al. 1990), membrane curvature (Steck et al. 1988) and membrane composition (Wimley et al. 1991) with the desorption of the lipid from the donor membrane being the rate limiting step (McLean et al. 1981). This raises the question whether the long transfer half times obtained in some artificial lipid systems are relevant for biological micro-environments in which two opposed membranes are tightly attached to each other such as MCS.

The first point to consider here is the distance between donor and acceptor membranes. The closer the two membranes, the less the hydrophobic lipid surface is exposed to the hydrophilic surrounding during the inter-membrane transfer step. Indeed, reducing the distance between donor and acceptor membrane by occasional collision was shown to accelerate PC transfer between liposomes (Jones et al. 1989) as well as phosphatidic acid transfer between liposomes and cells (Longmuir et al. 1989). In experiments on PC transfer the exchange half time was reduced by half if the vesicle concentration was 10 - fold increased (Jones et al. 1989).

What is the situation at ER-PM MCS? On the one hand, the high occupancy of proteins on the membrane periphery could prevent direct contact between the two opposed lipid bilayers. Most of the up to now identified ER-PM tethers are large proteins (Henne et al. 2015) arguing against direct contact between the membranes. On the other hand, EM images of the contacts seem to suggest the exact opposite (Orci et al. 2009, Fernández-Busnadiego et al. 2015 and figure 1.1). The average distance at ER-PM MCS was proposed to range between 7 and 30 nm (Carrasco et al. 2011), although exact measurement seem to largely depend on the fixation or embedding method used for electron microscopy. Therefore, in comparison to the *in vitro* data, it is still unclear whether the distance between ER and PM at MCS may promote or rather diminish SLT.

Membrane curvature additionally influences SLT. Spontaneous cholesterol transfer, for example, was shown to strongly depend on the curvature of the acceptor structure (Steck et al. 1988) or inversely of the donor vesicle (Thomas et al. 1988). The high curvature may disturb lipid packing thereby facilitating the rate limiting desorption step. Considering the fact that some of the tethering proteins at ER-PM MCS insert with hairpin structures into the ER (Giordano et al. 2013) an elevated curvature of the ER membrane is probable. Indeed, a recent cryo-electron tomography study on ER-PM MCS in COS-7 cells (Fernández-Busnadiego et al. 2015) as well as a conventional EM study in HeLa cells (Orci et al. 2009) occasionally observed such curved ER membranes at the predicted contact sites. As a result, the desorption step for lipid transfer from the ER to the PM could be

facilitated.

Another very influential difference between the artificial lipid systems previously used to study SLT and native MCS are the protein domains within the hydrophobic core of the native membranes (section 1.3.1). Again, two opposing scenarios are possible in this context: Either protein-lipid interactions stabilize the bilayers and thus prohibit SLT, or TM proteins perturb lipid bilayer structure and enhance SLT. Along these lines, the insertion of specific TM peptides has been reported to induce otherwise restricted lipid trans-bilayer movement in vesicles (Kol et al. 2003).

In summary, the ER-PM MCS, as well as other MCS, could on the one hand offer a perfect micro-environment for SLT providing greatly enhanced transfer kinetics of lipids compared to the *in vitro* studies. On the other hand, the possibility exists that SLT is blocked for instance through protein shielding of donor and acceptor membrane. The question of SLT at MCS is therefore highly relevant for the understanding of cell biological processes and thus merits further investigation. In this context, PM sheets provide an accessible native experimental system.

5.2.4 No evidence for SLT of PC and cholesterol

To address the question of SLT at ER-PM MCS, the preparation was used to investigate whether PC or cholesterol would transfer spontaneously. In short, for neither of the two lipids evidence for spontaneous trans-bilayer movement at the isolated ER-PM MCS was observed.

Spontaneous transfer of PC

When pPC was labeled on PM sheets, the fluorescence intensity of the ER spots reflected the expected natural concentration gradient of PC between the ER and PM (section 4.2.1.3). This concentration gradient did not dissipate when freshly prepared sheets were incubated for up to 2 h (section 4.2.3.1) in line with the absence of SLT. Conversely, the gradient even increased upon incubation. A possible explanation for this observation could be the pPC transport against the concentration gradient. However, a more detailed analysis revealed that this effect was primarily caused by a decrease in PM fluorescence, which may be explained by PM resident phospholipases cleaving the propargyl head group of pPC to which the label is attached. It cannot be excluded that phospholipase cleavage proceeds faster than the SLT and therefore the gradient rather increases although PC moves from the ER to the PM. In this scenario however, ER spots should also decrease in fluorescence, which was not the case.

Additional evidence for a lack of SLT stems from an experiment directly observing the fluorescently labeled BP-PC on PM sheets. FLAP revealed a lateral movement of lipids within the PM but no lipid flux along the PC gradient from the ER into the PM (section 4.2.3.1). This finding corroborates the above mentioned incubation experiment.

A related experiment was conducted in another study (Spitta 2012): The presumed objects of research in this former study were PC platforms, which were later on identified to represent ER-PM MCS (section 4.2.1.2). The author used the same metabolic labeling for PC as in the here presented work. When single PC spots (ER-PM MCS) on PM sheets were bleached, their fluorescence recovered within a few seconds. The majority of spots recovered up to 30% of their original fluorescence and occasionally spots even reached full recovery. The author hypothesized to observe a lipid exchange between the PM and the PC platforms (ER-PM MCS). In contrast, recovery of the spots in the bleached area has not been observed in this study (see figure 4.24). Further, it was not possible to reproduce the findings of Spitta 2012 in a similarly conducted FRAP experiment (data not shown). This discrepancy could be attributed to the following technical differences.

Firstly, a 10-fold higher azido-sBP concentration was used for cycloaddition to pPC in the Spitta study. The concomitant higher labeling density may have lead to quenching before and de-quenching after bleaching which could have been falsely interpreted as fluorescence recovery. Additionally, the study of Spitta 2012 presumed the PC enrichments to be integral parts of the PM and accordingly, the experiment was designed for a 2D structure. Thus, some of the spots could largely extent into the periphery of the PM. This reservoir would be bleached less efficiently and may thus cause some recovery. Furthermore, the study of Spitta 2012 included around 70 spots in total, while the FLAP approach enabled to obtain results from 80 - 180 spots for each of the three independent experiments. Finally, it is important to consider another difference between the FRAP and the FLAP approach: While FRAP is designed to detect lipid transfer from the PM back to the ER, FLAP addresses the opposite transfer direction. Since SLT is expected to proceed along the concentration gradient, FLAP is the more suitable approach for studying SLT of PC.

When studying SLT it is also important to take temporal aspects into account. Formally, it could be possible that SLT already takes place within the first few minutes after sheeting. This would result in a readily equilibrated system from the beginning and exclude the study of gradient neutralization. Although this hypothesis cannot be fully excluded, a strong argument against it is provided by the experiment in section 4.2.3.1. Using the carrier

HPαCD, lipid transfer from the ER is driven by the concentration gradient to the PM. This positive control also shows that the sensitivity of the system is high enough to detect fluorescence changes based on lipid transfer. From a methodological point of view using HPαCD as a carrier might not be the optimal solution, since cyclodextrins are only partly specific for the lipid type they take up (Zidovetzki et al. 2007). A more specific and less invasive method could be the application of a PC specific lipid transfer protein such as PC-TP (Wirtz et al. 1972). However, specificity was not crucial in this study and the ability to process a desorption-adsorption cycle of pPC (see figure 4.22) identified HPαCD as a suitable tool for the purpose of a positive control for lipid transfer between ER and PM membranes.

Another important technical aspect to consider is the labeling of lipids. Most of the organic dyes available for lipid labeling are only slightly smaller or even larger than the lipids themselves. Therefore, lipid labeling with fluorophores always raises concerns about their influence on lipid behavior (Sezgin et al. 2011). In the FLAP experiment a sBP was linked to the propargyl head group of pPC before investigating SLT. Although the sBP molecule is bulky in comparison to the PC backbone, it is unlikely to account for the lack of lipid flux for the following reasons. Firstly, addition of the sBP increases the overall hydrophilicity and thus the solubility of PC in the aqueous solvent (Maier et al. 2002). An increased solubility, however, should facilitate rather than reduce SLT (see above, section 5.2.3) Secondly, the headgroup of phospholipids was shown to have less impact on SLT than the hydrophobic fatty acid parts (Massey et al. 1982). By applying metabolic labeling at the choline head group the natural fatty acid composition remains unaffected (Jao et al. 2009). Instead of introducing a single lipid species, the major advantage of metabolic labeling is the inclusion of all PC species that are naturally present in cellular membranes. For these reasons, it is rather unlikely that the fluorescent headgroup prevents SLT of sBP-PC.

While the absence of SLT was observed for pPC or sBP-PC, it cannot be excluded, that other glycerophospholipids (GPLs) are able to move between the bilayers. In principle, there could be a hydrophobicity threshold that determines an energy barrier for lipid desorption from the bilayer. *In vitro* experiments on vesicles showed a highly accelerated transfer of lyso-GPLs in comparison to GPL with two fatty acids (McLean et al. 1984). Additionally, the degree of saturation could induce local lipid perturbation, thus facilitating desorption of the lipid. As mentioned above the usage of metabolic head group labeling provides the great advantage of considering all natural PC species with respect

to their fatty acid distribution (Jao et al. 2009). Still, for a more comprehensive study on the effect of hydrophobicity on SLT at contact sites, one possibility is to incorporate GPLs of different fatty acid length and saturation into the PM and compare their ability to transfer into the ER membranes.

Spontaneous cholesterol transfer

Cholesterol is capable to transfer spontaneously between artificial membrane vesicles (Jones et al. 1990, McLean et al. 1981) and the transfer is accelerated if vesicles exhibit high bilayer curvature (Thomas et al. 1988). Therefore, cholesterol seemed to be an interesting lipid to probe for SLT in the ER-PM MCS preparation. When filipin was used to stain cholesterol, the ER membranes were not detectable on the background of the bright PM staining (section 4.2.3.2), which reflects the different cholesterol contents of the two membranes (Meer et al. 2011).

The formation of complexes with SM was previously suggested to lower the effective cholesterol concentration in the PM (Baumann et al. 2005) and can be considered as a thermodynamic trap. Thus, the expected direction of spontaneous cholesterol flux in cells is from the site of synthesis, the ER, to the PM. However, when ER membranes were loaded in the cell-free system with detectable amounts of cholesterol, this artificially established concentration gradient persisted. This was even the case when the overall cholesterol concentration was depleted ruling out an artifact of overloading. This finding further supports the idea that there is no spontaneous lipid movement at ER-PM MCS in this experimental system.

A MβCD-cholesterol complex was used for cholesterol loading of the ER membranes. It might be argued that the lack of cholesterol transfer is caused by a change in the overall lipid composition through the lipid carrier cyclodextrin. Particularly the exchange of sphingomyelin could strongly effect the outcome of the experiment for the above mentioned reason. However, the heptameric β-cyclodextrins are known to have a higher specificty for cholesterol than for other lipids (Zidovetzki et al. 2007). In experiments on monolayers using a similar concentration of 1.4 mM MβCD, for example, only 5% sphingomyelin relative to cholesterol was extracted (Ohvo et al. 1996). Therefore, the MβCD-cholesterol complex can be considered as a suitable tool for the purpose of this study.

It is important to keep in mind that filipin is not able to detect low cholesterol levels such as the natural cholesterol content of a few percentage of total ER lipids (Radhakrishnan et al. 2008)(see figure 4.25). This is of minor importance for the study presented here, because the mere ability to load ER spots with cholesterol already argues against SLT.

Still, for a more precise approach of cholesterol transfer, in particular when assessing LTP mediated transfer, a more sensitive method for cholesterol detection is desirable. One possibility may be the usage of alkyne cholesterol for visualization by cycloaddition of reporter azides (Hofmann et al. 2014).

The data presented in this study are in contrast to a recent work on cholesterol movement in Niemann-Pick disease (NPC) 1 and NPC 2 fibroblasts. The authors reported a rapid exchange between the entire intracellular cholesterol pool and the PM, even if cells were fixed with glutaraldehyde, which should prevent protein and vesicle mediated transfer (Lange et al. 2012). A possible explanation for the high inter-membrane mobility of cholesterol in Lange et al. 2012 is the special lipid composition of the NPC1/2 cell membranes. These cells are known to accumulate high amounts of cholesterol and glycolipids in their lysosomes and late endosomes (Bi et al. 2010). Moreover, the lipid transfer in Lange et al. 2012 extends to the entire cell and does not differentiate between compartments involved in the transport, while our study enables the precise investigation of lipid transfer between ER and PM. Interestingly, fixation enhanced the mobility of cholesterol in NPC1/2 cells (Lange et al. 2012). Although the authors show that the cells are not permeable for cell viability dyes, it is formally possible that fixation changes membrane properties such as tension or lipid order. This could further enhance the spontaneous transfer of lipids through destabilization of membrane structure. Although I cannot exclude that under certain circumstances, as for example the absence of functional NPC1 and NCP2 proteins, cholesterol exhibits high solubility, there is no evidence for a SLT at normal cellular cholesterol levels at ER-PM MCS. In order to clarify the role of specific proteins, further research could be undertaken on PM sheets of NPC1/2 cells to investigate spontaneous cholesterol transfer.

5.2.5 Possible role for lipid transfer proteins

Several reports in the past decade suggested lipid transfer protein (LTP) mediated lipid transport at MCS. Thus, the question arises why I observed no lipid transfer, independent of SLT (section 4.2.3).

The answer to this question requires a more detailed response: Possible candidates for LTPs at ER-PM MCS are the oxy-sterol-binding related proteins (ORPs) for cholesterol and the extended synaptotagmins (E-Syt) for glycerophospholipids. Both protein classes are located at MCS and are able to simultaneously bind to the ER and the PM (Schulz et al. 2009, Giordano et al. 2013). For the yeast ORP homolog Osh4 the simultaneous binding

of phosphoinosotides and sterols within a hydrophobic pocket of the protein stimulated the idea of PI dependent sterol transfer from the ER to the PM (Saint-Jean et al. 2011). Still, the exact role of ORPs in sterol transport is under debate and alternative functions such as e.g. sensing of cholesterol levels and regulation of lipid pathways are discussed (Beh et al. 2012). As to the E-Syts, two recent studies report on the ability to transport glycerophospholipids *in vitro* (Yu et al. 2016, Saheki et al. 2016). Both studies highlight the calcium dependence of the transport. However, the exact molecular mechanism and regulation of E-Syt mediated lipid transfer at ER-PM MCS has been not fully elucidated yet.

The lack of lipid transfer in our experimental system therefore supports the idea that LTPs are highly regulated, presumably by cytosolic factors, which are missing in the preparation. It further corroborates the concept that LTPs are only activated in specific situations such as the accumulation of DAG upon activation of PLC (Saheki et al. 2016).

Further work is necessary to unravel the role of LTPs in lipid transfer at MCS. The experimental system presented in our study can be used to study such mechanisms, since it provides direct access to the site of action and allows for sensitive microscopic analysis in the absence of SLT and vesicular trafficking.

5.3 Reduced dimensionality in supra-molecular structures

The supra-molecular structures addressed in this study are examples for higher order assemblies of molecules that physically separate particular environments (see section 1.3.2). At the same time their components are in constant exchange with the surroundings. Such structures are not restricted to the PM environment but are ubiquitously present in cells (Hartwell et al. 1999). In principal, these supra-molecular assemblies can influence biological processes in two ways: either they create reaction centers to accelerate and promote processes or conversely they shield molecules from participating in particular reactions (Adam et al. 1968, M. A. McCloskey et al. 1986). An example for the latter are complexes of histones and DNA, in which the DNA is densely packed restricting for example access of the transcription machinery. Reaction promoting structures are, for instance, ribosomes, composed of large assemblies of proteins, DNA and RNA working synergistically for protein synthesis.

How can the two supra-molecular subjects of the present thesis be classified in this context?

For the syntaxin clusters two different scenarios are conceivable: One the one hand,

syntaxin clusters could represent reaction centers for vesicle docking and fusion (Lang et al. 2001). This hypothesis is corroborated by the finding that $PI(4,5)P_2$, which is necessary for neuronal exocytosis (Milosevic et al. 2005), accumulates at syntaxin clusters thereby priming exocytic sites (Aoyagi et al. 2005). Arguing with the timing of overlap between syntaxin cluster formation and vesicle docking, Barg et al. 2010 report on the formation of syntaxin accumulation after the docking of vesicles. This is in line with the observation from super-resolution imaging that vesicles rather dock at PM areas of low SNARE abundance (L. Yang et al. 2012).

One the other hand the clusters could, similar to the histone example above, withhold syntaxin molecules. Such "storage" would shield the proteins and thereby prevent unwanted interactions of otherwise highly reactive SNARE motifs. This hypothesis is supported by previous reports on reduced SNARE reactivity within syntaxin clusters (Bar-On et al. 2009). Another argument for the shielding function of the cluster micro-environment can be extracted from the here addressed cluster density: at intermolecular distances between syntaxin molecules of maximally about 6 - 7 nm (Sieber et al. 2007) accessibility for interaction partners could be strongly reduced as shown in the present work for antibody binding (see section 4.1.2). In principle, the shielding of syntaxin molecules within the cluster could not only be a protective mechanism, but might be important to maintain adequate amounts of reactive syntaxin in a reservoir to enable fast release when necessary (Bar-On et al. 2009).

The ER-PM MCS seem to take over a two-sided function regarding their involvement in lipid transfer: On the one hand they probably restrict the ability of lipids to transfer between the two membranes spontaneously, as suggested in the present work. One reason could be that the energetic costs for desorption of the lipids are too high despite high curvature or close apposition of the membranes. A major factor in this context could be high protein density in the inter-membrane cleft between ER and PM. Generally speaking, prevention of SLT at ER-PM MCS might be essential for cellular functions. As described in section 1.3 membrane peripheries are built up by sensitive lipid-lipid and protein-lipid interactions that mutually depend on each other. The membrane lipid composition plays a central role and needs to be tightly regulated. In case of SLT, it would be difficult for cells to preserve lipid asymmetry against concentration gradients. Prevention of lipids leakage at MCS could help to preserve lipid homeostasis and allow for more precise regulation of lipid composition.

However, the putative lack of SLT does not establish ER-PM MCS as lipid transfer

prohibiting environments *per se*. Quite the contrary, it could stress the importance of regulated protein-mediated lipid transfer at those sites, which has been of high interest recently (Saheki et al. 2016, Yu et al. 2016). For the formation of a lipid transfer promoting micro-environment additional factors could be necessary, such as adaptor proteins, the protein-regulated intermembrane spacing or curvature. Therefore, the MCS could act as a regulatory gate that only allows specific lipids at a certain time to pass from one membrane to another.

In conclusion, reduced dimensionality within the supra-molecular structures at the cytoplasmic periphery does not necessarily result in mere promotion or restriction of reactions but rather allows for refined regulation of particular biological processes. The methods developed in this work conserve the fragile supra-molecular assemblies within the native membrane surroundings. Therefore, they may serve as a starting point for further analysis of the enigmatic biological role of these structures and their molecular architecture.

Bibliography

Adam, G. and Delbrück, M. (1968). *Reduction of dimensionality in biological diffusion processes.* Ed. by A. Rich and N. Davidson. London: W.H. Freeman and Company, pp. 198–215.

Alberts, B., Johnson, A., Lewis, J., Raff, M., Roberts, K., and Walter, P. (2002). *Molecular Biology of the Cell, Fourth Edition*, p. 1616.

Almeida, P. F. F., Vaz, W. L. C., and Thompson, T. E. (2005). "Lipid diffusion, free area, and molecular dynamics simulations." In: *Biophysical journal* 88.6, pp. 4434–4438.

Aoyagi, K., Sugaya, T., Umeda, M., Yamamoto, S., Terakawa, S., and Takahashi, M. (2005). "The activation of exocytotic sites by the formation of phosphatidylinositol 4,5-bisphosphate microdomains at syntaxin clusters." eng. In: *The Journal of biological chemistry* 280.17, pp. 17346–17352.

Banjade, S. and Rosen, M. K. (2014). "Phase transitions of multivalent proteins can promote clustering of membrane receptors." In: *eLife* 3.

Barg, S., Knowles, M. K., Chen, X., Midorikawa, M., and Almers, W. (2010). "Syntaxin clusters assemble reversibly at sites of secretory granules in live cells". In: *Proceedings of the National Academy of Sciences of the United States of America* 107.48, pp. 20804–20809.

Bar-On, D., Gutman, M., Mezer, A., Ashery, U., Lang, T., and Nachliel, E. (2009). "Evaluation of the Heterogeneous Reactivity of the Syntaxin Molecules on the Inner Leaflet of the Plasma Membrane". In: *Journal of Neuroscience* 29.39, pp. 12292–12301.

Bar-On, D., Winter, U., Nachliel, E., Gutman, M., Fasshauer, D., Lang, T., and Ashery, U. (2008). "Imaging the assembly and disassembly kinetics of cis -SNARE complexes on native plasma membranes". In: *FEBS Letters* 582.23-24, pp. 3563–3568.

Bar-On, D., Wolter, S., Linde, S. van de, Heilemann, M., Nudelman, G., Nachliel, E., Gutman, M., Sauer, M., and Ashery, U. (2012). "Super-resolution imaging reveals the internal architecture of nano-sized syntaxin clusters". In: *The Journal of biological chemistry* 287.32, pp. 27158–27167.

Batoulis, H., Schmidt, T. H., Weber, P., Schloetel, J.-G., Kandt, C., and Lang, T. (2016). "Concentration Dependent Ion-Protein Interaction Patterns Underlying Protein Oligomerization Behaviours". In: *Scientific Reports* 6, p. 24131.

Baumann, N. A., Sullivan, D. P., Ohvo-Rekilä, H., Simonot, C., Pottekat, A., Klaassen, Z., Beh, C. T., and Menon, A. K. (2005). "Transport of newly synthesized sterol to the sterol-enriched plasma membrane occurs via nonvesicular equilibration." In: *Biochemistry* 44.15, pp. 5816–26.

Beh, C. T., McMaster, C. R., Kozminski, K. G., and Menon, A. K. (2012). "A detour for yeast oxysterol binding proteins." In: *The Journal of biological chemistry* 287.14, pp. 11481–8.

Bennett, H. J., Davenport, J. B., Collins, R. F., Trafford, A. W., Pinali, C., and Kitmitto, A. (2013). "Human junctophilin-2 undergoes a structural rearrangement upon binding PtdIns(3,4,5)P3 and

the S101R mutation identified in hypertrophic cardiomyopathy obviates this response." In: *The Biochemical journal* 456.2, pp. 205–17.

Betzig, E., Patterson, G. H., Sougrat, R., Lindwasser, O. W., Olenych, S., Bonifacino, J. S., Davidson, M. W., Lippincott-Schwartz, J., and Hess, H. F. (2006). "Imaging Intracellular Fluorescent Proteins at Nanometer Resolution". In: *Science* 313.5793.

Bi, X. and Liao, G. (2010). "Cholesterol in Niemann-Pick Type C disease." In: *Sub-cellular biochemistry* 51, pp. 319–35.

Bilkova, E., Pleskot, R., Rissanen, S., Sun, S., Czogalla, A., Cwiklik, L., Róg, T., Vattulainen, I., Cremer, P. S., Jungwirth, P., et al. (2017). "Calcium Directly Regulates Phosphatidylinositol 4,5-Bisphosphate Headgroup Conformation and Recognition". In: *Journal of the American Chemical Society* 139.11, pp. 4019–4024.

Bogaart, G. van den, Meyenberg, K., Risselada, H. J., Amin, H., Willig, K. I., Hubrich, B. E., Dier, M., Hell, S. W., Grubmuller, H., Diederichsen, U., et al. (2011). "Membrane protein sequestering by ionic protein-lipid interactions." In: *Nature* 479.7374, pp. 552–5.

Brini, M., Marsault, R., Bastianutto, C., Alvarez, J., Pozzan, T., and Rizzuto, R. (1995). "Transfected aequorin in the measurement of cytosolic Ca2+ concentration ([Ca2+]c). A critical evaluation." In: *The Journal of biological chemistry* 270.17, pp. 9896–903.

Brotherus, J. R., Griffith, O. H., Brotherus, M. O., Jost, P. C., Silvius, J. R., and Hokin, L. E. (1981). "Lipid-protein multiple binding equilibriums in membranes". In: *Biochemistry* 20.18, pp. 5261–5267.

Brown, D. A. and London, E. (2000). "Structure and function of sphingolipid- and cholesterol-rich membrane rafts." In: *The Journal of biological chemistry* 275.23, pp. 17221–4.

Brown, R. E. (1992). "Spontaneous lipid transfer between organized lipid assemblies". In: *Biochimica et biophysica acta* 1113.3-4, pp. 375–389.

Bulbarelli, A., Sprocati, T., Barberi, M., Pedrazzini, E., and Borgese, N. (2002). "Trafficking of tail-anchored proteins: transport from the endoplasmic reticulum to the plasma membrane and sorting between surface domains in polarised epithelial cells." In: *Journal of cell science* 115.Pt 8, pp. 1689–1702.

Campbell, N. A. and Reece, J. B. (2001). *Biology*. 6th Editio. Benjamin Cummings.

Carrasco, S. and Meyer, T. (2011). "STIM proteins and the endoplasmic reticulum-plasma membrane junctions." In: *Annual review of biochemistry* 80, pp. 973–1000.

Carvalho, K., Ramos, L., Roy, C., and Picart, C. (2008). "Giant Unilamellar Vesicles Containing Phosphatidylinositol(4,5)bisphosphate: Characterization and Functionality". In: *Biophysical Journal* 95.9, pp. 4348–4360.

Chandler, D. (2005). "Interfaces and the driving force of hydrophobic assembly". In: *Nature* 437.7059, pp. 640–647.

Christian, A. E., Haynes, M. P., Phillips, M. C., and Rothblat, G. H. (1997). "Use of cyclodextrins for manipulating cellular cholesterol content." In: *Journal of lipid research* 38.11, pp. 2264–72.

Contreras, F.-X., Ernst, A. M., Haberkant, P., Björkholm, P., Lindahl, E., Gönen, B., Tischer, C., Elofsson, A., Heijne, G. von, Thiele, C., et al. (2012). "Molecular recognition of a single sphingolipid species by a protein's transmembrane domain." In: *Nature* 481.7382, pp. 525–9.

Coskun, Ü. and Simons, K. (2011). "Cell membranes: The lipid perspective". In: *Structure* 19.11, pp. 1543–1548.

Derler, I., Jardin, I., Stathopulos, P. B., Muik, M., Fahrner, M., Zayats, V., Pandey, S. K., Poteser, M., Lackner, B., Absolonova, M., et al. (2016). "Cholesterol modulates Orai1 channel function". In: *Science Signaling* 9.412, ra10–ra10.

Di Paolo, G. and De Camilli, P. (2006). "Phosphoinositides in cell regulation and membrane dynamics". In: *Nature* 443.7112, pp. 651–657.

Dietrich, C., Bagatolli, L. A., Volovyk, Z. N., Thompson, N. L., Levi, M., Jacobson, K., and Gratton, E. (2001). "Lipid rafts reconstituted in model membranes." In: *Biophysical journal* 80.3, pp. 1417–28.

Doherty, G. J. and McMahon, H. T. (2008). "Mediation, modulation, and consequences of membrane-cytoskeleton interactions." In: *Annual review of biophysics* 37, pp. 65–95.

Dupuy, A. D. and Engelman, D. M. (2008). "Protein area occupancy at the center of the red blood cell membrane". In: *Proceedings of the National Academy of Sciences of the United States of America* 105.8, pp. 2848–2852.

Eggeling, C., Ringemann, C., Medda, R., Schwarzmann, G., Sandhoff, K., Polyakova, S., Belov, V. N., Hein, B., Middendorff, C. von, Schönle, A., et al. (2009). "Direct observation of the nanoscale dynamics of membrane lipids in a living cell." In: *Nature* 457.7233, pp. 1159–1162.

Elias, P. M., Friend, D. S., and Goerke, J. (1979). "Membrane sterol heterogeneity. Freeze-fracture detection with saponins and filipin." In: *The journal of histochemistry and cytochemistry : official journal of the Histochemistry Society* 27.9, pp. 1247–60.

Engelman, D. M. and Rothman, J. E. (1972). "The planar organization of lecithin-cholesterol bilayers." In: *The Journal of biological chemistry* 247.11, pp. 3694–7.

Fagone, P. and Jackowski, S. (2009). "Membrane phospholipid synthesis and endoplasmic reticulum function." In: *Journal of lipid research* 50 Suppl.Suppl, S311–6.

Fairn, G. D., Schieber, N. L., Ariotti, N., Murphy, S., Kuerschner, L., Webb, R. I., Grinstein, S., and Parton, R. G. (2011). "High-resolution mapping reveals topologically distinct cellular pools of phosphatidylserine". In: *The Journal of Cell Biology* 194.2, pp. 257–275.

Ferguson, K. M., Lemmon, M. A., Schlessinger, J., and Sigler, P. B. (1995). "Structure of the high affinity complex of inositol trisphosphate with a phospholipase C pleckstrin homology domain." In: *Cell* 83.6, pp. 1037–46.

Fernández-Busnadiego, R., Saheki, Y., Camilli, P. de, and De Camilli, P. (2015). "Three-dimensional architecture of extended synaptotagmin-mediated endoplasmic reticulum-plasma membrane contact sites". In: *Proceedings of the National Academy of Sciences of the United States of America*, p. 201503191.

Fischer, M. A., Temmerman, K., Ercan, E., Nickel, W., and Seedorf, M. (2009). "Binding of Plasma Membrane Lipids Recruits the Yeast Integral Membrane Protein Ist2 to the Cortical ER". In: *Traffic* 10.8, pp. 1084–1097.

Florian, J. A., Kosky, J. R., Ainslie, K., Pang, Z., Dull, R. O., and Tarbell, J. M. (2003). "Heparan sulfate proteoglycan is a mechanosensor on endothelial cells." In: *Circulation research* 93.10, e136–42.

Ford, M. G. J., Mills, I. G., Peter, B. J., Vallis, Y., Praefcke, G. J. K., Evans, P. R., and McMahon, H. T. (2002). "Curvature of clathrin-coated pits driven by epsin". In: *Nature* 419.6905, pp. 361–366.

Fugler, L., Clejan, S., and Bittman, R. (1985). "Movement of cholesterol between vesicles prepared with different phospholipids or sizes." In: *The Journal of biological chemistry* 260.7, pp. 4098–102.

Gil, T., Ipsen, J. H., Mouritsen, O. G., Sabra, M. C., Sperotto, M. M., and Zuckermann, M. J. (1998). "Theoretical analysis of protein organization in lipid membranes". In: *Biochimica et Biophysica Acta (BBA) - Reviews on Biomembranes* 1376.3, pp. 245–266.

Giordano, F., Saheki, Y., Idevall-Hagren, O., Colombo, S. F., Pirruccello, M., Milosevic, I., Gracheva, E. O., Bagriantsev, S. N., Borgese, N., and De Camilli, P. (2013). "PI(4,5)P(2)-dependent and Ca(2+)-regulated ER-PM interactions mediated by the extended synaptotagmins." In: *Cell* 153.7, pp. 1494–509.

Gowrishankar, K., Ghosh, S., Saha, S., C., R., Mayor, S., and Rao, M. (2012). "Active Remodeling of Cortical Actin Regulates Spatiotemporal Organization of Cell Surface Molecules". In: *Cell* 149.6, pp. 1353–1367.

Halemani, N. D., Bethani, I., Rizzoli, S. O., and Lang, T. (2010). "Structure and dynamics of a two-helix SNARE complex in live cells." In: *Traffic* 11.3, pp. 394–404.

Hartwell, L. H., Hopfield, J. J., Leibler, S., and Murray, A. W. (1999). "From molecular to modular cell biology". In: *Nature* 402.supp, pp. C47–C52.

Heerklotz, H. (2002). "Triton Promotes Domain Formation in Lipid Raft Mixtures". In: *Biophysical Journal* 83.5, pp. 2693–2701.

Helle, S. C. J., Kanfer, G., Kolar, K., Lang, A., Michel, A. H., and Kornmann, B. (2013). "Organization and function of membrane contact sites". In: *Biochimica et Biophysica Acta - Molecular Cell Research* 1833.11, pp. 2526–2541.

Henne, W. M., Liou, J., and Emr, S. D. (2015). "Molecular mechanisms of inter-organelle ER–PM contact sites". In: *Current Opinion in Cell Biology* 35, pp. 123–130.

Heo, W. D., Inoue, T., Park, W. S., Kim, M. L., Park, B. O., Wandless, T. J., and Meyer, T. (2006). "PI(3,4,5)P3 and PI(4,5)P2 lipids target proteins with polybasic clusters to the plasma membrane." In: *Science (New York, N.Y.)* 314.5804, pp. 1458–61.

Hermann, M., Klein, R., and Schultz, T. (2014). "Segmentation-free quantification of spots on a homogeneous background". In: *2014 IEEE Conference on Visual Analytics Science and Technology (VAST)*. IEEE, pp. 253–254.

Heumann, R., Kachel, V., and Thoenen, H. (1983). "Relationship between NGF-mediated volume increase and "priming effect" in fast and slow reacting clones of PC12 pheochromocytoma cells". In: *Experimental Cell Research* 145.1, pp. 179–190.

Heuser, J. (2000). "The production of 'cell cortices' for light and electron microscopy". In: *Traffic (Copenhagen, Denmark)* 1.7, pp. 545–552.

Hofmann, K., Thiele, C., Schött, H.-F., Gaebler, A., Schoene, M., Kiver, Y., Friedrichs, S., Lütjohann, D., and Kuerschner, L. (2014). "A novel alkyne cholesterol to trace cellular cholesterol metabolism and localization." In: *Journal of lipid research* 55.3, pp. 583–91.

Holthuis, J. C. M. and Menon, A. K. (2014). "Lipid landscapes and pipelines in membrane homeostasis." In: *Nature* 510.7503, pp. 48–57.

Homsi, Y., Schloetel, J.-G., Scheffer, K. D., Schmidt, T. H., Destainville, N., Florin, L., and Lang, T. (2014). "The extracellular δ-domain is essential for the formation of CD81 tetraspanin webs." In: *Biophysical journal* 107.1, pp. 100–13.

Honigmann, A., Bogaart, G. van den, Iraheta, E., Risselada, H. J., Milovanovic, D., Mueller, V., Müllar, S., Diederichsen, U., Fasshauer, D., Grubmüller, H., et al. (2013). "Phosphatidylinositol 4,5-bisphosphate clusters act as molecular beacons for vesicle recruitment." In: *Nature structural & molecular biology* 20.6, pp. 679–86.

Hoover, P. J. and Lewis, R. S. (2011). "Stoichiometric requirements for trapping and gating of Ca2+ release-activated Ca2+ (CRAC) channels by stromal interaction molecule 1 (STIM1)." In: *Proceedings of the National Academy of Sciences of the United States of America* 108.32, pp. 13299–304.

Ipsen, J. H., Karlström, G., Mouritsen, O. G., Wennerström, H., and Zuckermann, M. J. (1987). "Phase equilibria in the phosphatidylcholine-cholesterol system." In: *Biochimica et biophysica acta* 905.1, pp. 162–72.

Irie, T., Fukunaga, K., and Pitha, J. (1992). "Hydroxypropylcyclodextrins in parenteral use. I: Lipid dissolution and effects on lipid transfers in vitro." In: *Journal of pharmaceutical sciences* 81.6, pp. 521–3.

Jahn, R. and Fasshauer, D. (2012). "Molecular machines governing exocytosis of synaptic vesicles." In: *Nature* 490.7419, pp. 201–7.

Jahn, R., Lang, T., and Südhof, T. C. (2003). "Membrane Fusion". In: *Cell* 112.4, pp. 519–533.

Jao, C. Y., Roth, M., Welti, R., and Salic, A. (2009). "Metabolic labeling and direct imaging of choline phospholipids in vivo". In: *Proceedings of the National Academy of Sciences of the United States of America* 106.36, pp. 15332–15337.

Jesus, A. J. de and Allen, T. W. (2013). "The determinants of hydrophobic mismatch response for transmembrane helices". In: *Biochimica et Biophysica Acta (BBA) - Biomembranes* 1828.2, pp. 851–863.

Jiao, X., Zhang, N., Xu, X., Oppenheim, J. J., and Jin, T. (2005). "Ligand-induced partitioning of human CXCR1 chemokine receptors with lipid raft microenvironments facilitates G-protein-dependent signaling." In: *Molecular and cellular biology* 25.13, pp. 5752–62.

Jones, J. D. and Thompson, T. E. (1989). "Spontaneous phosphatidylcholine transfer by collision between vesicles at high lipid concentration". In: *Biochemistry* 28.1, pp. 129–134.

Jones, J. D. and Thompson, T. E. (1990). "Mechanism of spontaneous, concentration-dependent phospholipid transfer between bilayers". In: *Biochemistry* 29.6, pp. 1593–1600.

Kahlenberg, A., Walker, C., and Rohrlick, R. (1974). "Evidence for an Asymmetric Distribution of Phospholipids in the Human Erythrocyte Membrane". In: *Canadian Journal of Biochemistry* 52.9, pp. 803–806.

Kahya, N., Brown, D. A., and Schwille, P. (2005). "Raft Partitioning and Dynamic Behavior of Human Placental Alkaline Phosphatase in Giant Unilamellar Vesicles". In: *Biochemistry* 44.20, pp. 7479–7489.

Kaiser, H.-J., Lingwood, D., Levental, I., Sampaio, J. L., Kalvodova, L., Rajendran, L., and Simons, K. (2009). "Order of lipid phases in model and plasma membranes." In: *Proceedings of the National Academy of Sciences of the United States of America* 106.39, pp. 16645–16650.

Keenan, T. W. and Morre, D. J. (1970). "Phospholipid class and fatty acid composition of Golgi apparatus isolated from rat liver and comparison with other cell fractions". In: *Biochemistry* 9.1, pp. 19–25.

Khuong, T. M., Habets, R. L. P., Kuenen, S., Witkowska, A., Kasprowicz, J., Swerts, J., Jahn, R., Bogaart, G. van den, and Verstreken, P. (2013). "Synaptic PI(3,4,5)P3 Is Required for Syntaxin1A Clustering and Neurotransmitter Release". In: *Neuron* 77.6, pp. 1097–1108.

Kilch, T., Alansary, D., Peglow, M., Dorr, K., Rychkov, G., Rieger, H., Peinelt, C., and Niemeyer, B. A. (2013). "Mutations of the Ca2+-sensing Stromal Interaction Molecule STIM1 Regulate Ca2+ Influx by Altered Oligomerization of STIM1 and by Destabilization of the Ca2+ Channel Orai1". In: *Journal of Biological Chemistry* 288.3, pp. 1653–1664.

Kirchhausen, T. (2000). "Clathrin". In: *Annual Review of Biochemistry* 69.1, pp. 699–727.

Klar, T. A., Engel, E., and Hell, S. W. (2001). "Breaking Abbe's diffraction resolution limit in fluorescence microscopy with stimulated emission depletion beams of various shapes". In: *Physical Review E* 64.6, p. 066613.

Kleene, R. and Schachner, M. (2004). "Glycans and neural cell interactions". In: *Nature Reviews Neuroscience* 5.3, pp. 195–208.

Klein, U., Gimpl, G., and Fahrenholz, F. (1995). "Alteration of the myometrial plasma membrane cholesterol content with beta-cyclodextrin modulates the binding affinity of the oxytocin receptor". In: *Biochemistry* 34.42, pp. 13784–13793.

Kol, M. A., Laak, A. N. C. van, Rijkers, D. T. S., Killian, J. A., Kroon, A. I. P. M. de, and Kruijff, B. de (2003). "Phospholipid Flop Induced by Transmembrane Peptides in Model Membranes Is Modulated by Lipid Composition". In: *Biochemistry* 42.1, pp. 231–237.

Kuerschner, L., Ejsing, C. S., Ekroos, K., Shevchenko, A., Anderson, K. I., and Thiele, C. (2005). "Polyene-lipids: a new tool to image lipids". In: *Nature methods* 2.1, pp. 39–45.

Kumar, M., Mommer, M. S., and Sourjik, V. (2010). "Mobility of cytoplasmic, membrane, and DNA-binding proteins in Escherichia coli." In: *Biophysical journal* 98.4, pp. 552–9.

Kunze, A., Svedhem, S., and Kasemo, B. (2009). "Lipid Transfer between Charged Supported Lipid Bilayers and Oppositely Charged Vesicles". In: *Langmuir* 25.9, pp. 5146–5158.

Kusumi, A., Sako, Y., and Yamamoto, M. (1993). "Confined lateral diffusion of membrane receptors as studied by single particle tracking (nanovid microscopy). Effects of calcium-induced differentiation in cultured epithelial cells." In: *Biophysical journal* 65.5, pp. 2021–40.

Kusumi, A., Suzuki, K. G. N., Kasai, R. S., Ritchie, K., and Fujiwara, T. K. (2011). "Hierarchical mesoscale domain organization of the plasma membrane." In: *Trends in biochemical sciences* 36.11, pp. 604–15.

Lacruz, R. S. and Feske, S. (2015). "Diseases caused by mutations in ORAI1 and STIM1". In: *Annals of the New York Academy of Sciences* 1356.1, pp. 45–79.

Lang, T., Bruns, D., Wenzel, D., Riedel, D., Holroyd, P., Thiele, C., and Jahn, R. (2001). "SNAREs are concentrated in cholesterol-dependent clusters that define docking and fusion sites for exocytosis". In: *EMBO Journal* 20.9, pp. 2202–2213.

Lang, T., Margittai, M., Hölzler, H., and Jahn, R. (2002). "SNAREs in native plasma membranes are active and readily form core complexes with endogenous and exogenous SNAREs." In: *The Journal of cell biology* 158.4, pp. 751–60.

Lange, Y., Ye, J., and Steck, T. L. (2012). "Activation mobilizes the cholesterol in the late endosomes-lysosomes of Niemann Pick type C cells." In: *PloS one* 7.1, e30051.

Lemmon, M. A. and Ferguson, K. M. (2000). "Signal-dependent membrane targeting by pleckstrin homology (PH) domains". In: *Biochem. J* 350, pp. 1–18.

Lenne, P.-F., Wawrezinieck, L., Conchonaud, F., Wurtz, O., Boned, A., Guo, X.-J., Rigneault, H., He, H.-T., and Marguet, D. (2006). "Dynamic molecular confinement in the plasma membrane by microdomains and the cytoskeleton meshwork." In: *The EMBO journal* 25.14, pp. 3245–3256.

Lev, S. (2010). "Non-vesicular lipid transport by lipid-transfer proteins and beyond." In: *Nature reviews. Molecular cell biology* 11.10, pp. 739–750.

Lev, S. (2012). "Nonvesicular lipid transfer from the endoplasmic reticulum". In: *Cold Spring Harbor Perspectives in Biology* 4.10, a013300.

Levine, T. (2004). "Short-range intracellular trafficking of small molecules across endoplasmic reticulum junctions". In: *Trends in Cell Biology* 14.9, pp. 483–490.

Li, Y. and Prinz, W. A. (2004). "ATP-binding cassette (ABC) transporters mediate nonvesicular, raft-modulated sterol movement from the plasma membrane to the endoplasmic reticulum". In: *Journal of Biological Chemistry* 279.43, pp. 45226–45234.

Lillemeier, B. F., Mörtelmaier, M. A., Forstner, M. B., Huppa, J. B., Groves, J. T., and Davis, M. M. (2010). "TCR and Lat are expressed on separate protein islands on T cell membranes and concatenate during activation". In: *Nature Immunology* 11.1, pp. 90–96.

Lillemeier, B. F., Pfeiffer, J. R., Surviladze, Z., Wilson, B. S., and Davis, M. M. (2006). "Plasma membrane-associated proteins are clustered into islands attached to the cytoskeleton." In: *Proceedings of the National Academy of Sciences of the United States of America* 103.50, pp. 18992–7.

Liou, J., Fivaz, M., Inoue, T., and Meyer, T. (2007). "Live-cell imaging reveals sequential oligomerization and local plasma membrane targeting of stromal interaction molecule 1 after Ca2+ store depletion." In: *Proceedings of the National Academy of Sciences of the United States of America* 104.22, pp. 9301–6.

Lohmann, D. (2013). "Posttranlational modifications of Ancient Ubiquitous Protein 1 control intracellular Lipid Droplet clustering". Dissertation. University of Bonn.

Longmuir, K. J. and Malinick, L. a. (1989). "Transfer of phosphatidic acid from liposomes to cells is collision dependent". In: *The American journal of physiology* 256.3 Pt 1, pp. C522–31.

Maier, O., Oberle, V., and Hoekstra, D. (2002). "Fluorescent lipid probes: some properties and applications (a review)". In: *Chemistry and physics of lipids* 116.1-2, pp. 3–18.

Malecz, N., McCabe, P. C., Spaargaren, C., Qiu, R., Chuang, Y., Symons, M., and Al., et (2000). "Synaptojanin 2, a novel Rac1 effector that regulates clathrin-mediated endocytosis." In: *Current biology : CB* 10.21, pp. 1383–6.

Manford, A. G., Stefan, C. J., Yuan, H. L., MacGurn, J. A., and Emr, S. D. (2012). "ER-to-Plasma Membrane Tethering Proteins Regulate Cell Signaling and ER Morphology". In: *Developmental Cell* 23.6, pp. 1129–1140.

Marsh, D. and Horváth, L. I. (1998). "Structure, dynamics and composition of the lipid-protein interface. Perspectives from spin-labelling." In: *Biochimica et biophysica acta* 1376.3, pp. 267–96.

Marsh, J. A. and Teichmann, S. A. (2015). "Structure, dynamics, assembly, and evolution of protein complexes." en. In: *Annual review of biochemistry* 84, pp. 551–75.

Marshall, M. R., Pattu, V., Halimani, M., Maier-Peuschel, M., Müller, M.-L., Becherer, U., Hong, W., Hoth, M., Tschernig, T., Bryceson, Y. T., et al. (2015). "VAMP8-dependent fusion of recycling endosomes with the plasma membrane facilitates T lymphocyte cytotoxicity". In: *The Journal of Cell Biology* 210.1.

Martin, W. and Russell, M. J. (2003). "On the origins of cells: a hypothesis for the evolutionary transitions from abiotic geochemistry to chemoautotrophic prokaryotes, and from prokaryotes to nucleated cells." In: *Philosophical transactions of the Royal Society of London. Series B, Biological sciences* 358.1429, 59–83, discussion 83–5.

Massey, J. B., Gotto, A. M., and Pownall, H. J. (1982). "Kinetics and mechanism of the spontaneous transfer of fluorescent phospholipids between apolipoprotein-phospholipid recombinants. Effect of the polar headgroup." In: *The Journal of biological chemistry* 257.10, pp. 5444–8.

McCloskey, M. A. and Poo, M. M. (1986). "Rates of membrane-associated reactions: reduction of dimensionality revisited." In: *The Journal of cell biology* 102.1, pp. 88–96.

McCloskey, M. and Poo, M. M. (1984). "Protein diffusion in cell membranes: some biological implications." In: *International review of cytology* 87, pp. 19–81.

McLaughlin, S., Wang, J., Gambhir, A., and Murray, D. (2002). "PIP(2) and proteins: interactions, organization, and information flow." In: *Annual review of biophysics and biomolecular structure* 31, pp. 151–175.

McLean, L. R. and Phillips, M. C. (1981). "Mechanism of cholesterol and phosphatidylcholine exchange or transfer between unilamellar vesicles." In: *Biochemistry* 20.10, pp. 2893–900.

McLean, L. R. and Phillips, M. C. (1984). "Kinetics of phosphatidylcholine and lysophosphatidylcholine exchange between unilamellar vesicles." In: *Biochemistry* 23.20, pp. 4624–30.

McMahon, H. T., Boucrot, E., Aimon, S., Callan-Jones, A., Berthaud, A., Pinot, M., Toombes, G. E., Bassereau, P., Bigay, J., Antonny, B., et al. (2015). "Membrane curvature at a glance." In: *Journal of cell science* 128.6, pp. 1065–70.

McMullen, T. P., Lewis, R. N., and McElhaney, R. N. (1994). "Comparative differential scanning calorimetric and FTIR and 31P-NMR spectroscopic studies of the effects of cholesterol and androstenol on the thermotropic phase behavior and organization of phosphatidylcholine bilayers." In: *Biophysical journal* 66.3 Pt 1, pp. 741–52.

Meer, G. van (2011). "Dynamic transbilayer lipid asymmetry". In: *Cold Spring Harbor Perspectives in Biology* 3.5, pp. 1–11.

Meer, G. van and Kroon, A. I. P. M. de (2011). "Lipid map of the mammalian cell." In: *Journal of cell science* 124.Pt 1, pp. 5–8.

Meer, G. van, Voelker, D. R., and Feigenson, G. W. (2008). "Membrane lipids: where they are and how they behave". In: *Nature reviews. Molecular cell biology* 9.2, pp. 112–124.

Meijering, E., Dzyubachyk, O., and Smal, I. (2012). "Methods for cell and particle tracking". In: *Methods in enzymology* 504, pp. 183–200.

Meilhac, N. and Destainville, N. (2011). "Clusters of Proteins in Biomembranes: Insights into the Roles of Interaction Potential Shapes and of Protein Diversity". In: *The Journal of Physical Chemistry B* 115.22, pp. 7190–7199.

Merklinger, E., Schloetel, J.-G., Spitta, L., Thiele, C., and Lang, T. (2016). "No Evidence for Spontaneous Lipid Transfer at ER–PM Membrane Contact Sites". In: *The Journal of Membrane Biology* 249.1-2, pp. 41–56.

Merklinger, E., Schloetel, J.-G., Weber, P., Batoulis, H., Holz, S., Karnowski, N., Finke, J., and Lang, T. (2017). "The packing density of a supramolecular membrane protein cluster is controlled by cytoplasmic interactions". In: *eLife* 6.

Messa, M., Fernández-Busnadiego, R., Sun, E. W., Chen, H., Czapla, H., Wrasman, K., Wu, Y., Ko, G., Ross, T., Wendland, B., et al. (2014). "Epsin deficiency impairs endocytosis by stalling the actin-dependent invagination of endocytic clathrin-coated pits." In: *eLife* 3, e03311.

Milosevic, I., Sørensen, J. B., Lang, T., Krauss, M., Nagy, G., Haucke, V., Jahn, R., and Neher, E. (2005). "Plasmalemmal phosphatidylinositol-4,5-bisphosphate level regulates the releasable vesicle pool size in chromaffin cells." In: *The Journal of neuroscience : the official journal of the Society for Neuroscience* 25.10, pp. 2557–65.

Milovanovic, D., Honigmann, A., Koike, S., Göttfert, F., Pähler, G., Junius, M., Müllar, S., Diederichsen, U., Janshoff, A., Grubmüller, H., et al. (2015). "Hydrophobic mismatch sorts SNARE proteins into distinct membrane domains". In: *Nature Communications* 6, p. 5984.

Misura, K. M., Scheller, R. H., and Weis, W. I. (2001). "Self-association of the H3 region of syntaxin 1A. Implications for intermediates in SNARE complex assembly." In: *The Journal of biological chemistry* 276.16, pp. 13273–82.

Mitra, K., Ubarretxena-Belandia, I., Taguchi, T., Warren, G., and Engelman, D. M. (2004). "Modulation of the bilayer thickness of exocytic pathway membranes by membrane proteins rather than cholesterol." In: *Proceedings of the National Academy of Sciences of the United States of America* 101.12, pp. 4083–8.

Mochly-Rosen, D., Khaner, H., and Lopez, J. (1991). "Identification of intracellular receptor proteins for activated protein kinase C." In: *Proceedings of the National Academy of Sciences of the United States of America* 88.9, pp. 3997–4000.

Moore, M. S., Mahaffey, D. T., Brodsky, F. M., and Anderson, R. G. (1987). "Assembly of clathrin-coated pits onto purified plasma membranes." In: *Science (New York, N.Y.)* 236.4801, pp. 558–63.

Morandell, S., Stasyk, T., Skvortsov, S., Ascher, S., and Huber, L. A. (2008). "Quantitative proteomics and phosphoproteomics reveal novel insights into complexity and dynamics of the EGFR signaling network." In: *Proteomics* 8.21, pp. 4383–401.

Mueller, V., Ringemann, C., Honigmann, A., Schwarzmann, G., Medda, R., Leutenegger, M., Polyakova, S., Belov, V. N., Hell, S. W., and Eggeling, C. (2011). "STED nanoscopy reveals molecular details of cholesterol- and cytoskeleton-modulated lipid interactions in living cells". In: *Biophysical Journal* 101.7, pp. 1651–1660.

Munro, S. (1995). "An investigation of the role of transmembrane domains in Golgi protein retention." In: *The EMBO journal* 14.19, pp. 4695–704.

Nooren, I. M. A. and Thornton, J. M. (2003). "Diversity of protein-protein interactions." In: *The EMBO journal* 22.14, pp. 3486–92.

Ohvo, H. and Slotte, J. P. (1996). "Cyclodextrin-mediated removal of sterols from monolayers: effects of sterol structure and phospholipids on desorption rate." In: *Biochemistry* 35.24, pp. 8018–24.

Oparin, A. (1924). "The origin of life". In: *Moscow Worker Publisher*.

Orci, L., Ravazzola, M., Le Coadic, M., Shen, W.-W., Demaurex, N., and Cosson, P. (2009). "From the Cover: STIM1-induced precortical and cortical subdomains of the endoplasmic reticulum". In: *Proceedings of the National Academy of Sciences of the United States of America* 106.46, pp. 19358–19362.

Pastan, I., Macchia, V., and Katzen, R. (1968). "A phospholipase specific for sphingomyelin from Clostridium perfringens." In: *The Journal of biological chemistry* 243.13, pp. 3750–5.

Patterson, G., Knobel, S., Sharif, W., Kain, S., and Piston, D. (1997). "Use of the green fluorescent protein and its mutants in quantitative fluorescence microscopy". In: *Biophysical Journal* 73.5, pp. 2782–2790.

Paul, G., Cardinale, J., and Sbalzarini, I. F. (2013). "Coupling Image Restoration and Segmentation: A Generalized Linear Model/Bregman Perspective". In: *International Journal of Computer Vision* 104.1, pp. 69–93.

Pawson, T. and Nash, P. (2000). "Protein-protein interactions define specificity in signal transduction." In: *Genes & development* 14.9, pp. 1027–47.

Pichler, H., Gaigg, B., Hrastnik, C., Achleitner, G., Kohlwein, S. D., Zellnig, G., Perktold, A., and Daum, G. (2001). "A subfraction of the yeast endoplasmic reticulum associates with the plasma membrane and has a high capacity to synthesize lipids". In: *European Journal of Biochemistry* 268.8, pp. 2351–2361.

Porter, K. R. and Palade, G. E. (1957). "Studies on the endoplasmic reticulum. III. Its form and distribution in striated muscle cells." In: *The Journal of biophysical and biochemical cytology* 3.2, pp. 269–300.

Prinz, W. A. (2014). "Bridging the gap: membrane contact sites in signaling, metabolism, and organelle dynamics." In: *The Journal of cell biology* 205.6, pp. 759–69.

Qian, H., Sheetz, M. P., and Elson, E. L. (1991). "Single particle tracking. Analysis of diffusion and flow in two-dimensional systems". In: *Biophysical journal* 60.4, pp. 910–921.

Radhakrishnan, A., Goldstein, J. L., McDonald, J. G., and Brown, M. S. (2008). "Switch-like Control of SREBP-2 Transport Triggered by Small Changes in ER Cholesterol: A Delicate Balance". In: *Cell Metabolism* 8.6, pp. 512–521.

Rickman, C., Medine, C. N., Dun, A. R., Moulton, D. J., Mandula, O. O., Halemani, N. D., Rizzoli, S. O., Chamberlain, L. H., and Duncan, R. R. (2010). "t-SNARE protein conformations patterned by the lipid microenvironment". In: *The Journal of biological chemistry* 285.18, pp. 13535–13541.

Rizk, A., Paul, G., Incardona, P., Bugarski, M., Mansouri, M., Niemann, A., Ziegler, U., Berger, P., and Sbalzarini, I. F. (2014). "Segmentation and quantification of subcellular structures in fluorescence microscopy images using Squassh". In: *Nature Protocols* 9.3, pp. 586–596.

Rizzuto, R. and Pozzan, T. (2006). "Microdomains of intracellular Ca2+: molecular determinants and functional consequences." In: *Physiological reviews* 86.1, pp. 369–408.

Saheki, Y., Bian, X., Schauder, C. M., Sawaki, Y., Surma, M. A., Klose, C., Pincet, F., Reinisch, K. M., and De Camilli, P. (2016). "Control of plasma membrane lipid homeostasis by the extended synaptotagmins". In: *Nature Cell Biology* 18.5, pp. 504–515.

Saint-Jean, M. de, Delfosse, V., Douguet, D., Chicanne, G., Payrastre, B., Bourguet, W., Antonny, B., and Drin, G. (2011). "Osh4p exchanges sterols for phosphatidylinositol 4-phosphate between lipid bilayers". In: *Journal of Cell Biology* 195.6, pp. 965–978.

Saka, S. K., Honigmann, A., Eggeling, C., Hell, S. W., Lang, T., and Rizzoli, S. O. (2014). "Multi-protein assemblies underlie the mesoscale organization of the plasma membrane". In: *Nature Communications* 5, p. 4509.

Sambrook, J. and Russell, D. W. (2001). *Molecular Cloning: A Laboratory Manual, 3rd ed.* 3rd. Cold Spring Harbor Laboratory Press.

Schiavo, G., Shone, C. C., Bennett, M. K., Scheller, R. H., and Montecucco, C. (1995). "Botulinum Neurotoxin Type C Cleaves a Single Lys-Ala Bond within the Carboxyl-terminal Region of Syntaxins". In: *Journal of Biological Chemistry* 270.18, pp. 10566–10570.

Schmidt, U., Guigas, G., and Weiss, M. (2008). "Cluster Formation of Transmembrane Proteins Due to Hydrophobic Mismatching". In: *Physical Review Letters* 101.12, p. 128104.

Schneiter, R., Brügger, B., Sandhoff, R., Zellnig, G., Leber, A., Lampl, M., Athenstaedt, K., Hrastnik, C., Eder, S., Daum, G., et al. (1999). "Electrospray ionization tandem mass spectrometry (ESI-MS/MS) analysis of the lipid molecular species composition of yeast subcellular membranes reveals acyl chain-based sorting/remodeling of distinct molecular species en route to the plasma membrane." In: *The Journal of cell biology* 146.4, pp. 741–54.

Schreiber, A., Fischer, S., and Lang, T. (2012). "The amyloid precursor protein forms plasmalemmal clusters via its pathogenic amyloid-beta domain". In: *Biophysical journal* 102.6, pp. 1411–1417.

Schulz, T. A., Choi, M.-G., Raychaudhuri, S., Mears, J. A., Ghirlando, R., Hinshaw, J. E., and Prinz, W. A. (2009). "Lipid-regulated sterol transfer between closely apposed membranes by oxysterol-binding protein homologues." In: *The Journal of cell biology* 187.6, pp. 889–903.

Schulz, T. A. and Creutz, C. E. (2004). "The tricalbin C2 domains: lipid-binding properties of a novel, synaptotagmin-like yeast protein family." In: *Biochemistry* 43.13, pp. 3987–95.

Schütz, D., Zilly, F., Lang, T., Jahn, R., and Bruns, D. (2005). "A dual function for Munc-18 in exocytosis of PC12 cells". In: *European Journal of Neuroscience* 21.9, pp. 2419–2432.

Seul, M. and Andelman, D. (1995). "Domain Shapes and Patterns: The Phenomenology of Modulated Phases". In: *Science* 267.5197, pp. 476–483.

Sezgin, E. and Schwille, P. (2011). "Fluorescence Techniques to Study Lipid Dynamics". In: *Cold Spring Harbor Perspectives in Biology* 3.11, a009803–a009803.

Shen, W.-W., Frieden, M., and Demaurex, N. (2011). "Remodelling of the endoplasmic reticulum during store-operated calcium entry." In: *Biology of the cell / under the auspices of the European Cell Biology Organization* 103.8, pp. 365–80.

Shibata, Y., Shemesh, T., Prinz, W. A., Palazzo, A. F., Kozlov, M. M., and Rapoport, T. A. (2010). "Mechanisms determining the morphology of the peripheral ER". In: *Cell* 143.5, pp. 774–788.

Sieber, J. J., Willig, K. I., Heintzmann, R., Hell, S. W., and Lang, T. (2006). "The SNARE motif is essential for the formation of syntaxin clusters in the plasma membrane." In: *Biophysical journal* 90.8, pp. 2843–2851.

Sieber, J. J., Willig, K. I., Kutzner, C., Gerding-Reimers, C., Harke, B., Donnert, G., Rammner, B., Eggeling, C., Hell, S. W., Grubmüller, H., et al. (2007). "Anatomy and dynamics of a supramolecular membrane protein cluster." In: *Science (New York, N.Y.)* 317.5841, pp. 1072–6.

Simons, K. and Ikonen, E. (1997). "Functional rafts in cell membranes". In: *Nature* 387.6633, pp. 569–572.

Simons, K. and Van Meer, G. (1988). "Lipid sorting in epithelial cells". In: *Biochemistry* 27.17, pp. 6197–6202.

Solon, J., Streicher, P., Richter, R., Brochard-Wyart, F., and Bassereau, P. (2006). "Vesicles surfing on a lipid bilayer: self-induced haptotactic motion". In: *Proceedings of the National Academy of Sciences of the United States of America* 103.33, pp. 12382–12387.

Somerharju, P. (2015). "Is Spontaneous Translocation of Polar Lipids Between Cellular Organelles Negligible?" en. In: *Lipid insights* 8.Suppl 1, pp. 87–93.

Sørensen, J. B., Wiederhold, K., Müller, E. M., Milosevic, I., Nagy, G., Groot, B. L. de, Grubmüller, H., and Fasshauer, D. (2006). "Sequential N- to C-terminal SNARE complex assembly drives priming and fusion of secretory vesicles". In: *The EMBO Journal* 25.5, pp. 955–966.

Spitta, L. F. (2012). "Phosphatidylcholine is organized in long-lived plasmalemmal platforms". Dissertation. University of Bonn.

Stachowiak, J. C., Schmid, E. M., Ryan, C. J., Ann, H. S., Sasaki, D. Y., Sherman, M. B., Geissler, P. L., Fletcher, D. A., and Hayden, C. C. (2012). "Membrane bending by protein-protein crowding." In: *Nature cell biology* 14.9, pp. 944–9.

Stathopulos, P. B., Schindl, R., Fahrner, M., Zheng, L., Gasmi-Seabrook, G. M., Muik, M., Romanin, C., and Ikura, M. (2013). "STIM1/Orai1 coiled-coil interplay in the regulation of store-operated calcium entry". In: *Nature Communications* 4, pp. 1–24.

Stauffer, T. P., Ahn, S., and Meyer, T. (1998). "Receptor-induced transient reduction in plasma membrane PtdIns(4,5)P2 concentration monitored in living cells". In: *Current biology : CB* 8.6, pp. 343–346.

Steck, T. L. (1974). "The organization of proteins in the human red blood cell membrane. A review." In: *The Journal of cell biology* 62.1, pp. 1–19.

Steck, T. L., Kezdy, F. J., and Lange, Y. (1988). "An activation-collision mechanism for cholesterol transfer between membranes". In: *The Journal of biological chemistry* 263.26, pp. 13023–13031.

Steck, T. L., Weinstein, R. S., Straus, J. H., and Wallach, D. F. (1970). "Inside-out red cell membrane vesicles: preparation and purification." In: *Science (New York, N.Y.)* 168.3928, pp. 255–7.

Stein, A., Weber, G., Wahl, M. C., and Jahn, R. (2009). "Helical extension of the neuronal SNARE complex into the membrane". In: *Nature* 460.7254, pp. 525–528.

Steyer, J. A. and Almers, W. (2001). "A real-time view of life within 100 nm of the plasma membrane". In: *Nature Reviews Molecular Cell Biology* 2.4, pp. 268–275.

Stiban, J., Caputo, L., and Colombini, M. (2008). "Ceramide synthesis in the endoplasmic reticulum can permeabilize mitochondria to proapoptotic proteins". In: *Journal of lipid research* 49.3, pp. 625–634.

Sud, M., Fahy, E., Cotter, D., Brown, A., Dennis, E. A., Glass, C. K., Merrill, A. H., Murphy, R. C., Raetz, C. R. H., Russell, D. W., et al. (2007). "LMSD: LIPID MAPS structure database." In: *Nucleic acids research* 35.Database issue, pp. D527–32.

Sutton, R. B., Fasshauer, D., Jahn, R., and Brunger, A. T. (1998). "Crystal structure of a SNARE complex involved in synaptic exocytosis at 2.4 A resolution." In: *Nature* 395.6700, pp. 347–53.

Takamori, S., Holt, M., Stenius, K., Lemke, E. a., Grønborg, M., Riedel, D., Urlaub, H., Schenck, S., Brügger, B., Ringler, P., et al. (2006). "Molecular anatomy of a trafficking organelle". In: *Cell* 127.4, pp. 831–846.

Thomas, P. D. and Poznansky, M. J. (1988). "Effect of surface curvature on the rate of cholesterol transfer between lipid vesicles." In: *The Biochemical journal* 254.1, pp. 155–60.

Thompson, J. L. and Shuttleworth, T. J. (2013). "How many Orai's does it take to make a CRAC channel?" In: *Scientific reports* 3, p. 1961.

Toulmay, A. and Prinz, W. a. (2012). "A conserved membrane-binding domain targets proteins to organelle contact sites." In: *Journal of cell science* 125.Pt 1, pp. 49–58.

Uhlén, M., Fagerberg, L., Hallström, B. M., Lindskog, C., Oksvold, P., Mardinoglu, A., Sivertsson, Å., Kampf, C., Sjöstedt, E., Asplund, A., et al. (2015). "Tissue-based map of the human proteome". In: *Science* 347.6220.

Varma, R., Campi, G., Yokosuka, T., Saito, T., and Dustin, M. L. (2006). "T cell receptor-proximal signals are sustained in peripheral microclusters and terminated in the central supramolecular activation cluster." In: *Immunity* 25.1, pp. 117–27.

Veatch, S. L. and Keller, S. L. (2003). "Separation of liquid phases in giant vesicles of ternary mixtures of phospholipids and cholesterol." In: *Biophysical journal* 85.5, pp. 3074–83.

Vicidomini, G., Moneron, G., Han, K. Y., Westphal, V., Ta, H., Reuss, M., Engelhardt, J., Eggeling, C., and Hell, S. W. (2011). "Sharper low-power STED nanoscopy by time gating." In: *Nature methods* 8.7, pp. 571–3.

Vreja, I. C., Nikić, I., Göttfert, F., Bates, M., Kröhnert, K., Outeiro, T. F., Hell, S. W., Lemke, E. A., and Rizzoli, S. O. (2015). "Super-resolution Microscopy of Clickable Amino Acids Reveals the Effects of Fluorescent Protein Tagging on Protein Assemblies." In: *ACS nano* 9.11, pp. 11034–41.

Wächtershäuser, G. (1988). "Before enzymes and templates: theory of surface metabolism." In: *Microbiological reviews* 52.4, pp. 452–84.

Watt, S. A., Kular, G., Fleming, I. N., Downes, C. P., and Lucocq, J. M. (2002). "Subcellular localization of phosphatidylinositol 4,5-bisphosphate using the pleckstrin homology domain of phospholipase C delta1." In: *The Biochemical journal* 363.Pt 3, pp. 657–66.

Weitz, S., Destainville, N., Melnik, L., Choe, H. W., and Ernst, O. P. (2013). "Attractive asymmetric inclusions in elastic membranes under tension: cluster phases and membrane invaginations". In: *Soft Matter* 9.32, p. 7804.

Wilkins, M. H., Blaurock, A. E., and Engelman, D. M. (1971). "Bilayer structure in membranes." In: *Nature: New biology* 230.11, pp. 72–6.

Williams, R. T., Manji, S. S., Parker, N. J., Hancock, M. S., Van Stekelenburg, L., Eid, J. P., Senior, P. V., Kazenwadel, J. S., Shandala, T., Saint, R., et al. (2001). "Identification and characterization of the STIM (stromal interaction molecule) gene family: coding for a novel class of transmembrane proteins." In: *The Biochemical journal* 357.Pt 3, pp. 673–85.

Willig, K. I., Rizzoli, S. O., Westphal, V., Jahn, R., and Hell, S. W. (2006). "STED microscopy reveals that synaptotagmin remains clustered after synaptic vesicle exocytosis." In: *Nature* 440.7086, pp. 935–939.

Wimley, W. C. and Thompson, T. E. (1991). "Phosphatidylethanolamine enhances the concentration-dependent exchange of phospholipids between bilayers". In: *Biochemistry* 30.17, pp. 4200–4204.

Wirtz, K. W., Kamp, H. H., and Deenen, L. L. van (1972). "Isolation of a protein from beef liver which specifically stimulates the exchange of phosphatidylcholine." In: *Biochimica et biophysica acta* 274.2, pp. 606–17.

Wu, M. and De Camilli, P. (2012). "Supported Native Plasma Membranes as Platforms for the Reconstitution and Visualization of Endocytic Membrane Budding". In: *Methods in cell biology.* Vol. 108, pp. 1–18.

Wu, M., Huang, B., Graham, M., Raimondi, A., Heuser, J. E., Zhuang, X., and De Camilli, P. (2010). "Coupling between clathrin-dependent endocytic budding and F-BAR-dependent tubulation in a cell-free system". In: *Nature Cell Biology* 12.9, pp. 902–908.

Wu, M., Buchanan, J., Luik, R. M., and Lewis, R. S. (2006). "Ca2+ store depletion causes STIM1 to accumulate in ER regions closely associated with the plasma membrane." In: *The Journal of cell biology* 174.6, pp. 803–13.

Yang, L., Dun, A. R., Martin, K. J., Qiu, Z., Dunn, A., Lord, G. J., Lu, W., Duncan, R. R., and Rickman, C. (2012). "Secretory vesicles are preferentially targeted to areas of low molecular SNARE density." In: *PloS one* 7.11. Ed. by L. Johannes, e49514.

Yang, X., Xu, P., Xiao, Y., Xiong, X., and Xu, T. (2006). "Domain requirement for the membrane trafficking and targeting of syntaxin 1A." In: *The Journal of biological chemistry* 281.22, pp. 15457–63.

Yeung, T., Gilbert, G. E., Shi, J., Silvius, J., Kapus, A., and Grinstein, S. (2008). "Membrane Phosphatidylserine Regulates Surface Charge and Protein Localization". In: *Science* 319.5860, pp. 210–213.

Yu, H., Liu, Y., Gulbranson, D. R., Paine, A., Rathore, S. S., and Shen, J. (2016). "Extended synaptotagmins are Ca2+-dependent lipid transfer proteins at membrane contact sites." In: *Proceedings of the National Academy of Sciences of the United States of America* 113.16, pp. 4362–7.

Zacharias, D. A., Violin, J. D., Newton, A. C., and Tsien, R. Y. (2002). "Partitioning of Lipid-Modified Monomeric GFPs into Membrane Microdomains of Live Cells". In: *Science* 296.5569, pp. 913–916.

Zambrano, F., Fleischer, S., and Fleischer, B. (1975). "Lipid composition of the golgi apparatus of rat kidney and liver in comparison with other subcellular organelles". In: *Biochimica et Biophysica Acta (BBA) - Lipids and Lipid Metabolism* 380.3, pp. 357–369.

Zenisek, D., Steyer, J. A., and Almers, W. (2000). "Transport, capture and exocytosis of single synaptic vesicles at active zones." In: *Nature* 406.6798, pp. 849–54.

Zhang, X., Zhang, L., Tong, H., Peng, B., Rames, M. J., Zhang, S., and Ren, G. (2015). "3D Structural Fluctuation of IgG1 Antibody Revealed by Individual Particle Electron Tomography". In: *Scientific Reports* 5, p. 9803.

Zidovetzki, R. and Levitan, I. (2007). "Use of cyclodextrins to manipulate plasma membrane cholesterol content: Evidence, misconceptions and control strategies". In: *Biochimica et Biophysica Acta (BBA) - Biomembranes* 1768.6, pp. 1311–1324.

Zilly, F. E., Halemani, N. D., Walrafen, D., Spitta, L., Schreiber, A., Jahn, R., and Lang, T. (2011). "Ca2+ induces clustering of membrane proteins in the plasma membrane via electrostatic interactions." In: *The EMBO journal* 30.7, pp. 1209–1220.

Zilly, F. E., Sørensen, J. B., Jahn, R., Lang, T., Sorensen, J. B., Jahn, R., and Lang, T. (2006). "Munc18-bound syntaxin readily forms SNARE complexes with synaptobrevin in native plasma membranes". In: *PLoS Biology* 4.10, pp. 1789–1797.

Acknowledgements

I would like to express my gratitude to my supervisor Prof. Dr. Thorsten Lang for providing me with the opportunity to work in his group and for many fruitful discussions. I have greatly benefited from his steady support, his caring supervision and his scientific enthusiasm.

I would like to thank Prof. Dr. Christoph Thiele for inspiring discussions, providing important “click” tools and for helpful advice.

For his steady support during my thesis, various ingenious ImageJ macros and help with STED experiments and image analysis, I am deeply grateful to Dr. Jan-Gero Schloetel. Furthermore, I greatly appreciate the valuable advice of Dr. Lars Kürschner and his help with electron microscopy, even though it did not make it into this thesis. Many thanks to Nora Karnovski and Jerome Finke for help with the 3D STED experiment. I would further like to thank Dr. Jan van Üüm, Dr. Anna Aschenbrenner and Helena Batoulis for proofreading this thesis.

I want to thank all members of the LIMES Institute for the nice working atmosphere. AG Kolanus, AG Thiele and AG Burgdorf shared a lot of expertise, important instruments and reagents. Special thanks to Elvira, Jenny and Rita from the scullery for their kind help. I am further thankful for the TRR83 of the DFG and the "NRW International Graduate Research School LIMES - Chemical Biology" of the ministry for innovation, science and research of North Rhine-Westphalia that provided the necessary funding.

I am thankful to the members of my thesis committee Prof. Dr. Thorsten Lang, Prof. Dr. Christoph Thiele, PD. Dr. Reinhard Bauer and Prof. Dr. Ulrich Kubitscheck for taking the time to evaluate this thesis.

I would like to express my deepest gratitude to my lab mates, namely Helena Batoulis, Martina Bettio, Dennis de Coninck, Jerome Finke, Yahya Homsi, Nora Karnowski, Ines Lauria, Shirisha Nagotu, Jan-Gero Schloetel, Thomas Schmidt, Luis Spitta, Arne Schreiber, Jan van Üüm, David Walrafen and Pascal Weber for many lively discussions, help at any time and the great atmosphere inside and outside the lab. It has been so much fun with you guys!

I would like to thank the members of the "Fightclub" for the heartfelt friendship since the very beginning of the studies in Tübingen and for sharing good and bad times of the PhD.

I owe my deepest gratitude to my parents for always supporting me and for having a steadfast belief in me. Your love gives me strength and keeps me grounded. Above all, I would like to thank Jan for his patience during the stressful times. Your incredible support, your love and the stupid jokes are irreplaceable.